Department of Physics
Indian Institute of Technology Guwahati
Ph.D. Thesis

Frustrated antiferromagnets and role of Dzyaloshinskii-Moriya interaction

Kallol Mondal

Thesis Supervisor: Prof. Charudatt Kadolkar

May, 2020

Frustrated antiferromagnets and role of Dzyaloshinskii-Moriya interaction

A Thesis submitted for the award of the degree of
Doctor of Philosophy in Physics
by

Kallol Mondal

Thesis Supervisor: **Prof. Charudatt Kadolkar**

Department of Physics
Indian Institute of Technology Guwahati
Guwahati - 781039, Assam, India

May, 2020

Statement

The work contained in the thesis entitled "**Frustrated antiferromagnets and role of Dzyaloshinskii-Moriya interaction**" has been carried out at the Department of Physics, Indian Institute of Technology Guwahati, India by me under the supervision of Prof. Charudatt Kadolkar. The material of this thesis has not been submitted elsewhere for any other degree. Works presented in the thesis are all my own unless referenced to the contrary in the text.

(Kallol Mondal) Date:
May, 2020
Department of Physics
Indian Institute of Technology Guwahati
Guwahati - 781039, India

Disclaimer

The bibliography included in this thesis is, by no means complete but contains the ones which are consulted thoroughly by me. I apologize for inadvertently missing out some of the research papers, review articles and other scientific documents pertaining to the focus of this thesis which should also have been cited. For illustration purpose some of the figures in this thesis are taken from other sources and properly cited.

Certificate

It is certified that the work contained in the thesis entitled "**Frustrated antiferromagnets and role of Dzyaloshinskii-Moriya interaction**" by Mr. Kallol Mondal (Roll no.-126121017), a Ph.D. student of the Department of Physics, Indian Institute of Technology Guwahati is carried out under my supervision and has not been submitted elsewhere for the award of any other degree.

(Prof. Charudatt Kadolkar) Date:
May, 2020
Department of Physics
Indian Institute of Technology Guwahati
Guwahati - 781039, India

Dedicated to

Kounish

Acknowledgement

Looking back at the seven and a half years I have spent at IITG, and I find myself very fortunate to have interacted with so many remarkable people. In these years at IITG have not only made me somewhat of an expert in a few specialized areas of physics but have also greatly transformed me as a person. Now I will express my gratitude to all those who have made a significant impact during this long journey.

First, I would like to thank my supervisor Prof. Charudatt Kadolkar for taking me as his Ph.D. student. I have always been motivated by his problem-solving skills and tried to follow him. It has been a privilege to be associated with a physicist like him and to have benefited from his immense wealth of ideas.

I am indebted to the members of the doctoral committee, Prof. Sitangshu Bikash Santara, Prof. Malay Kumar Nandy, Prof. K. V. Srikanth, and Prof. Subhradip Ghosh for their useful suggestions to improve my scientific understanding during the yearly assessments of my research work. Their insightful comments also helped to clarify several basic concepts.

I also thank all HODs (Prof. Saurabh Basu, Prof. Poulose Poulose, and Prof. Subhradip Ghosh) for their various academic help during my Ph.D. I would like to thank all the technical assistants, the academic and non-academic staff of the department who helped me in various ways during my research period. I especially thank Basab-da for his support in different computer related issues and also for giving me shelter during the CAA- protest, which I will never forget. I am also thankful to Param Ishan, IIT Guwahati, for the supercomputer facility. I thank the Department of Physics IIT Guwahati, India, for allowing me to utilize the Newton cluster, funded under the FIST program by DST, India.

I would also like to thank Dr. Laura Messio for sharing her codes and data, which helped me a lot during my initial days.

Life outside of physics has been incredibly rich and fulfilling too, and thanks go to all my friends. I am extremely fortunate to have seniors like Bishu-da, Himangsu-da, Tapas-da, Bappa-da, Kartik-da, Arnab-da, Ramesh-da, Bhargav-da, and Debashis

da. Here, I have got some amazing friends like Ramiz, Sudin da, Sourav, Ashis, Koushik, Noor, Anabilda, Abhijit, Rahul, and Atanu. We have great memories and will cherish forever. I would like to thank my batchmates Venky, Bibhuti, Ram Kumar, Prahlad, and my juniors Srikrishna, Sheuly, Sayan, Pratap, Sumit, Karuna, Pulak, SS Goutam Buddha, Sneha(Mataji), Sanjib, Gobinda and others. Outside the department, I must thank our football group(FootBong), where I have got some amazing players as my friend like Subhankar, Gourab, Anirban, Sourav(Bharatiya), Uday, Barreto da, Shantiram, Soumen(Boss), Debashis(Mahan DK). Then, I have never dreamt of acting in a movie, so thanks go to all the members of Cinephile Production, specially Ramiz, Krishnanjan, Basabendu, Srimoy, Sunando-da, and Ashmita-di. Last but not least, the friend list will not be complete without my childhood friend Moonni(Arpita Roy Mukherjee), Payel, Mantu, Chinmoy, Sourav, my M. Sc. mate Amitabha and Senapati. Especially, I am indebted to Moonni for her help during my tough days.

Finally, I would like to thank all my family members, especially my parents and my elder brother, for their unconditional love, support, freedom, and sacrifices for me.

May, 2020 Kallol Mondal

Abstract

In this thesis, we have extensively worked on the nature of the ground state of different frustrated magnets, especially on kagome lattice and the possible magnetic long-range order state in those systems. Due to low dimensionality, a higher degree of frustration and larger quantum fluctuations makes kagome Heisenberg antiferromagnet(KHAF) a suitable candidate to host a quantum spin liquid ground state. In the isotropic case, i.e., in the absence of DMI, the ground state of kagome Heisenberg antiferromagnet is argued to be a $\mathbb{Z}_2$ chiral topological spin liquid. We have mainly focused on the effect of anisotropies like Dzyaloshinskii-Moriya interaction(DMI) on the ground state manifold of kagome Heisenberg antiferromagnet. So, the presence of DMI can be identified as a perturbation to the Heisenberg Hamiltonian. So, it is expected that the DMI can potentially destroy the spin liquid state and induce magnetic order in the system through a quantum phase transition. DMI is a special kind of anisotropy that arises in a lattice where there is a lack of inversion symmetry and originates from the spin-orbit coupling. Up to what extent DMI induces magnetic order in the system and understanding the zero temperature magnetic structure is the objective of the present thesis.

Since there is a possibility of a magnetic long-range order state, induced by DMI, we have used *Schwinger boson mean-field theory*(**SBMFT**) to study the above problems. SBMFT is an elegant way to study both the long-range ordered state as well as spin liquid state. Magnetic long-range order is induced by the condensations of Schwinger bosons. Now, the effect of the in-plane component and out-of-plane component of DMI is quite different. The planar component favors the canting of the spins from the kagome plane leading to the non-coplanar spin structure, whereas the out-of-plane component favors the planar spin structure. Thus, we have considered two separate problems when the in-plane component is small compared to the out-of-plane component of DMI, and the other one, when both are comparable or in-plane component, is dominant over the out-of-plane component.

In our first work, we have calculated the ground state phase diagram when the in-plane component is quite small compared to the out-of-plane component, and that is the case of Herbertsmithite. This material does not show any sign of freezing down to very low temperatures, but the experimental results predict the presence of DMI. It was not very clear why this material does not freeze, and the possible explanation was the presence of a quantum critical point. Thus we have computed the ground-state phase diagram using SBMFT. We have calculated properties associated with

each of the phases to interpret the experimental result of Herbertsmithite.

In the next work, we investigate the possible *regular magnetic order*(RMO) for the spin models based on **group theoretical approach** for kagome and triangular lattices. The main reason to study these RMOs is that they are the good variational candidates for the ground states of these kinds of frustrated magnets. In this thesis, we followed the prescription introduced by Messio et al. (L. Messio, C. Lhuillier, and G. Misguich, Phys. Rev. B, 2011, 83, 184401) for $p6m$ group and extended their work for different subgroups of $p6m$, i.e., $p3$, $p31m$, $p3m1$, and $p6$ in Hermann-Mauguin notations. We have listed all the possible classical ground state spin configurations for these groups.

In our last work, we consider the case where the in-plane component is dominant over the out-of-plane component, which is the case of vesignieite. Motivated by the experimental result of vesignieite that the ground state in $Q = 0$ magnetic long-range order state, we looked at the mean-field *Ansatz*, which mimics the above ground state in the large S-limit. We have obtained the ground-state phase diagram of this model and calculated properties of different phases. In order to have better insight into the problem, we have also studied the above model numerically using *exact diagonalization*(**ED**) up to a system size $N = 30$. We have compared the obtained results from these two approaches. We have made an attempt to interpret the experimental of vesignieite result from our calculation.

List of Publications

Journal Publications

1. **Kallol Mondal** and Charudatt Kadolkar, *Schwinger boson mean field theory of the kagome Heisenberg antiferromagnet with Dzyaloshinskii-Moriya interaction*, Phys. Rev. B **95**, 134404 (2017)

2. **Kallol Mondal** and Charudatt Kadolkar, $Q = 0$ *order in quantum kagome Heisenberg antiferromagnet*, arXiv:2001.10885 (communicated to Phys. Rev. B)

3. **Kallol Mondal** and Charudatt Kadolkar, *Regular magnetic order in kagome and triangular lattice* (To be submitted)

Conference Publications

4. **Kallol Mondal** and Charudatt Kadolkar. *Study of Ising antiferromagnet with Dzyaloshinskii-Moriya interaction.* Proceeding of International Conference on Condensed Matter and Applied Physics, Vol. 1728, p. 020158. AIP Publishing, 2016.

5. **Kallol Mondal** and Charudatt Kadolkar. *Ground state phase diagram of kagome Heisenberg antiferromagnet with Dzyaloshinskii- Moriya interaction.* AIP Conference Pro- ceedings 2072, 020008 (2019).

Conferences/workshops/Schools attended

1. Attended **Workshop on Current Trends in Frustrated Magnetism**, February 2015, Department of Physics, Jawaharlal Neheru University, Delhi.

2. Presented poster at **International Conference on Condensed Matter and Applied Physics**, organised by Dept. of Physics, Govt. Engineering College Bikaner, Nov 2015

3. Attended **Workshop on Frontier in Condensed Matter Physics**, organised by I.O.P Bhubaneswar, February 2016

4. Oral presentation at **National Conference on Frontier in Modern Physics**, August 2018, Department of Physics, Adamas University, Kolkata

5. Presented poster at, **2nd Annual Conference on Quantum Condensed Matter**, July 2019, Department of Physics, IISC Bangalore, India.

Contents

List of Figures

List of Tables

Chapter 1

Introduction

Understanding the ground state of different quantum magnets, especially, the frustrated antiferromagnets is a long-sought goal in condensed matter physics. For a magnetic material of those kinds, the degrees of freedom are magnetic moments, completely localized on a given lattice. The macroscopic magnetic properties are remarkably different from those of atoms and molecules, though the fundamental constituents remain the same. This is due to the fact the macroscopic properties are collective in nature and purely quantum mechanical, involving a huge number of particles. Typically, when a magnetic material is cooled below a critical temperature, the magnetic moments tend to align in a particular pattern like, parallel or anti-parallel to minimize their free energy. These two patterns correspond to a well-known ferromagnet or antiferromagnet depending on their sign of exchange coupling J. As we lower the temperature, thermal fluctuations become smaller and smaller. Typically, lower thermal energy leads to an ordered ground state. However, there are magnetic materials where there exist multiple competing magnetic interactions, and the ground states tend to deviate from the usual magnetic long-range order. The most familiar example is edge-sharing triangular lattice and corner-sharing kagome lattice, where the magnetic interactions are frustrated by the triangular geometry of the lattice. The ground state becomes disordered due to large quantum fluctuations for low values of spin [1]. Materials with such a completely disordered zero-temperature phase are termed as quantum spin liquids (QSL) [2]. However, QSL is not merely a disordered state, and there are other exciting features that make the study of quantum spin liquids even more fascinating. The quantum spin liquids are highly entangled states with no spontaneous symmetry breaking at absolute zero. Hence they can not be explained in the paradigm of Landaus symmetry breaking theory [3, 4]. Another exciting feature of quantum spin liquid is the

fractional excitations. The spin liquids are classified based on the topological order introduced by Wen [5]. Because of the frustration induced by the geometry with vertex sharing triangles, the Heisenberg antiferromagnetic model on kagome lattice (KHAF) is considered as the best candidate to host the spin liquid ground states.

However, the presence of anisotropy plays a vital role in deciding the fate of the ground states, especially if the ground state is disordered. There is a special kind anisotropy that appears if there is a lack of inversion symmetry in the crystal, known as the Dzyaloshinskii-Moriya(DM) interaction [6, 7], which arises from the spin-orbit coupling. Up to what extent this DM interaction influences the disordered ground state and establishes long-range order in the spin system is the focus of the present thesis. We use the Schwinger boson framework and exact diagonalization to study the above problem.

We must mention that the quantum spin liquids possess very rich physics, and each of those phases is interesting in their own way since these phases emerge with unconventional orders and excitations. It turns out the magnetically ordered phases of those materials can also be non-trivial. Specifically, the classical ground state of those quantum magnets may appear with "accidental degeneracies" that may be lifted by quantum fluctuations. In that case, quantum fluctuations induce order in the system, known as "order form disorder" [8–10]'. Therefore, a systematic study of possible long-range order states for a given lattice is highly relevant. Based on symmetry consideration, applying a group theoretical approach, we investigate the possible "regular magnetic order", in kagome and triangular lattice, which falls into the category of wallpaper group $p6, p3, p3m1$, and $p31m$.

1.1 Spin models and magnetic long-range roder

Theoretical models of many insulating crystals with localized electrons typically starts with the Heisenberg Hamiltonian with interacting spins

$$H = \frac{1}{2}\sum_{ij} J_{ij}\mathbf{S}_i \cdot \mathbf{S}_j \tag{1.1}$$

where i and j are the site index. The model can be defined on any lattice. Here, we will mainly concentrate on kagome and triangular lattice. $\mathbf{S}_i$ and $\mathbf{S}_j$ are the spin operators at i-th and j-th site respectively. The components of spin operators on the same lattice sites obey the standard angular momentum commutation relations

$$[\mathbf{S}_j^\alpha, \mathbf{S}_k^\beta] = i \sum_\gamma \epsilon_{\alpha\beta\gamma}\ \mathbf{S}_j^\gamma \delta_{jk} \quad \text{where} \quad \alpha, \beta, \gamma = \{x, y, z\} \tag{1.2}$$

and the spins sitting at different site will commute with each other. $\epsilon_{\alpha\beta\gamma}$ is the Levi-Civita symbol. All the spin operators wall have spin S and $\mathbf{S}_i^2$ have the eigenvalue $S(S+1)$. The spin interaction of the form $\mathbf{S}_i \cdot \mathbf{S}_j$ as referred in Eqn. 1.1 is known as exchange interaction and the coupling constant J_{ij} is known as exchange integral. Now, we can define the operator *total spin* as $S^a = \sum_{i=1}^N S_i^a$. If then Hamiltonian commutes with this operator, then we can say that the Hamiltonian is SU(2) invariant. It can be shown that each of the three components of *total spin* $\vec{S} = \sum_i \vec{S}_i$ commutes with the dot product $\vec{S}_i \cdot \vec{S}_j$ i.e. $[\vec{S}, \vec{S}_i \cdot \vec{S}_j] = 0$.

The spin-half anti-ferromagnetic Heisenberg model also arises as a limit of the Hubbard model at half-filling for large onsite Coulomb repulsion [11, 12]. When the electrons are not localized to the lattice sites, then a better description of the problem is given by the Hubbard model, which also includes charge fluctuations. The Hamiltonian for the Hubbard model is given by

$$H_{\text{Hubbard}} = -\sum_{ij,\alpha} t_{ij} C_{i\alpha}^\dagger C_{j\alpha} + U \sum_i (n_i - 1) n_i \tag{1.3}$$

where $C_{i\alpha}^\dagger$ and $C_{j\alpha}$ are creation and annihilation operators respectively and α can be $\pm\frac{1}{2}$ on site i and n_i is the occupation density. The operators satisfy anti-commutation relations, given by $\{C_{i\alpha}^\dagger, C_{j\beta}\} = \delta_{\alpha,\beta}\delta_{ij}$. The coupling t_{ij} represents the hopping ampilitude from site i to j and U is the Coulomb energy cost to occupy the same site for two electrons. In the $U >> t$ limit, there is on avergae one electron per site and the charge fluctuations become negligible. It can be shown that at $J_{ij} \sim 4t_{ij}^2/U$, the Hubbard model reduces to the above Heisenberg model. However, when the strength of U and t are comparable, then the two models are inequivalent.

Heisenberg Hamiltonian can successfully capture the physics of low-temperature magnetic structure and still a cherished model to understand the collective behavior of many spins arranged in a lattice. However, despite deceptive simplicity, exact solutions are extremely difficult to obtain. Even the most sophisticated techniques are used to get the approximate ground states of frustrated magnets. In the present thesis, we will mainly focus on the Heisenberg model to study the ground states of quantum antiferromagnets.

In a conventional ferromagnet, the ground state is where all the spins are aligned in the same direction, resulting in a spontaneous magnetization. However, the anti-

ferromagnetic ground state is a bit more complicated and exactly known for few spin systems like a 1D spin chain. In that case, for bipartite lattices, the possible ground state consists of two sublattices with mutually antiparallel spins is known as Neel state. But it turns out that Neel state is not an eigenstate of Heisenberg Hamiltonian. So, the Neel state can be considered as a trial ground state for the variational approach.

Even though the interaction between the spins is short-ranged interactions, there exists a correlation between the spins situated at each site of the lattice, separated by a distance that is larger than the effective distance between nearest neighbors. Magnetic long-range orders are characterized by such correlations. Different macroscopic properties are the manifestation of such correlations. Spin-spin correlation length gives a measure of the magnetic long-range order in quantum spin systems. The correlation length is basically the effective distance at which the spin-spin correlation is not zero. The correlation length is infinite if the system is perfectly ordered. As temperature increases, the thermal fluctuations wash out these orderings, and the correlation length becomes finite. At sufficiently high temperature, the spins becomes uncorrelated and stabilizes the *paramagnetic* state, are in some sense liquid of spin. This order-disorder transition occurs at a critical temperature T_c.

From the symmetry point of view, one of the most remarkable properties of long-range order in the ground always posses lower symmetry than the Hamiltonian describing the system. For example, let us consider the Heisenberg Hamiltonian, which is SO(3) symmetric. If the ground state is ferromagnetic, i.e., the spins are aligned in a preferred direction. Then, SO(3) symmetry is reduced to SO(2). This phenomenon is known as *spontaneous symmetry breaking*. The phenomenon of broken symmetry has a deep impact on the ground state. Goldstone theorem states that spontaneous breaking of continuous symmetry implies that the low energy excitations of the ground state can be viewed as massless bosons known as *Goldstone bosons* or Goldstone modes. In quantum spin systems, the *Goldstone bosons* are called *magnons* or *spin waves*.

One of the most remarkable properties of these quantum magnets that in three dimensions, they exhibit spontaneous symmetry breaking and magnetic long-range order at finite temperature, but in the lower dimension, that is not the case. According to the Mermin-Wagner theorem, no long-range order is possible in 1D and 2D [13]. It has been found that in the case of 1D and 2D, the critical temperature $T_c = 0$. The introduction of infinitesimal temperature may lead to the finite correlation length, consistent with Mermin-Wagner Theorem.

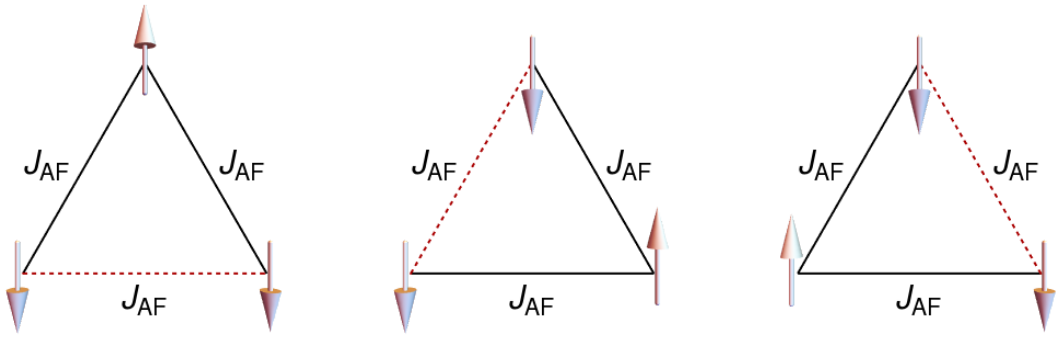

Figure 1.1: Geometric frustration on a triangular geometry for Ising spins. When the anti-parallel arrangement of two spins is fixed, the third one experiences conflicting preferences of orientation, which can never be simultaneously satisfied. The unsatisfied bonds are shown by a dashed red line, whereas the satisfied bonds are shown by a solid black line.

1.2 Frustration

The phenomenon of magnetic frustration occurs in a quantum spin system when the spins interact antiferromagnetically with each other. For the antiferromagnetic interaction, the interaction energy is minimized when the spins are aligned anti-parallel with respect to its neighbors. However, there are situations when the spins can not satisfy all interactions simultaneously. In that case, the interactions compete with each other in such a way that satisfaction of one of them leads to dissatisfaction of others. Frustration arises mainly due to the nature of the lattice geometry or due to the internally conflicting nature of a set of multiple couplings that acts in different ranges. The first one is often termed as *geometric frustration* and while the second one is called *exchange frustration* To illustrate the geometrical frustration, let us consider a lattice where the elementary plaquette is a triangle. Now consider, three Ising spins which are interacting antiferromagnetically are situated at the vertices of the triangle. The most energetically favorable configuration for a spin of one vertex will be anti-parallel to the others. But the very nature of the geometry makes it impossible to satisfy all three interactions simultaneously. Spins on the two vertices can be anti-parallel, but the remaining spins can not be anti-parallel to both of them simultaneously, leading to the frustration. There is a total of eight possible states. Among them, two are high energy states where all the spins are pointing in the same direction. The remaining states are six-fold degenerate, are described by 2 : 1 ratio of anti-parallel versus parallel spins, as shown in the Fig. 1.1. The minimum of total energy does not correspond to the minimum of each bond present

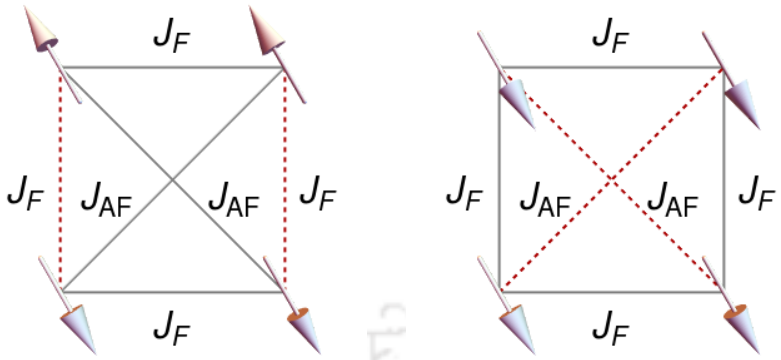

Figure 1.2: Exchange frustration on a square geometry for Ising spins. There are two types of couplings. The ferromagnetic coupling which acts between the nearest neighbor spins and the anti-ferromagnetic coupling, which acts between the next nearest neighbor spins. There is no way to satisfy all the interactions simultaneously, hence frustrated. The above diagram shows the two possible spin configurations with the same ground state energy. Here also, the unsatisfied bonds are shown by a dashed red line, whereas the satisfied bonds are shown by a solid black line.

in the system. In the case of exchange frustration, there is a conflicting preference between several competing interactions present in the system. For instance, let us consider the square geometry as shown in the Fig. 1.2. By the nature of square geometry, this is not frustrated by a single type of interaction. Now, if we consider ferromagnetic coupling between the nearest neighbor and antiferromagnetic between coupling between the next nearest neighbor. In this case, it is impossible to satisfy all these competing interactions to satisfy simultaneously, hence frustrated. In both types of frustration, the simultaneous satisfaction of all the competing interactions is not limited to these basic configurations. Rather, it is spanned over the entire lattice that has those elementary "plaquettes". The higher degree of frustration leads to greater quantum fluctuation, and the ground state often becomes disordered.

One of the most remarkable properties of these frustrated magnets is the dependence of magnetic susceptibility χ on temperature T. Ramirez introduced a simple prescription to measure frustration empirically that is widely used in literature [14]. At high temperature, magnetic susceptibility χ of a local-moment magnet often follows the Curie-Weiss form, given by

$$\chi^{-1} \propto (T - \Theta_{\mathrm{CW}}) \tag{1.4}$$

Where T is the temperature and Θ_{CW} be the Curie-Weiss constant, provides the

natural estimate of sign and the energy scale of exchange interactions. For example, Θ_{CW} negative implies that the interactions are antiferromagnetic and it gives a qualitative scale of magnetic ordering for the unfrustrated magnet.

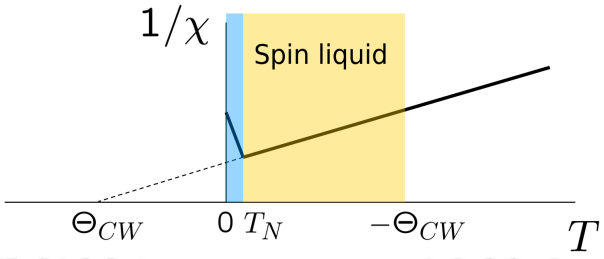

Figure 1.3: Characteristic Succeptibilty behaviour in frustrated system. The susceptibility follows a Curie-Weiss law much below the Curie-Weiss temperature Θ_{CW}.

Without frustration, magnetic ordering is supposed to be at a temperature scale set by $|\Theta_{\mathrm{CW}}|$. But in case of highly frustrated magnets, the spins do not order at much lower temperature and even some cases at absolute zero. Now, to extract the Θ_{CW}, it is convenient to plot χ^{-1} vs T(see Fig. 1.3) . Let, T_c be the critical temperature at which the magnetic moment freezes, then the frustration parameter f can be obtained from $f = |\Theta_{\mathrm{CW}}|/T_c$. It turns out that the frustration parameter greater than five indicates a lack of magnetic ordering due to frustration. The spin liquid regime is found to be in the temperature range $T_c < T < |\Theta_{\mathrm{CW}}|$. Some selected example of frustrated magnetic materials is listed in the Table 1.1 .

Material	**Lattice**	**Spin**	$\boldsymbol{\Theta_{\mathrm{CW}}(K)}$	**Reference**
κ-(BEDT-TTF)$_2$ Cu$_2$(CN)$_3$	Triangular	$\frac{1}{2}$	-375	[15]
EtMe$_3$Sb[Pd(dmit)$_2$]$_2$	Triangular	$\frac{1}{2}$	-(375-325)	[16]
Volborthite	Kagome	$\frac{1}{2}$	-115	[17]
Herbertsmithite	Kagome	$\frac{1}{2}$	-314	[18]
Vesignieite	Kagome	$\frac{1}{2}$	-77	[19]
$Na_4Ir_3O_8$	Hyperkagome	$\frac{1}{2}$	-650	[20]
Cs_2CuCl_4	Triangular	$\frac{1}{2}$	-4	[21]

Table 1.1: Examples of frustrated magnetic material.

1.3 Unconventional phases

The most 'conventional phases' hosted by the Heisenberg model are those who possess magnetic order. These phases which break the transnational and spin rotational

symmetry are termed as conventional phases due to the following reasons. The order parameters are well defined; experimentally measurable quantities are readily accessible by existing theories, and excitations are known to be the 'magnons' with bosonic character. On the other hand, the unconventional phases are those ground state remains disordered mainly due to the frustration and strong quantum fluctuation. In the case of classical magnetic order, the spin behaves as well-defined classical vectors. First, let us consider the unfrustrated case in 1D, 2D, and 3D, i.e., linear spin chain, square lattice, and cubic lattice. For Neel order, the binding energy per site will be given by $-J/4, -J/2$ and $-3J/4$ for spin-1/2. Now, if we consider the singlets with spin expectation value zero at each site.

$$|\psi_{ij}\rangle = \frac{1}{\sqrt{2}}(\uparrow_i\downarrow_j |\rangle - |\downarrow_i\uparrow_j\rangle) \tag{1.5}$$

In this case, the binding energy per bond can be calculated quantum mechanically. It turns out that in one dimension for $S = 1/2$, the formation of singlets is more energetically preferable as the binding energy per spin case singlet is $-\frac{3}{8}J$ and $-\frac{1}{4}J$ for Neel state. The one-dimensional spin chain can be solved exactly and turns out to be a useful example to understand the physics of quantum spin liquid in 2D. The exact solution of the 1D chain was done by Bethe [22], the obtained ground state energy per spin is found to be $-0.443J$ much lower than the nearest neighbor singlet($-\frac{3}{8}J$) and Neel state ($-\frac{1}{4}J$). The possible explanation was the formation of the singlet is not restricted to the nearest neighbor, and the ground state is the macroscopic superposition of all possible singlet pairings. This was identified as the quantum spin liquid in 1D.

In the case of 2D, the Mermin-Wagner theorem discards the possibility of magnetic long-range order. So, to find the nature of the ground state of the 2D system, especially frustrated magnets, is a long-sought goal in condensed matter physics. There is no complete theory which decides the fate of the ground states of these frustrated magnets in contrast to metals, which is well described by Fermi liquid theory [23]. Quantum spin liquids and valence bonds solids are a typical example of unconventional phases in quantum magnets.

1.3.1 Quantum spin liquids

The idea of 'quantum spin liquids' was first introduced by P Anderson [2] in 1973. He proposed that the ground state of two-dimensional quantum antiferromagnets may not be magnetically long-range ordered. Instead, there can be more exotic states

which do not break any symmetry and remain 'disordered' even at absolute zero. According to Anderson's picture, the ground state wave function consists of linear superposition of a large number of singlets and widely known as "resonating valence bond(RVB)" wave function. Over the years, the idea of quantum spin liquid(QSL) has been conflated with the usual notions of liquid in the classical sense. The main features of quantum spin liquid as follows.

Absence of magnetic long-range order : Quantum spin liquid is a state in which the spin-spin correlation $\langle S_i^{\alpha} S_j^{\beta} \rangle$ decays to zero at a large distances, $|R_i - R_j| \to \infty$. This definition is rather very simple, inadequate, and has several limitations. According to the Mermin-Wagner theorem, any system having dimension $D \leq 2$ with a continuous spin rotation symmetry can not be ordered even at $T = 0$. The spin nematic state [24], which satisfies the above criterion but breaks the spin rotation symmetry. This spin nematic states tend to show long-range order in the four-spin correlations [25–27]. A valence bond crystal (VBC) also has short-range spin-spin correlations and also satisfies the above criterion. But VBC shows the signature of ordering in the four-spin correlations also breaks lattice symmetries; hence, it can not be classified as the quantum spin liquid. QSLs do not possess any conventional magnetic order but possess a different type of ordering termed as topological order, originally introduced by X-G Wen [28].

No broken symmetry even at zero temperature : Quantum spin liquid is a state without any spontaneously broken symmetries even at $T = 0$; hence it can not be explained in the paradigm of Landau's symmetry breaking theory. This definition excludes the VBC ground state. But this definition is also not adequate to describe quantum spin liquid.

Quantum spin liquid is a state with fractional excitations : These factional excitations are called 'spinons'. These spinons carry quantum numbers (usually the total spin), which are fractions of the local elementary degrees of freedom. The spinons are said to be deconfined if it is possible to separate these quasi-particles infinitely away from each other at the cost of only a finite amount of energy.

Quantum Entanglement : Quantum spin liquid is a highly entangled quantum object. In general, quantum entanglement is the property of some special states where the measurement of one observable affects the outcome of the measurement of others. In mathematical language, those states can not be written as the direct product of the pure states even under an arbitrary local change of basis. In quantum spin liquid, we characterize the entanglement of the phases, not the individual quantum states. So, we are talking about a phase in which no representative member of the

phase is not entangled. Thus the ground state can not be continuously deformed into product state while staying in the state. Here, the continued deformation can be interpreted as a continuous change in the ground state wave function while slowly varying the local Hamiltonian parameters. The continuous change can be made in such a way that a non zero gap is maintained above the ground state throughout the process. In a many-body system, the entanglement is often studied by calculating what is called *entanglement entropy*.

1.3.2 Valence bond solids

A valence bond is a natural building block of the non-magnetic ground states of these frustrated magnets. Valence bond refers to a pair of spin that, owing to antiferromagnetic coupling, forms a spin-0 singlet object. A valence bond is a non-classical object with maximum entanglement between the pairing spins(see Fig. 1.4). The ground state becomes non-magnetic with spin-0 when all the spins in a spin system become the part of these valence bonds, which are static and localized. In a mathematical language, the ground state can be described by the direct product of each valence bonds, and each of the spins is highly entangled to its valence bonds partner. This ground state is known to be the valence bond solids(VBS) and found to be the ground state of different material [29–31]. Valence bond solids are of particular interest since Bose-Einstein condensation of magnons can be realized experimentally in a material that hosts this kind of ground state [32].

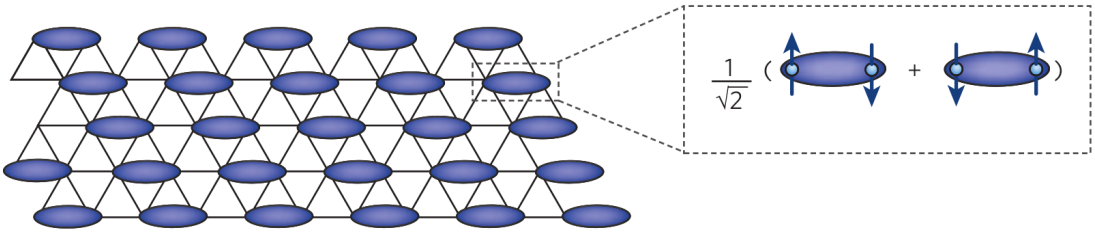

Figure 1.4: Pictorial representation of valence bond states. Entangled pairs in the valence bonds are shown by ovals on triangular lattice. (Figure is taken from Ref. [1])

As discussed earlier, VBS can not be classified as the quantum spin liquid as the arrange of spins are not unique; hence, it breaks lattice symmetries. To build the quantum spin liquid, the valence bond solid should enjoy strong quantum fluctuations. In that case, the ground state becomes a superposition of different configurations of the valence bonds, i.e., different ways of partitioning the spins into

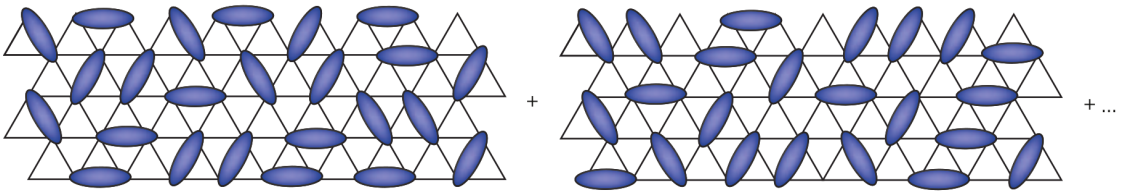

Figure 1.5: Resonating valence bond states where the wave function is superposition of different valence bond states. Here, valence bonds are short ranged and is restricted to nearest neighbor. (Figure is taken from Ref. [1])

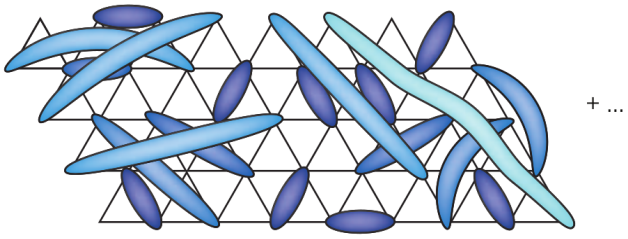

Figure 1.6: Spins in long range valence bond states, where the spins are less tightly bound and therefore can be easily excited in to a state with non-zero spin. (Figure is taken from Ref. [1])

valence bonds. Thus, there will be a resonance between different valence bond partitions. This is the picture suggested by Anderson [2] and argued to be the underlying physics of high-temperature superconductivity. This type of ground state appropriately termed as the resonating valence bond(RVB) analogous to Benzene. So, RVB can be regarded as more of a liquid rather than solids.

However, the RVB wave functions in principle should contain the valence bonds of all possible lengths, not necessarily restricted to only nearest neighbor or short-ranged. Considering the distribution of weights on valence bond configuration of short lengths, we obtained short-range RVBs(see Fig. 1.5) such as gapped $\mathbb{Z}_2$ spin liquids, and for long lengths, we obtain long-range RVBs(see Fig. 1.6) such as algebraic spin liquids. More interestingly, we can have more intermediate states between the above two extreme cases. One can use the gauge structure and symmetries two classify these spin liquids as pioneered by Wen [5]. $U(1)$ analogs of these $\mathbb{Z}_2$ spin liquids phases, are termed as $U(1)$ spin liquids. These $U(1)$ spin liquid states support gapped spinons, gapped monopoles, and gapless photons [33, 34]. Experimentally, these phases are easier to probe since the gapless photons will appear in the low-

energy physical properties of the system. For example, an additional T^3 contribution to the specific heat from photons could easily be observed. There have been recent theoretical studies of three-dimensional models in which possible $U(1)$ spin liquid states are reported [35–37].

Finally, the study of quantum spin liquid is fascinating as it is associated with rich physics also may host the underlying physics of high-temperature superconductivity. In addition to that quantum spin liquid also posses great application potential, for instance, the long-range entanglement of the spins are the essential ingredient for quantum communication [38] and also topological quantum computation [39]

1.4 Anisotropies

In real spin systems, several perturbations come into play, which could, in principle, alter the low-temperature magnetic structure. There are cases where the exchange interaction is not restricted to the nearest neighbor, and the next-nearest neighbor and next-next-nearest neighbor may become significant [40]. The most obvious one is the distortion, where some of the bonds may differ from each other. In addition to that, Even for the undistorted network, there are other interactions that come into play. Below we discuss the main perturbations, which play a vital role in deciding the fate of the ground state.

1.4.1 Dzyaloshinskii-Moriya interaction

Weak ferromagnetism of antiferromagnet of antiferromagnetic crystal such as α-Fe_2O_3 and the carbonate of Mn and Co was a controversial problem from a long time. So, the question was asked whether the origin of weak ferromagnetism is an intrinsic property of the crystal. Dzyaloshinskii first gave a phenomenological explanation that the weak ferromagnetism is possible without breaking the symmetry of the original state [6]. Since this theory is a phenomenological one and does not clarify how this interaction arises and also the strength of the interaction. Later, Moriya showed that the interaction occurs naturally in the perturbation theory due to the spin-orbit coupling with low symmetry [41]. Moriya's approach was an extension of anisotropic superexchange theory already introduced by Anderson [42] to include the spin-orbit coupling. Moriya argued that the spin-orbit coupling generates the excited state in one of the magnetic ions, and hence, the process of virtual transition leads to an anisotropic correction to the isotropic part. Moriya concluded that the

coupling constant is linear in spin-orbit coupling. Using second order perturbation theory, Moriya showed that the general effective spin Hamiltonian describing the interaction between the two spins $\hat{S}_k$ and $\hat{S}_l$ is given by

$$\hat{H}_{\text{Spin}} = J\hat{S}_k \cdot \hat{S}_l + \hat{S}_k \cdot \overleftrightarrow{A}_{kl} \cdot \hat{S}_l + D_{kl} \cdot \hat{S}_k \times \hat{S}_l \tag{1.6}$$

The first term denotes the isotropic symmetric exchange. The second and the third term represents the symmetric $\overleftrightarrow{A}_{kl} = \overleftrightarrow{A}_{lk}$ and anti-symmetric $D_{kl} = D_{lk}$ anisotropies respectively. The anti-symmetric Dzyaloshinskii-Moriya (DM) interaction has the following form

$$H'_{kl} = \vec{\mathbf{D}}_{kl} \cdot (\vec{\mathbf{S}}_k \times \vec{\mathbf{S}}_l) \tag{1.7}$$

For a given spin configuration, the allowed component of DMI is restricted by the symmetry of the crystal. As mentioned in Ref.[7], the rules for the DM vectors are following. Let us consider two magnetic ions are located at points A and B, respectively. If C be the point bisecting the bond, then.

- When a center of inversion is located at C, $\vec{D} = 0$.
- When a mirror plane perpendicular to AB passes through C, $\vec{D}$ lies in the mirror plane or $\vec{D} \perp AB$
- When there is a mirror plane including A and B, D is perpendicular to the mirror plane
- When a two-fold rotation axis perpendicular to AB passes through C, D is perpendicular to the two-fold axis.
- When there is an n-fold axis $n \geq 2$ along AB, $\vec{D}||AB$

These symmetry rules have immediate consequences. For instance, in the case of square lattice and triangular lattice, the center of every bond is the center of inversion. So the first rule implies that in those cases, DM interaction should not exist. But in the case of kagome lattice, every midpoint of a bond is not a center of inversion, so DM interaction is allowed. For a perfect two dimensional lattice, if the lattice plane is itself a mirror plane, then the in-plane component should vanish according to the third rule.

Since this interaction term has the directional sense due to the presence of vector cross product, we must follow a convention whether the bond is taken $i \to j$ or $j \to i$. Our conventions for the bonds will be presented where appropriate.

1.4.2 Dipole-dipole interactions

In general, the dipole-dipole interactions are long ranged and weak, typically do not decide the fate of magnetic ordering and related physical observables [43]. From the knowledge of electrodynamics, the dipole-dipole interaction can be written in the following form

$$\hat{H}_{dd} = -\frac{1}{2}\sum_{i,j,i\neq j}\frac{\mu^2}{|\mathbf{R}_{ij}|^3}\Big[3(\mathbf{S}_i\cdot\hat{\mathbf{R}}_{ij})(\mathbf{S}_j\cdot\hat{\mathbf{R}}_{ij}) - (\mathbf{S}_i\cdot\mathbf{S}_j)\Big] \tag{1.8}$$

where the sums are sites i and j. $\hat{\mathbf{R}}_{ij}$ is the unit vector in the direction of $\mathbf{R}_{ij} = \mathbf{R}_i - \mathbf{R}_j$. The magnetic moment associated with spins are denoted by μ where $\mu = g\mu_B$, g is the effective g-factor and μ_B be the Bohr magneton.

Interestingly, the contribution of this anisotropy becomes vital if the isotropic exchange does not allow magnetic ordering at finite temperature. According to the Mermin-Wagner theorem, in the presence of $SU(2)$ symmetry, there will be no magnetic long-range order in 2-D quantum magnets at finite temperature. Inclusion of dipole-dipole interaction breaks the SU(2) symmetry may lead to the possibility of magnetic long-range ordering. The addition of the above anisotropy may result in a nonzero gap in the excitation spectrum.

1.4.3 Single ion uniaxial anisotropies

Single ion uniaxial anisotropies are induced by the local crystal field through the spin-orbit coupling. This type of anisotropy generally appears in kagome, and triangular lattice due to the layered nature of the materials has the following form

$$H' = -D\sum_i (S_i^z)^2 \tag{1.9}$$

Where D is the strength of the coupling. For the pure Heisenberg model on kagome and triangular lattices, the ground states typically involve coplanar spin configuration. However, the presence of this type of anisotropy may lead to the collinear spin arrangement. There are several rare-earth quantum magnets where the single ion uniaxial anisotropies are quite dominant. For instance, the quantum kagome anti-

ferromagnet Nd-langasite($Nd_3Ga_5SiO_{14}$) where $D \sim 10K$ and $J \sim 1.5K$ [44]. The classical ground state of such collinear spin arrangement becomes highly degenerate.

1.5 Kagome lattice spin systems : theoretical review

Quantum Kagome Heisenberg antiferromagnet with spin-1/2 is a potential candidate to host a quantum spin-liquid ground state. Corner sharing triangles with a high degree of frustration and small spin, with large quantum fluctuations make it a suitable candidate for quantum spin liquids [45, 46]. So, the quantum kagome Heisenberg antiferromagnet has been studied extensively over the years. However, the fate of the ground state is still undecided [1, 45, 47, 48]. The proposed ground state includes valence bond solids [49–53], gapless quantum spin liquids [54–56] and gapped spin liquids [57–62]. Very early on, Elser et al. [63] suggested that the ground state of nearest neighbor Heisenberg Hamiltonian with antiferromagnetic interaction is nonmagnetic, which might be a QSL [59] or a VBS. Then, Lecheminant et al. [64] predicted a gapless QSL ground state based on exact diagonalization studies up to a system size of 27 spins. In 2007, Y Ran et al. [65], based on Gutzwiller projected fermion variational calculation argued that the ground state is a gapless U(1) Dirac spin liquid. Based on the series expansion calculation by Rajiv R. P. Singh [66] predicted a VBS state as a ground state. The VBS state was leading numerical candidate as a ground state of kagome Heisenberg antiferromagnet for several years, Then, S Yan et al. [48] came up with a pioneering DMRG calculation and conclusively demonstrated the lack of VBS order and strongly suggested a gapped QSL state, which was supported by other DMRG calculation [67]. A finite spin gap in the thermodynamic limit is also reported from DMRG calculation [48, 67, 68]. It turns out that the magnitude of the spin gap is method dependent and qualitatively in agreement with the gapped $\mathbb{Z}_2$ topological spin liquid theory [59]. The large scale numerical diagonalization results for a system size $N = 42$ predicts the ground state to be gapless spin liquid in the thermodynamic limit [69], consistent with U(1) Dirac spin liquid theory [65] and variational method [70, 71]. Schwinger boson mean-field theory predicts the chiral topological spin liquid as the ground state of kagome Heisenberg natiferromagnet [72].

The ground state of spin-1/2 quantum kagome Heisenberg antiferromagnet is still an open problem as the present techniques are not enough to resolve the issue in the thermodynamic limit. Even when the most sophisticated methods are used to get the approximate ground state.

1.5.1 Role of DM interaction

The introduction of DM interaction has a deep impact on the ground state manifold [73]. Hermele et al. [54] argued that an infinitesimal strength of DMI may induce long-range magnetic order and hence can not be neglected. Exact diagonalization results predict the presence of quantum critical point $D_c = 0.1J$ where there is moment free phase at one side and Neel phase on the other as suggested by Cepas et al. [74]. Huh et al. has proposed a quantum critical theory [75] about the presence of quantum critical point, already suggested by Cepas. Schwinger boson formalism also agrees qualitatively about the presence of the critical point as shown by L Messio et al. [76]

One of the challenges of the search for QSL among materials is the presence of anisotropies like DMI. Typically, DMI reduces symmetry and quantum fluctuations and leads to magnetic long-range order.

1.6 Quantum spin liquids in experiment

It should be noted that to probe quantum spin liquids, the experiments should be performed ideally at absolute zero temperature, but that is not achievable. In practice, the measuring temperature T must be very less than the characteristic temperature of the exchange couplings of the material. So, the properties at the measuring temperature can be interpreted as the properties of the zero temperature state, provided that there is no further phase transition below the temperature. The detection of quantum spin liquids in experiments is still a challenging problem because of its peculiar properties like unbroken lattice symmetries and the absence of local order parameters. The search for quantum spin liquids necessarily involves frustrated spin systems where the spin-spin interaction dominantly antiferromagnetic, which does not freeze to the lowest achievable temperature. The measurement of magnetic susceptibility provides useful insights into this aspect. One can perform Curie-Weiss fit to the high-temperature susceptibility to calculate the Curie-Weiss temperature Θ_{CW} that characterizes the strength of antiferromagnetic exchange coupling. In Table 1.1 we have listed the Θ_{CW} for few frustrated magnets.

Measurement of specific heat also provides useful information to probe the magnetic freezing. Magnetic ordering at low temperature shows a λ- type peak in specific heat vs. temperature plot. For quantum spin liquids, such a sharp peak does not generally appear unless there is topological phase transition [77]. Furthermore, it

can provide information about low-temperature magnetic excitations. One can calculate the residual magnetic entropy by subtracting the phonon contribution. The possibility of magnetic ordering at low temperature can be estimated by examining the released entropy at the measuring temperature [78, 79]. Apart from the above macroscopic measurements, one can perform the microscopic measurements like muon spin relaxation (μSR) and Nuclear magnetic resonance(NMR) to probe the spin liquid ground states. These microscopic probes are very sensitive to the local magnetic environment, thus can be used to detect the spin freezing [80–82]. Inelastic neutron scattering experiments give better insights to the magnetic ordering in a spin system. The inelastic neutron cross-section is proportional to the dynamical spin structure factor; hence there is a direct connection between theory and experiment.

One of the unorthodox features of quantum spin liquids is fractional excitations and long-range quantum entanglement. Since the later one is hard to characterize, so the identification of QSL's is mostly based on the former, for instance, the predictions of spinons in RVB model [2]. These spinons are charge-neutral carrying a fractional spin $S = 1/2$, are deconfined in the lattice. For a particular type of spin liquid, for example, U(1) gapless spin liquids where the low energy effective model has a U(1) gauge symmetry. In that case, the spinons form a Fermi sea, very similar to that formed by electrons in a metal [83]. To identify the presence of fractional excitations, the techniques which are sensitive to the magnetic excitations such as inelastic neutron scattering, thermal conductivity, Nuclear magnetic resonance, electron spin resonance, as well as terahertz spectroscopies are used extensively.

The search for the realization of quantum spin liquids in Heisenberg quantum antiferromagnet has several rare earth materials, listed below. However, each of them suffers from anisotropies or some distortion.

Herbertsmithite: This material is strongly suspected of hosting the quantum spin liquid ground state. In Herbertsmithite($ZnCu_3(OH)_6Cl_2$), the spin-1/2 Cu^{++} forms a perfect kagome structure [18, 84–87]. The high temperature susceptibility is well described by the spin-1/2 Heisenberg model with nearest-neighbor coupling. More interestingly, in addition to that, there is the presence of Dzyaloshinskii-Moriya interaction (DMI), which is around 10% of the exchange coupling. This material does not show any sign of freezing down to 50 mK as predicted from SQUID magnetometry, and the specific heat follows a T^{α} behavior with $\alpha \approx 1$. In contrast, a higher power law is found for the magnons in the case of ordered antiferromagnets. Inelastic neutron scattering experiments on single-crystal reveals diffusive dynamic

structure factor for a broad range of momenta and energy down to 2 K, in contrast to that sharp Bragg peaks appear in magnetically long-range ordered state [88]. This indicates the existence of deconfined fractional excitation in contrast to $S = 1$ spin-wave excitation in the case of ordered magnets.

Vesignieite : The mineral vesignieite ($BaCu_3V_2O_8(OH)_2$) [19] is also an interesting case. This material has the kagome structure with minute 0.07% bond-length difference due to two inequivalent Cu^{+2} sites [89]. The magnetism of this material is mainly dominated by the nearest neighbor antiferromagnetic interaction $J = 53K$. In this material, the magnetic ordering is found surprisingly at a very large temperature of $T = 9K$, unlike Herbertsmithite. Electron spin resonance(ESR) spectra reveal that there is a strong presence of DM anisotropy, which may lead to the magnetic ordering [89–92]. Unlike Herbertsmithite, in this case, the dominant anisotropy is an in-plane component of DMI, which is estimated to be $D_p = 0.19J$, whereas the out-of-plane component is $D_z = 0.07J$. The ground state is found to possess $Q = 0$ magnetic long-range order with canted structure, and the canting angle is found to be $3^o < \phi < 9^o$ [93]. However, a recent NMR study predicts that the ground state posses hexagonal multi-K structure with dominant third neighbor antiferromagnetic interaction, and the magnetic ordering temperature is also reported to be $9K$ [94]. So, the true nature of the ground state is yet to be understood.

Volborthite : Volborthite($Cu_3V_2O_7(OH)_2{\cdot}2H_2O$) is magnetic insulator with distorted kagome structure with inequivalent exchange couplings [95–97]. Naturally, it is expected that the lattice distortion may play a vital role in the determination of magnetism in this material. The freezing temperature of $1K$ is much lower than the measured Curie-Weiss temperature of $140K$, which indicates the strong presence of frustration. Nuclear magnetic resonance experiment shows a series of distinct magnetic phases with the increase of external magnetic field [97–99]

Kapellasite : The mineral Kapellasite($ZnCu_3(OH)_6Cl_2$) is a polymorph of Herbertsmithite that means they have the same chemical formula but different crystallographic structures [100, 101]. This material has a structurally perfect kagome structure [102] but suffers from a large amount of disorder. It turns out that $\sim 27\%$ of Zn^{+2} lies in the kagome plane and $\sim 12\%$ of Cu^{+2} occupies the Zn sites [101]. Above all, there exists third neighbor exchange interaction, which is as strong as the first neighbor coupling [103]. No spin freezing is found down to 20 mk, so it remains a potential candidate for quantum spin liquid [103]

1.7 Overview of the thesis

In this thesis, we extensively study the effect of DM interaction on the ground state of kagome Heisenberg antiferromagnet. We use the Schwinger boson mean-field theory and exact diagonalization to study the said problem. We also investigate the possible regular magnetic order in $p6, p3, p3m1$, and $p31m$ wallpaper group, which includes the kagome and triangular geometry. We use a simple group theoretical approach to obtain the possible regular magnetic order for each of the wallpaper groups. In the following, we briefly describe the outline of the thesis.

- In **Chapter-1**, we introduce the motivation and underlying basic concepts of quantum spin liquids. Particularly, we focus on the key features of quantum spin liquids, which makes the underlying physics of the quantum spin system fascinating. We discuss factors like frustration, low dimensionality, and quantum fluctuation, which promote this unconventional ground state. We also briefly introduce the Heisenberg model and the anisotropies, which can spoil the spin-liquid phase and establish magnetic long-range order. In this context, the impact of the Dzyaloshinskii-Moriya interaction on the ground state is the main focus of the present thesis. We present a brief survey of literature about the work done on this topic so far.

- In **Chapter-2**, we introduce the basics of Schwinger boson formalism and why we use this framework. We discuss the gauge redundancy associated with the framework. Now, to construct the mean-field theory, we define bond operators accordingly. For this mean-field treatment, the choice of the mean-field Anstze comes from the group-theoretical analysis, known as the projective symmetry group(PSG) analysis. We briefly introduce the PSG analysis and all the possible *Ansätze* for $p6m$ wallpaper group. In the discussion, we include all the symmetric *Ansätze*, which do not break any lattice symmetry or spin rotation symmetry as well as the chiral *Ansätze*, which breaks the time-reversal symmetry (and also minimal lattice symmetry). These *Ansätze* will serve as the trial ground state in the SBMFT calculation, as discussed later.

- In **Chapter-3**, we study the ground-state phase diagram of the Heisenberg model with added Dzyaloshinskii-Moriya interaction, using the Schwinger boson mean-field theory framework. Following the experimental result of Herbertsmithite, we consider the DM interaction as a staggered one, which only has an out-of-plane component. In our mean-field treatment, we consider the

chiral *Ansätze* as well as the symmetric *Ansätze* to calculate the ground-state phase diagram. We also present the details of our constrained optimization algorithm to calculate the mean-field parameters. We draw the phase diagram in the space of parameters S(spin) and θ where $\theta = D/J$, D be the strength of DM interaction. We calculated the properties associated with each of the phases present in the phase diagram and interpreted our results with the experimental result of Herbertsmithite.

- In **Chapter-4**, we study a family of spin configurations, termed as regular magnetic order(RMO), specifically in kagome and triangular lattices. These special spin configurations respect all the symmetries of the given lattice modulo global spin transformation. We calculate the RMOs for the wallpaper group $p6, p3, p3m1$, and $p31m$, which includes kagome and triangular lattice. Here, we present the definition of RMOs and the notations needed for the group theoretical approach. We present the algebraic structure of each of the group and explain how to construct the RMOs. Then, we list all the possible RMOs in triangular and kagome lattice for each of the groups.

- In **Chapter-5**, we study the effect of both the in-plane(D_p) and out-of-plane(D_z) component of DMI on the ground state of kagome Heisenberg antiferromagnet using SBMFT framework. To construct the mean-field theory, we first looked at the possible classical ground state of the model and considered the mean-field *Ansatz*, which mimics the classical ground state in the large S limit. Since the experimental results predict that the ground state of vesignieite possesses $Q = 0$ magnetic order, we mainly focus on the ground state with Q = 0 magnetic order. We present the ground-state phase diagram in the parameter space of D_p and D_z for different values of spin$s$. We have calculated properties associated with each of the phases present in the phase diagram.

- In **Chapter-6**, we study the effect of both the in-plane(D_p) and out-of-plane(D_z) component of DMI on the ground state of kagome Heisenberg antiferromagnet, numerically using exact diagonalization and compared the results from SBMFT as well as the classical case. We briefly demonstrate the details of the matrix-vector product and Arnoldis method. We calculate various physical quantities to investigate the zero-temperature magnetic structure up to a system size $N = 30$ for different shapes and extrapolated to obtain the result in the thermodynamic limit. We calculate the ground-state phase diagram for

the above model and properties associated with each of the phases. We have interpreted the experimental result of vesignieite.

- In **Chapter-7**, we conclude with a summary of the essential outcomes of the thesis. We also describe the possible extensions of our work.

Chapter 2

Schwinger Boson Framework

A general framework to study the spin-liquid states of quantum magnets is the application of effective theories where the building blocks are quasi-particles associated with fractional quantum numbers. In that case, the description of spin-liquid states involves deconfined spinons, whereas the long-range order implies glued spinons. There are two distinct approaches, one with chargeless fermions and the other with Schwinger bosons.

In the first approach, the spin is represented by spin-half charge-neutral fermions with a constraint on the number of fermions per site, and then a mean-field theory is constructed. This mean-field treatment can be viewed as a variational calculation where the spin-wave function can be obtained after the projection to remove the empty or doubly occupied sites. Wen came up with the idea of classifying the spin-liquid states based on the concept of the projective symmetry group(PSG) [5].

Another way to describe the spin liquid state is to use the Schwinger boson formalism, where the spin at each site is represented by bosons. One of the advantages of Schwinger boson formalism is that it enables us to describe a disordered state as well as a magnetically ordered state. Magnetic long-range order is induced by boson condensation, and the spin liquid states will have gapped bosonic spinons. The idea of classifying the spin liquid state using PSG analysis was introduced by Wen [5] for the fermionic case was extended by Wang and Vishwanath in case of bosonic spinons [61]. In these two works, the definition of the spin-liquid states(strictly symmetric spin liquids) was restricted to the spins systems that do not break any symmetries like lattice symmetries, spin rotation symmetry, and time-reversal symmetry, hence we miss out the whole family of chiral spin liquids. Later, L Messio et al. [104] extended their work for time-reversal symmetry breaking mean-field *Ansätze* on kagome and triangular lattice.

Within the SBMFT, Messio et al. argued that the ground state kagome Heisenberg antiferromagnet in the absence of DMI is possibly a chiral topological spin liquid [72]. It breaks the time-reversal symmetry and is gapped. So, in this chapter, we briefly describe the Schwinger boson formalism and how to construct the chiral *Ansätze* for kagome lattice.

2.1 Schwinger boson mean-field theory

SBMFT provides an approximate way to treat the problem where the approximate ground state is supposed to capture the basic features of the ground state, which are not known a-priori. In this thesis, we mainly concentrate on the Heisenberg model. Let, N is the total number of sites, and S be the length of each spin. The Hamiltonian is invariant under a list of symmetries, e.g., lattice symmetries, spin rotation symmetry, time reversal, etc. that form a group, the symmetry group.

2.1.1 Schwinger boson representation of spin

In Schwinger Boson formalism, the spin operators are mapped into two 'flavors' Schwinger bosons via following relation [91]

$$S_i^\alpha = \frac{1}{2}\begin{pmatrix} a_i^\dagger & b_i^\dagger \end{pmatrix} \sigma^\alpha \begin{pmatrix} a_i \\ b_i \end{pmatrix} \tag{2.1}$$

where i is the site index and $\alpha = x, y, z$. σ^α are the Pauli matrices. The operator a and b follows the usual bosonic commutation relation

$$[a_i, a_j^\dagger] = [b_i, b_j^\dagger] = \delta_{ij}$$

The relation in Eqs.(2.1) ensures that the commutation relation $[S_i^\alpha, S_i^\beta] = i\epsilon^{\alpha\beta\delta} S_i^\delta$ is preserved. The total spin satisfies the relation $\hat{S}_i^2 = \frac{\hat{n}_i}{2}(\frac{\hat{n}_i}{2} + 1)$ where $\hat{n}_i = a_i^\dagger a_i + b_i^\dagger b_i$ is the number operator, gives the total number of bosons at each site i. This mapping has immediate consequences. First, the Hilbert space is enlarged, which may result in unphysical states. Second, to restore the physical Hilbert space, one must introduce the single occupancy constraint for the spin-1/2 case. For a faithful representation of the Hilbert space, the single-occupancy constraint is written as

$$a_i^\dagger a_i + b_i^\dagger b_i = 2S \quad \forall\ i \tag{2.2}$$

The above constraint is implemented by using the Lagrange multiplier, which can be thought of as a scalar potential.

Above all, there is an emergent, local $U(1)$ gauge symmetry $a_i \to e^{i\phi(i)}a_i$ and $b_i \to e^{i\phi(i)}b_i$ where $\phi \in [0, 2\pi]$ which leaves any physical observable invariant. Therefore the description of spins via slave particle necessarily has the bosons are coupled to the gauge field. This will result in two drastically different types of phases. First, the gauge field may be confined in that case; the quasi-particle operators do not represent the particle that can move freely across the lattice. So the enlarged Hilbert space is not a good approach. On the other hand, if the gauge field is deconfining, then the low energy excitations are not spins, but some emergent particles are called ' spinons.' These spinons are deconfined and associated with the fractional quantum number. For example, in the case of the Heisenberg model, the excitations for magnetically ordered states involves a spin-flip. This results in a change of spin quantum number by $1\hbar$, whereas the spinon excitations can carry fractional spin quantum number $\hbar/2$.

2.1.2 Definition of bond operators

In standard mean-field treatment, the mean-field parameters are often used as order parameters such as magnetization. The mean field Hamiltonian breaks few symmetries of the original Hamiltonian. In this mean-field treatment, we do not want to break any symmetries to describe the quantum spin liquids. Thus we want to rewrite the Hamiltonian in terms of quadratic boson operators with global spin rotations. Normally SU(2) symmetric Hamiltonian can be decoupled in terms of SU(2) invariant bond operator, given by

$$\hat{A}_{ij} = \frac{1}{2}\epsilon_{\alpha\beta}c_{i\alpha}c_{j\beta} \quad \text{and} \quad \hat{B}_{ij} = \frac{1}{2}c^{\dagger}_{i\alpha}c_{j\alpha} \tag{2.3}$$

The indices of c, α and β can take values 1 and 2, indicate the type of boson a and b respectively. i and j are the lattice sites. These bond operators satisfies the following equations

$$: \hat{B}^{\dagger}_{ij}\hat{B}_{ij} : + \hat{A}^{\dagger}_{ij}\hat{A}_{ij} = \frac{1}{4}\hat{n}_i(\hat{n}_j - \delta_{ij}) \tag{2.4}$$

where :: means the normal ordering of the operators.

The Heisenberg Hamiltonian can be decoupled in terms of these bond operators

in the following way

$$\begin{aligned} \hat{S}_i \cdot \hat{S}_j &= :\hat{B}^\dagger_{ij}\hat{B}_{ij}: -\hat{A}^\dagger_{ij}\hat{A}_{ij} && (2.5)\\ &= 2:\hat{B}^\dagger_{ij}\hat{B}_{ij}: -S^2 && (2.6)\\ &= S^2 - 2\hat{A}^\dagger_{ij}\hat{A}_{ij} && (2.7) \end{aligned}$$

The first equation is valid for any boson number, but the last two are valid when the occupation constraint is obeyed strictly. The bond operator $\hat{A}^\dagger_{ij}$ creates singlet at the bond ij whereas $\hat{B}^\dagger_{ij}$ is responsible for coherent hopping of the Schwinger bosons from the site i to site j.

2.1.3 Mean-field approximation

Now we make two approximations to make the resulting Hamiltonian solvable. Implementation of occupation constraint strictly implies solving the problem exactly, which is a difficult problem to solve. So first, we relax the constraint and implement it on the average sense, that is

$$\langle \hat{n}_i \rangle = \kappa \tag{2.8}$$

Where $\langle\cdot\rangle$ implies the expectation value over the mean-field states and the average boson density κ can take any value, not necessarily be an integer. This continuous parameter κ can be varied with two extreme limit $\kappa \to \infty$ (classical limit) and $\kappa \to 0$ (extreme quantum limit). The constraint can be implemented by introducing a Lagrange multiplier λ_i at each site (λ can be thought as chemical potential)

Second, we use the standard mean-field decoupling scheme, and the fluctuation of the bond operators are neglected

$$\begin{aligned} \hat{A}^\dagger_{ij}\hat{A}_{ij} &= \langle\hat{A}^\dagger_{ij}\rangle\hat{A}_{ij} + \hat{A}^\dagger_{ij}\langle\hat{A}_{ij}\rangle - |\langle\hat{A}_{ij}\rangle|^2 && (2.9)\\ \hat{B}^\dagger_{ij}\hat{B}_{ij} &= \langle\hat{B}^\dagger_{ij}\rangle\hat{B}_{ij} + \hat{B}^\dagger_{ij}\langle\hat{B}_{ij}\rangle - |\langle\hat{B}_{ij}\rangle|^2 && (2.10) \end{aligned}$$

We replace the $\langle\hat{A}_{ij}\rangle$ and $\langle\hat{B}_{ij}\rangle$ by complex number $\mathcal{A}_{ij}$ and $\mathcal{B}_{ij}$ where $\mathcal{A}_{ij} = -\mathcal{A}_{ji}$ and $\mathcal{B}_{ij} = \mathcal{B}^*_{ji}$. The set of mean field parameters $\{\mathcal{A}_{ij}, \mathcal{B}_{ij}\}$ appearing in the mean field Hamiltonian are called mean field *Ansatz*. For transitionally invariant states, the chemical potential $\mu_i = \mu$ is taken to be uniform and the bond parameters have same magnitude on symmetry related bonds.

This mean-field decoupling can be identified as the first term of a large N expansion of Sp(N) theory [105]. The mean-field Hamiltonian can be regarded as

a saddle-point solution of the Sp(N) action after Hubbard-Stratonovich transformation [106]. This mean-field Hamiltonian is quadratic in bosonic operator can be diagonalized. The mean-field Hamiltonian, after Fourier transformation can be written in the following form

$$\hat{H}_{\mathrm{MF}} = \sum_{q} \phi_q^\dagger M_q \phi_q + \epsilon_0 \tag{2.11}$$

where M_q is a complex matrix with dimension $2m \times 2m$, ϵ_0 is a constant which depends on the mean field parameters $\mathcal{A}_{ij}, \mathcal{B}_{ij}$ and Lagrange multiplier λ and $\phi_q^\dagger = \left[a_{1q}^\dagger, ...a_{mq}^\dagger, b_{1,-q}, ...b_{m,-q}\right]$ with m be the number sites within the unit cell. The mean field parameters can be obtained from the following self consistency equations

$$\mathcal{A}_{ij} = \langle \hat{\mathcal{A}}_{ij} \rangle \quad \& \quad \mathcal{B}_{ij} = \langle \hat{\mathcal{B}}_{ij} \rangle \tag{2.12}$$

which are equivalent to extremization of free energy F_{MF}

$$\frac{\partial F_{\mathrm{MF}}}{\partial \mathcal{A}_{ij}} = 0 \quad \text{and} \quad \frac{\partial F_{\mathrm{MF}}}{\partial \mathcal{B}_{ij}} = 0 \tag{2.13}$$

And the constraint

$$\langle \hat{n}_i \rangle = \kappa \quad \Leftrightarrow \quad \frac{\partial F_{\mathrm{MF}}}{\partial \lambda_i} = 0 \tag{2.14}$$

These conditions implies that we need to figure out the saddle point of the free energy $F_{\mathrm{MF}}(\mathcal{A}_{ij}, \mathcal{B}_{ij}, \lambda_i)$. Each *Ansatz* describes a particular ground state up to an equivalence relation described in the next section. Next, we focus on the possible mean-field *Ansätze* based on the projective symmetric group(PSG) analysis.

2.2 Search for possible mean-field Ansätze

The number of mean-field parameter increases rapidly with system size even for nearest neighbor coupling only. The presence of the Lagrange multiplier makes it even more difficult as we will be dealing with constraint optimization. G Misguich et al. [107] has calculated the mean-field parameters for square and triangular lattice without applying any symmetry assumption up to a system size $N = 36$. The obtained mean-field solutions turned out to be highly symmetric, but the excited mean-field solution is highly inhomogeneous. Therefore the search for quantum spin liquid ground state is remarkably simplified if we demand that the mean-field *Ansatz* is invariant under some of the symmetries(if not all the symmetries of the original

Hamiltonian). Since this prescription has some gauge redundancy, symmetries can act on the quasi-particle operators projectively, keeping the physical observables invariant. Here we briefly describe how to find all the possible mean-field *Ansätze* for kagome lattice.

2.2.1 Gauge redundancy and Flux

In Schwinger boson representation, there is a U(1) gauge redundancy characterized by an angle $\theta \in [0, 2\pi]$ at each site. Let $\mathcal{G} \simeq U(1)^N$ be the set of gauge transformation, and $\hat{G}$ be the operator that implements the associated gauge transformation. Then

$$b_{r\sigma} \rightarrow e^{i\theta(r)} b_{r\sigma} = G^\dagger b_{r\sigma} G \tag{2.15}$$

$$b^\dagger_{r\sigma} \rightarrow e^{-i\theta(r)} b^\dagger_{r\sigma} = G b^\dagger_{r\sigma} G^\dagger \tag{2.16}$$

where G is given by

$$G = \exp\big(i \sum_r b^\dagger_{r\sigma} b_{r\sigma} \theta(r)\big) \tag{2.17}$$

Equivalent action of G on the mean field *Ansatz* is given by

$$\mathcal{A}_{ij} \rightarrow \mathcal{A}_{ij} e^{i(\theta(i)+\theta(j))} \tag{2.18}$$

$$\mathcal{B}_{ij} \rightarrow \mathcal{B}_{ij} e^{-i(\theta(i)-\theta(j))} \tag{2.19}$$

So that the mean-field Hamiltonian H_{MF} is unchanged by the action of G. The physical observables are gauge independent, but the mean-field parameters $\mathcal{A}_{ij}$ and $\mathcal{B}_{ij}$ are not. Now, when we choose an *Ansatz*, eventually, the gauge symmetry is broken. If two mean-field Hamiltonian leads to the same physical properties, then the mean-field *Ansatz* must be linked by a gauge transformation. There are two physical observables that are directly connected to the mean-field *Ansatz*. Mean-field parameter modulii which are related to the scalar product of two spins and are thus one of the physical observable [104]. Another one is the flux. The flux is defined by the arguments of the Wilson loop operators such as $\langle \hat{A}_{ij} \mathcal{A}^\dagger_{jk} \hat{A}_{kl} \mathcal{A}^\dagger_{li} \rangle$ and $\langle \hat{B}_{ij} \hat{B}_{jk} \hat{B}_{ki} \rangle$. The flux can be used to distinguish different *Ansätze*. The gauge invariance of flux requires two conditions. First, each site index i must appear in an even number of times. Second, the set of operators with site index i can be grouped in pairs such that their products of each pair remain gauge invariant. It is also to be noted that one can mix $\hat{A}_{ij}$ and $\hat{B}_{ij}$ operators while defining the flux such as

$\text{Arg}\langle\hat{A}_{ij}\mathcal{A}^{\dagger}_{jk}\mathcal{B}^{\dagger}_{kl}\hat{A}_{lm}\mathcal{A}^{\dagger}_{mi}\rangle$. In this formalism, averages of products of the operators are replaced by the product of averages of the operator as an approximation. This can be justified in large N limit i.e. $N \to \infty$. For example

$$\langle\hat{B}_{ij}\hat{B}_{jk}....\hat{B}_{li}\rangle \to \mathcal{B}_{ij}\mathcal{B}_{jk}....\mathcal{B}_{li} \tag{2.20}$$

The physical meaning of this flux can be found in Ref [104]. They have shown that in the classical limit, fluxes are related simple geometrical quantities corresponding to the orientation of the spins.

2.2.2 Projective symmetry group

Let χ be the group of lattice symmetries of the original Hamiltonian. If we take any element $X \in \chi$, then

$$X : b_{j\sigma} \to b_{X(j)\sigma} \tag{2.21}$$

And X acts on the *Ansatz* in the following way

$$\mathcal{A}_{jk} \to \mathcal{A}_{X(j)X(k)} \quad \text{and} \quad \mathcal{B}_{jk} \to \mathcal{B}_{X(j)X(k)} \tag{2.22}$$

Now, we will focus on the lattice symmetries. As we discussed earlier, that physical properties are gauge invariant. Similarly, if the mean-field *Ansatz* before and after the action of X will lead to the same physical properties, then they must be related by a gauge transformation. So, we can say that there exists at least one gauge transformation G_X corresponding to X such that $G_X X$ leaves the mean-field *Ansatz* invariant. The set of all transformations of $\mathcal{G} \times \chi$ that leaves the mean-field *Ansatz* invariant is known as the projective symmetry group(PSG) of the *Ansatz*. However, there are some elements of PSG that are purely local transformation and also form a subgroup. This subgroup is known as the invariant gauge group(IGG). This emergent gauge group describes the spin-liquid phase obtained. For each lattice symmetry $X \in \chi$ and $G_X X \in$ PSG, then $G_X X$ must be isomorphic to IGG.

2.2.3 Algebraic projective symmetry group

A mean-field *Ansatz* is characterized by its IGG as well as the PSG, and also from the group structure, we know which symmetries it preserves. Reversely, if we want to figure out all the *Ansätze* by imposing the lattice symmetries, we do the following steps. First, figure out the set, which is known as algebraic PSG [5, 61]. These are the subgroups of $\mathcal{G} \times \chi$ that obeys the algebraic constraints involving the generators

of the group. The second step is to find the all compatible *Ansätze* with the algebraic PSG for a given lattice.

The symmetry group χ is characterised by its generators $x_1, x_2, ...x_p$. A generator x_a has an order $n_a \in \mathbb{N}$ so that $x_a^{n_a}$ becomes identity. For any element $X \in \chi$, there exists a unique ordered product such that

$$X = x_1^{k_1}, x_2^{k_2}, ..., x_p^{k_p} \text{ where } 0 \leq k_a < n_a \text{ (if } n_a \text{ is finite)}, k_a \in \mathbb{Z} \text{ (if not)} \quad (2.23)$$

For any unordered product, the algebraic constraints between the generator can be used to order the product. Each of the constraint between the generators implies that a constraint on the gauge transformation G_{x_a} corresponding to the generator x_a. Basically, the subgroup of $\mathcal{G} \times \chi$ that respects all the algebraic constraints between the generators are the desired algebraic PSG.

To explain this concept, let us consider a simple example where the group χ is generated by two translation T_1 and T_2. Both of these generators has the order $n_1 = n_2 = \infty$. As discussed earlier, $X \in \chi$ can be written as a product of the generator as $X = T_1^{m_1} T_2^{m_2} T_1^{m_3} T_2^{m_4}$..... And we want to write X as the ordered product $X = T_1^{p_1} T_2^{p_2}$. The associated algebraic relation between these generator is given by $T_1 T_2 = T_2 T_1$. Thus we have $p_1 = m_1 + m_3 + ...$ and $p_2 = m_2 + m_4 + ...$ This implies constraint on the gauge transformation G_{T_1} and G_{T_2} associated with the generators T_1 and T_2. Now, if we have an *Ansatz* which is unchanged by G_{T_1} and G_{T_2} . Then their inverse $T_1^{-1} G_{T_1}^{-1}$ and $T_2^{-1} G_{T_2}^{-1}$ will also be an element of PSG. Accordingly, the product $G_{T_1} T_1 G_{T_2} T_2 T_1^{-1} G_{T_1}^{-1} T_2^{-1} G_{T_2}^{-1} \in$ PSG. Thus,

$$\begin{aligned}
G_{T_1} T_1 G_{T_2} T_2 T_1^{-1} G_{T_1}^{-1} T_2^{-1} G_{T_2}^{-1} &\in \text{PSG} \\
G_{T_1} T_1 G_{T_2} (T_1^{-1} T_1) T_2 T_1^{-1} (T_2^{-1} T_2) G_{T_1}^{-1} T_2^{-1} G_{T_2}^{-1} &\in \text{PSG} \\
G_{T_1} (T_1 G_{T_2} T_1^{-1}) T_1 T_2 T_1^{-1} T_2^{-1} (T_2 G_{T_1}^{-1} T_2^{-1}) G_{T_2}^{-1} &\in \text{PSG} \\
G_{T_1} (T_1 G_{T_2} T_1^{-1}) (T_2 G_{T_1}^{-1} T_2^{-1}) G_{T_2}^{-1} &\in \text{PSG}
\end{aligned}$$

This is pure gauge transformation and hence we can write

$$G_{T_1} (T_1 G_{T_2} T_1^{-1}) (T_2 G_{T_1}^{-1} T_2^{-1}) G_{T_2}^{-1} \in \text{IGG} \quad (2.24)$$

If we consider the IGG to be $\mathbb{Z}_2$. Then we can write in term of phases of the gauge transformation

$$\phi_{T_1}(i) + \phi_{T_2}(T_1^{-1} i) - \phi_{T_1}(T_2^{-1} i) - \phi_{T_2}(i) = p\pi \quad (2.25)$$

where p can take values either 0 or 1. Once all the PSG classes are known then the remaining work is to find the compatible *Ansatz* corresponding to each class. To check compatibility, we must have $\mathcal{A}_{ij} = \mathcal{A}_{X(i)X(j)}$. If this is satisfied then the *Ansatz* respects all the lattice symmetries by construction. Finally, for a complete definition of the *Ansatz* it is sufficient to provide the algebraic PSGs and the value of the mean-field parameters.

2.2.4 Chiral spin liquids

The family of co-planar states is obtained from the strictly symmetric(respects all lattice symmetries, spin rotation symmetries, and time-reversal symmetry) *Ansätze*. Hence, we miss out on the chiral spin liquid states. This prompts us to construct the chiral *Ansätze*, which breaks the time-reversal symmetry and some of the lattice symmetries. These chiral *Ansätze* leads to the non-coplanar spin orientation via Bose-condensation. The time-reversal symmetry acts on the mean-field *Ansatz* through complex conjugation of the mean-field parameters [5]. No transition is yet to know where the chiral ordered state is induced from time-reversal symmetric *Ansatz* through the Bose condensation process. These chiral *Ansätze* involves complex-valued fluxes, which evolves continuously with boson density. To obtain the possible chiral spin liquid states, one has to break the time-reversal symmetry at the mean-field level.

In the case of classical magnetic order with $SO(3)$ symmetry, any lattice transformation X from χ can be compensated by global spin rotation. But for $O(3)$ states, an inversion $\mathbf{S}_i \to -\mathbf{S}_i$ is required in addition to that. This led us to define the parity ϵ_X to be $+1$ if no spin inversion is required and -1 otherwise. Similarly, in the case of chiral spin liquids, the parity can be defined from the effect of $X \in \chi$ on the fluxes. If the flux is unchanged under the action of X, then the parity is defined to be $+1$ and -1 otherwise. With this idea, we define the weakly symmetric(WS) *Ansatz* as the *Ansatz*, which respects lattice symmetries up to time-reversal τ and the *Ansatz* which respects the lattice symmetries as well as time-reversal symmetry is termed as strictly symmetric(SS) *Ansatz*.

The construction of weakly symmetric *Ansatz* is based upon the concept of even and odd symmetries. Even and odd symmetries are termed on the basis of parity ϵ_X, as defined above. Let χ_e be the subgroup of χ, which are even. The subgroup χ_e includes at least all the squares of the elements of the group χ as $\epsilon_{X^2} = \epsilon_X^2 = 1$. Once we figure out χ_e, we define chiral algebraic PSGs of χ as the algebraic PSGs of χ_e.

Similarly, we can define χ_o, as the set of transformation which are odd ($\chi_o = \chi - \chi_e$). The group χ_o contains all the transformation which has undetermined parities.

Now, we want to extract the possible weakly symmetric *Ansätze* from the compatible chiral PSGs. To do this, we have to take care of the transformation of χ_o. We have the following constraints. First, The mean-field parameters ($\mathcal{A}$ and $\mathcal{B}$) linked by a transformation of χ_o must have the same magnitude. The second constraint comes from the flux. Flux is a gauge-invariant quantity, but the phases are not. Fluxes are sent to their opposite by the action of the elements of χ_o, much like τ, whereas it is unchanged by the elements of χ_e.

2.3 Chiral algebraic PSGs of lattices with triangular Bravias lattice

Let us consider the model Hamiltonian $\hat{H}$ that respects all the lattice symmetries as shown in Fig. 2.1(a). The wallpaper group is $p6m$ but the actual(spin) lattice can be triangular, kagome, honeycomb etc. Let (x, y) be the co-ordinate of an arbitrary point, then the effect of the generators on the co-ordinate are given by

$$T_1 : (x, y) \rightarrow (x + 1, y) \tag{2.26a}$$
$$T_2 : (x, y) \rightarrow (x, y + 1) \tag{2.26b}$$
$$R_6 : (x, y) \rightarrow (x - y, x) \tag{2.26c}$$
$$\sigma : (x, y) \rightarrow (y, x) \tag{2.26d}$$

The algebraic relation between the elements of χ are given by

$$T_2 T_1 = T_1 T_2 \tag{2.27a}$$
$$T_1 R_6 = R_6 T_2^{-1} \tag{2.27b}$$
$$T_2 R_6 = R_6 T_1 T_2 \tag{2.27c}$$
$$T_1 \sigma = \sigma T_2 \tag{2.27d}$$
$$\sigma T_1 = T_2 \sigma \tag{2.27e}$$
$$R_6^{-1} = [R_6]^5 \tag{2.27f}$$
$$\sigma^{-1} = \sigma \tag{2.27g}$$
$$R_6 \sigma = \sigma [R_6]^5 \tag{2.27h}$$

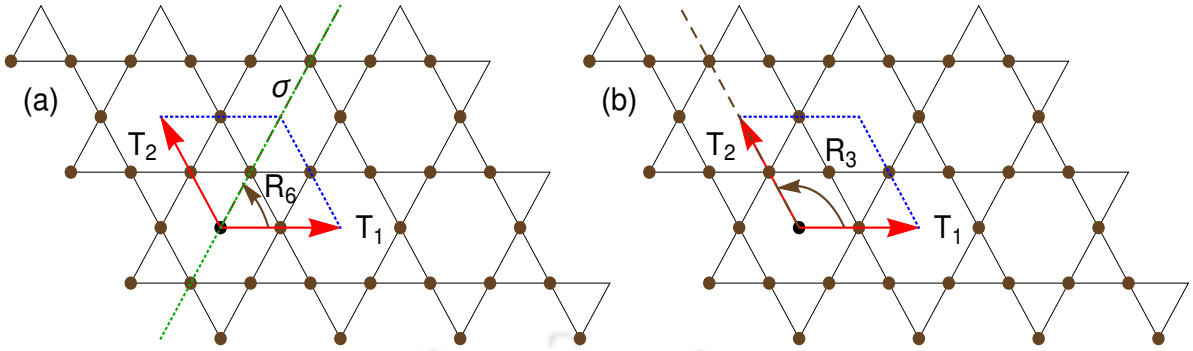

Figure 2.1: (a) Generators of the group χ and (b) generators of the group χ_e where T_i is the translation, σ is the reflection and R_i is the rotation of the order i.

Now, we have to determine the χ_e and χ_o. By construction χ_e includes the transformation which are even. So, it includes T_1^2, T_2^2 and $R_6^2 = R_3$. However, there exist more even transformation in χ_e. From Eq. 2.27(c) we get $\epsilon_{T_2}\epsilon_{R_6} = \epsilon_{R_6}\epsilon_{T_1}\epsilon_{T_2}$, which implies $\epsilon_{T_1} = +1$. Similarly, from Eq. 2.27(b) we get $\epsilon_{T_2} = +1$. So, the elements of χ_e are given by T_1, T_2 and R_3. The algebraic relations between the generators of the group χ_e are given by the following equations

$$T_2T_1 = T_1T_2 \tag{2.28a}$$
$$T_1R_3 = R_3T_2^{-1} \tag{2.28b}$$
$$T_2R_3 = R_3T_1T_2 \tag{2.28c}$$
$$R_3^3 = I \tag{2.28d}$$

Each of these relations enforces constraint on the gauge transformations associated with each of the generators of the group. Let, i be the site index, then Eqn. 2.28 implies

$$\phi_{T_2}(T_1^{-1}i) - \phi_{T_2}(i) = p_1\pi \tag{2.29a}$$
$$\phi_{R_3}(i) + \phi_{R_3}(R_3i) + \phi_{R_3}(R_3^2i) = p_2\pi \tag{2.29b}$$
$$\phi_{R_3}(i) - \phi_{R_3}(T_2^{-1}i) - \phi_{T_2}(i) = p_3\pi \tag{2.29c}$$
$$\phi_{T_2}(T_1^{-1}i) + \phi_{R_3}(T_2^{-1}T_1^{-1}i) + \phi_{T_2}(T_2R_3^2i) - \phi_{R_3}(i) = p_4\pi \tag{2.29d}$$

Here, the parameter p_1, p_2, p_3 and p_4 can take values either 0 or 1. If $[x]$ be the

integer part of x, then we define $x^* = x - [x]$. Solving Eqn. 2.29 we get

$$\begin{aligned} \phi_{T_1}(x,y) &= 0 && \text{(2.30a)} \\ \phi_{T_2}(x,y) &= p_1\pi x && \text{(2.30b)} \\ \phi_{R_3}(x,y) &= p_1\pi x\Big[y - \frac{x+1}{2}\Big] + g_{R_3}(x^*,y^*) && \text{(2.30c)} \end{aligned}$$

where the last term in Eqn. 2.30(c) involves the spin lattice, given by

$$g_{R_3}(x^*,y^*) = g_{R_3}((-y)^*,(x-y)^*) + g_{R_3}((y-x)^*,(-x)^*) = p_2\pi \tag{2.31}$$

2.3.1 Weakly summetric *Ansätze* on kagome lattice

In kagome lattice, the number of sites within the unit cell is three. Let us fix the origin at the center of the hexagon, then the co-ordinates of the three sites will be at $(\frac{1}{2},0),(0,\frac{1}{2})$ and $(\frac{1}{2},\frac{1}{2})$. For simplification, we apply the following gauge transformation to the Eqn. 2.30

$$G_1 : (x,y) \to -p_1\pi y x^*$$

We get the following equations

$$\begin{aligned} \phi_{T_1}(x,y) &= 0 && \text{(2.32a)} \\ \phi_{T_2}(x,y) &= p_1\pi[x] && \text{(2.32b)} \\ \phi_{R_3}(x,y) &= p_1\pi[x]\Big[[y] - \frac{[x]+1}{2} - [y^*-x^*]\Big] + g_{R_3}(x^*,y^*) && \text{(2.32c)} \end{aligned}$$

As shown in the Ref. [104], using proper gauge transformation we can set $g_{R_3} = 0$. Finally we are left with two sets of algbraic PSGs which are characterized by $p_1 = 0, 1$ as shown in Eqn. 2.32 with $g_{R_3} = 0$. Now, we can find all the compatible *Ansätze* for corresponding to these algebraic PSGs. We have focused on the nearest neighbor interaction in this thesis. So, we will only look for nearest neighbor *Ansätze* only but it can be extended for further neighbor also. To generate the whole lattice, two bonds are required which are denoted by red and blue color as shown in the Fig. 2.2. The *Ansatz* for the remaining bonds can be obtained using the PSG. To begin with, for chiral *Ansätze* the mean field parameters are complex. Now, using gauge freedom, we can choose the $\mathcal{A}_{ij}$ to be real for the reference blue bond. The mean men-field parameters for the chiral *Ansatz* are as shown in the Fig. 2.2. The general unit cell becomes twice large than the usual unit cell of kagome lattice is

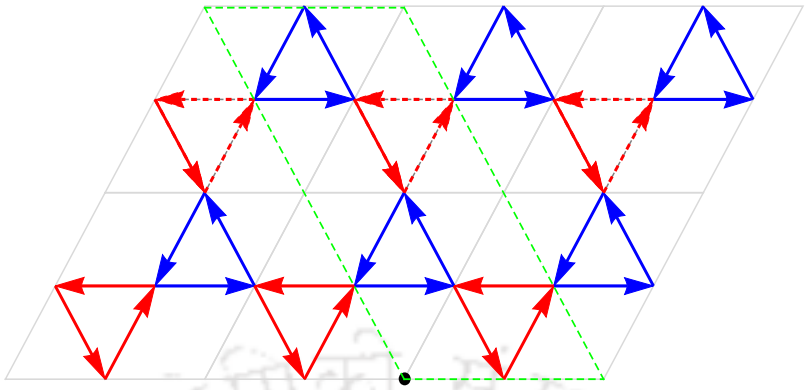

Figure 2.2: Description of the *Ansätze* that respects χ_e symmetry. In general, mean-field parameters $\mathcal{A}_{ij}$ and $\mathcal{B}_{ij}$ are complex. On the blue bonds the mean-field parameters $\mathcal{A}$ and $\mathcal{B}$ has modulus A_1 and B_1 with the phase zero and ϕ_{B_1} respectively. Whereas, on the red bonds $\mathcal{A}$ and $\mathcal{B}$ has modulus A_1' and B_1' with the phase $\phi_{A_1'}$ and$\phi_{B_1'}$ respectively. An extra phase $p_1\pi$ is to be added on the dashed bonds for $\mathcal{A}_{ij}$ and $\mathcal{B}_{ij}$.

due to the nonzero value of the parameter p_1.

Now, we can simplify things. So, we have got the mean field *Ansätze* with the parameter p_1, moduli A_1, A_1', B_1 and B_1' and the arguments ϕ_{A_1}, ϕ_{B_1} and $\phi_{B_1'}$.

Now, we will consider the symmetries of the group χ_o. R_6 rotations puts the following constraints on the moduli of the mean-field parameters $A_1 = A_1'$ and $B_1 = B_1'$. The effect of R_6 and σ on the flux gives constraint on the phases of the mean-field parameters. If we assume that both the mean field parameter are nonzero then, the effect of R_6 and σ on the flux through an elementary hexagon $\mathrm{Arg}(\mathcal{A}_{ij}\mathcal{A}^*_{jk}\mathcal{A}_{kl}\mathcal{A}^*_{lm}\mathcal{A}_{mn}\mathcal{A}^*_{ni})$ and through an elementary triangle $\mathrm{Arg}(\mathcal{A}_{ij}\mathcal{B}^*_{jk}\mathcal{A}_{ki})$ gives us the following constraints

$$(\epsilon_{R_6} + \epsilon_\sigma)\phi_{B_1} = 0 \tag{2.33a}$$

$$\epsilon_{R_6}\phi_{B_1} = \phi_{B_1'} \tag{2.33b}$$

$$(\epsilon_{R_6} + 1)\phi_{A_1'} = 0 \tag{2.33c}$$

$$(\epsilon_\sigma + 1)\phi_{A_1'} = 0 \tag{2.33d}$$

Solving these, we get the following possibilities

- $(\epsilon_{R_6}, \epsilon_\sigma) = (1, 1) : \phi_{B_1} = \phi_{B_1'} = 0$ or π and $\phi_{A_1'} = 0$ or π
- $(\epsilon_{R_6}, \epsilon_\sigma) = (1, -1) : \phi_{B_1} = \phi_{B_1'}$ and $\phi_{A_1'} = 0$ or π
- $(\epsilon_{R_6}, \epsilon_\sigma) = (-1, 1) : \phi_{B_1} = -\phi_{B_1'}$ and $\phi_{A_1'} = 0$ or π

- $(\epsilon_{R_6}, \epsilon_\sigma) = (-1, -1) : \phi_{B_1} = \phi_{B_1'}$ and $\phi_{B_1'} = 0$ or π

Finally, we are left with twenty different weakly symmetric mean-field *Ansätze* for kagome lattice as shown in the table below.

No.	p_1	$\phi_{A_1'}$	ϕ_{B_1}	$\phi_{B_1'}$
1	p_1	0	$\phi_{B_1'}$	0
2				π
3				Any
4			-$\phi_{B_1'}$	Any
5		π	$\phi_{B_1'}$	0
6				π
7				Any
8			-$\phi_{B_1'}$	Any
9		Any	$\phi_{B_1'}$	0
10				π

Table 2.1: List of weakly symmetric *Ansätze* for kagome lattice. Depending upon the value of p_1(can be either 1 or 0), we get total twenty different *Ansätze*.

2.4 Diagonalization of mean field Hamiltonian

In this section, we will briefly describe how to get the eigenmodes of the mean-field Hamiltonian given by Eqn. 2.11. Now construct new bosonic operator $\tilde{\phi}$, which is the linear combination of elements of ϕ to obtain the new diagonal matrix $\tilde{M}$. The Hamiltonian must be a positive definite matrix, to posses the ground state. In other words, the spectrum must be bounded from the below. So, the diagonal elements must be positive or zero. This can achieved through standard Bogolioubov transformation [11]. For periodic *Ansätze*, a Fourier transform led to the block-diagonal form of the M matrix, which has the dimension $2m \times 2m$ where m is the number of sites within the unit cell. We must mention that for 2×2 matrix, the diagonalization can be performed analytically but, if $m > 1$, then numerical calculations are required.

Consider the most general case, where the dimension of $\tilde{M}$ matrix is arbitrary [108]. Let us define the transformation matrix $\phi = P\tilde{\phi}$ where P has the dimension $2N \times 2N$, is known as the transformation matrix. Now we can put several condition on P. The most obvious one is that $\tilde{M}$ must be a diagonal matrix. Secondly, the first N element of the $\tilde{\phi}$ must be annihilation operators and the rest

will be creation operators and we have the following equations

$$P^{\dagger}MP = \tilde{M} \quad \text{and} \quad P^{\dagger}JP = J \tag{2.34}$$

where J is a diagonal matrix with dimension $2N \times 2N$. First N elements of the diagonal matrix is -1 and the last N diagonal elements are $+1$. This is often termed as paradiagonalization. We follow the following steps as prescribed in Ref [108]

- Matrix M must be positive definite which guarantees the unique ground state. Now if the eigenvalues comes out to be zero then the ground state exists but it is not unique.
- Perform the Cholesky decomposition of M and find the complex upper triangular square matrix K such that $M = K^{\dagger}K$.
- Look for an unitary matrix U, so that $L = U^{\dagger}KJK^{\dagger}U$ becomes diagonal. First N element of L will become positive and rest of them will be negative.
- The solution is given by $\tilde{M} = JL$ and $P = K^{-1}U\tilde{M}^{1/2}$

The ground state energy is given by

$$E_0 = \frac{1}{2}\sum_{i=1}^{N}\omega_i + \epsilon_0 \tag{2.35}$$

The elementary excitations are spinons with energies $\omega_1, \omega_2, \omega_3 \ldots\ldots\ldots \omega_N$.

Chapter 3

Role of Out-of-plane Component of DMI on the Ground State of KHAF

3.1 Introduction

Quantum spin liquids (QSL) [2] are the exotic states of matter without any broken symmetries even at $T = 0$, the states of matter which cannot be explained in the paradigm of Landaus's symmetry breaking theory [1, 1, 3, 4, 109]. The most promising candidate to possess spin liquid ground states is spin-1/2 kagome Heisenberg antiferromagnet (KHAF) due to its low-dimension, small-spin, and strong geometrical frustration [48, 55, 65, 110]. One of the challenges of the search for QSL among materials is the presence of anisotropies like the Dzyaloshinskii-Moriya (DM) interaction. Such interactions reduce symmetry and quantum fluctuations and lead to magnetic ordering. The Dzyaloshinskii-Moriya interaction [6, 7], arises when there is a lack of inversion symmetry in the lattice.

The mineral, Herbertsmithite, is an example where the spin-1/2 copper atoms form a kagome lattice. No magnetic order has been found down to 50 mK, with the exchange coupling being 170K [47, 84]. To explain the spin susceptibility enhancement of Herbertsmithite [111]at low temperature, a small value of Dzyaloshinskii-Moriya interaction has to be considered. The presence of DM interaction is also confirmed by paramagnetic resonance [112], where the DM interaction of strength of $0.08J$ is needed to explain the line width. Small values of DM interaction can produce long-range order in a spin system, especially in spin liquid ground states. So it was not clear why spins do not freeze in Herbertsmithite at low temperatures.

The effect of DM interaction on the kagome Heisenberg antiferromagnet has been studied by several groups [54, 74, 76, 113–115]. From exact diagonalization(ED)

Cepas et. al [74], they found that there is a critical point at $D_c = 0.1J$, where there is moment free phase at the lower side and Neel phase on the other. This result is consistent with experiments since the estimated DM interaction strength is about $0.08J$ in Herbertsmithite. Sachdev has proposed a quantum critical theory [75] about the critical point suggested by Cepas. Messio et al., [76] using Schwinger-boson mean-field theory (SBMFT), have calculated the phase diagram and showed that the results are qualitatively similar to the ED studies in small boson density region.

The purpose of this chapter is two-fold. In 2013, Messio et al. [72] showed that in the SBMFT framework, that the ground state of the Kagome Heisenberg antiferromagnet is chiral $\mathbb{Z}_2$ spin liquid. In their study of DM interaction, they had not considered the time-reversal breaking *Ansätze* [76]. This would change the phase diagram for a small strength of DM interaction. Secondly, they have considered only bond creation mean-field $\mathcal{A}$. However, the inclusion of a second boson hopping mean-field, $\mathcal{B}$ field, improves the quantitative agreement of the bandwidth in the excitation spectrum of the Heisenberg model on triangular lattice [116]. Flint and Coleman showed that these two fields together give a better description of these frustrated systems [106]. Thus, we, in this work, have considered chiral spin liquid *Ansatz* and also included the hopping mean-field.

The outline of the chapter is as follows. In Sec.II, we present the model and the brief of the Schwinger boson mean-field theory with two bond operators. In Sec.III, we have described the detailed algorithm for the numerical search of the optimum points. In the Sec.IV, we present the zero-temperature ground state phase diagram with properties associated with it and the effect of DM interaction on the QSL ground state. We have discussed the connection between the prediction of our model with experimental results. We have also calculated the dynamical structure factor of the different *Ansätze* in relevant phases in the Sec.V.

3.2 Model and formalism

The Hamiltonian for the nearest neighbor Heisenberg model with Dzyaloshinskii-Moriya interaction is given by

$$H = \sum_{\langle ij \rangle} \left[J\vec{S}_i \cdot \vec{S}_j + \vec{D}_{ij} \cdot (\vec{S}_i \times \vec{S}_j) \right] \tag{3.1}$$

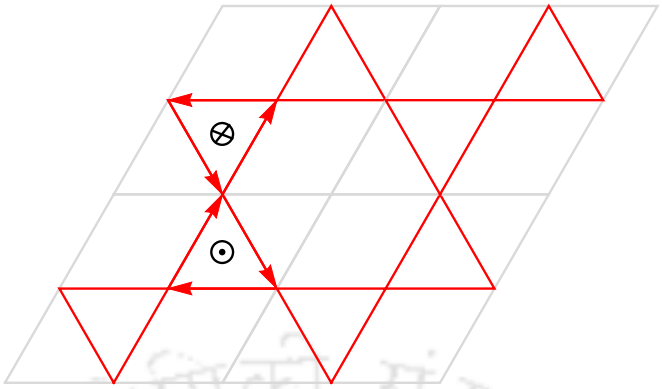

Figure 3.1: Bond directions for Dzyaloshinskii-Moriya interaction where the DM vector $\vec{D}$ (shown at the center of triangle) is staggered between up to down triangles.

with $\langle ij \rangle$ stands for a pair of neighbouring sites i and j. The pairs are directed due to the DM interaction and the directions are shown in Fig. 3.1. The Heisenberg coupling is assumed to be antiferromagnetic ($J > 0$). The DM vector is taken to be perpendicular to the plane of the lattice as shown in in Fig. 3.1 with constant magnitude D. The planar component of DM vector can be taken care of by rotating the spins appropriately as long as the planar component is small [74]. Introduction of the DM interaction reduces the global symmetry of the Heisenberg hamiltonian from $SU(2)$ to $U(1)$. However, the wallpaper group remains $P6m$.

It is expected that the DM interaction will induce long range order and hence using SBMFT approach is appropriate since it elegantly treats both ordered and spin liquid phases. In Schwinger boson representation the spin operators are mapped to the bosonic operators as follows,

$$S_i^\alpha = \frac{1}{2}\begin{pmatrix} a_i^\dagger & b_i^\dagger \end{pmatrix} \sigma^\alpha \begin{pmatrix} a_i \\ b_i \end{pmatrix} \tag{3.2}$$

where i is the site index and $\alpha = x, y, z$. σ^α are the Pauli matrices. This mapping is faithful only when the number of bosons is equal to $2S$, that is, $(a_i^\dagger a_i + b_i^\dagger b_i) = 2S$. This constraint, in principle, must be satisfied at each site. However, it is interesting to study the properties of the bosonic system by implementing this constraint on an average basis by treating $2S$ as a parameter. Let $\kappa = \langle n_i/2 \rangle$ be the boson density per flavor. The spin-wave function is then obtained by applying an appropriate projection operator.

We define bond creation operators as $\hat{A}_{ij}^\dagger = \frac{1}{2}(e^{i\theta_{ij}} a_i^\dagger b_j^\dagger - e^{-i\theta_{ij}} b_i^\dagger a_j^\dagger)$ and $\hat{B}_{ij}^\dagger = \frac{1}{2}(a_i a_j^\dagger + b_i b_j^\dagger)$ with $\theta_{ij} = D_{ij}/J$. The operator $A_{ij}^\dagger$ creates a mixture of a singlet

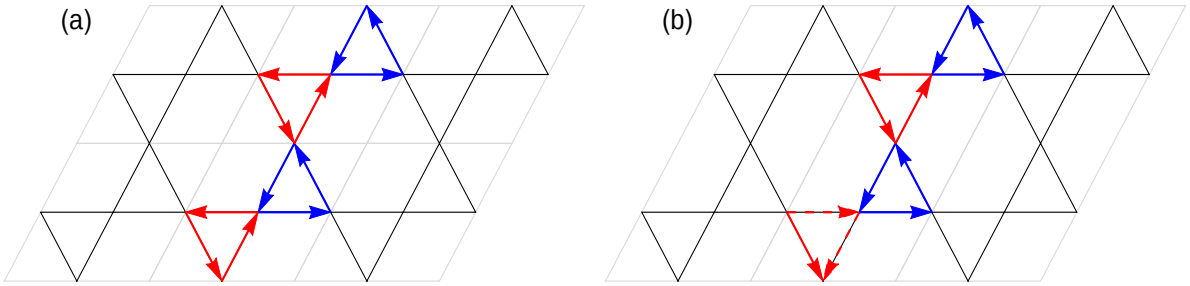

Figure 3.2: Grey lines mark the three-site unit cell for the $(0,0)$,$(\pi,0)$ *Ansatz* in the Fig. (a) and six-site unit cell for *cuboc1 Ansatz* in Fig. (b). The mean fields are defined as $\langle \mathcal{A}_{ij} \rangle = |\mathcal{A}|e^{i\phi_{\mathcal{A}}}$ and $\langle \mathcal{B}_{ij} \rangle = |\mathcal{B}|e^{i\phi_{\mathcal{B}}}$. In the Fig. (a), for $(0,0)$ *Ansatz* $\phi_{\mathcal{A}} = 0$ for both the red (down) triangles and blue (up) triangles. For $(\pi,0)$ *Ansatz* $\phi_{\mathcal{A}} = 0$ for red triangles and $\phi_{\mathcal{A}} = \pi$ for blue triangles. For both the *Ansätze* $\phi_{\mathcal{B}} = \pi$ for all bonds. In the Fig. (b), for *cuboc*1 *Ansatz*, $(\phi_A, \phi_B) = (\phi, \pi)$ for blue triangles where ϕ is arbitrary. For red triangles, for undashed lines $(\phi_A, \phi_B) = (0, \pi)$ and for dashed lines $(\phi_A, \phi_B) = (\pi, 0)$.

and a triplet on the bond, while $B_{ij}^{\dagger}$ is represents coherent hopping of the bosons between the sites. These definitions are slightly different from those used by Manuel et al [117]. We can rewrite the Hamiltonian in terms of these bond operators with an approximation that D/J is very small as,

$$H = \sum_{\langle ij \rangle} J\big[: \hat{B}_{ij}^{\dagger} \hat{B}_{ij} : - \hat{A}_{ij}^{\dagger} \hat{A}_{ij} \big] \tag{3.3}$$

where :: means normal order. We decouple the quartic term by introducing mean fields $\mathcal{A}_{ij} = \left\langle \hat{A}_{ij} \right\rangle$ and $\mathcal{B}_{ij} = \left\langle \hat{B}_{ij} \right\rangle$. Then the mean field hamiltonian is given by

$$H_{\mathrm{MF}} = \sum_{\langle ij \rangle} J\big[\mathcal{B}_{ij} \hat{B}_{ij}^{\dagger} - \mathcal{A}_{ij} \hat{A}_{ij}^{\dagger} \big] + \mathrm{H.C.} - \sum_{i} \lambda_i \hat{n}_i + \epsilon_0 \tag{3.4}$$

where $\epsilon_0 = \sum_{\langle ij \rangle} J(\mathcal{A}_{ij}|^2 - |\mathcal{B}_{ij}|^2) + 2S \sum_i \lambda_i$. The Lagrange multiplier λ_i has been added to constrain the mean boson number at each site.

The PSG analysis of $\mathbb{Z}_2$ spin liquids on kagome lattice was carried out by Wang and Vishwanath and they have shown that there are only four symmetric *Ansätze* possible [61]. They have labeled these *Ansätze* as $(0,0), (\pi,0), (0,\pi)$ and (π,π), based on the fluxes through the hexagon and the rhombus. These *Ansätze* respect time reversal symmetry and lead to planar long range order. However, Messio et al have shown that ground state of Heisenberg antiferromagnet on kagome lattice is possibly a chiral spin liquid which is termed as *cuboc1* [72]. A systematic enumeration of *weakly symmetric* spin liquids shows that there are 20 families of spin

liquid *Ansätze* on kagome lattice [104]. We restrict our choices to the four symmetric spin liquids since DM interaction prefers planar LRO and cuboc1 spin liquid since it energetically most favorable in absence of DM interaction. In all *Ansätze*, the magnitudes of $\mathcal{A}_{ij}$ and $\mathcal{B}_{ij}$ are same on all bonds, that is, $|\mathcal{A}_{ij}| = \mathcal{A}$ and $|\mathcal{B}_{ij}| = \mathcal{B}$. $\mathcal{A}$ and $\mathcal{B}$ are complex numbers and their phases are summarized in the caption of the Fig. 3.2. But Messio et. al [118] pointed out that one more *Ansatz*, termed as $A_4(0,1)$ results in a stable phase. So we also include $A_4(0,1)$ in our calculation.

We assume that the Lagrange multiplier is independent of sites and is equal to λ. Using Fourier transformation, the Hamiltonian can be written as

$$H_{\mathrm{MF}} = \sum_{q} \phi_q^\dagger N_q \phi_q + N\left[\lambda(2S+1) + 2(\mathcal{A}^2 - \mathcal{B}^2)\right] \tag{3.5}$$

where N is the number of sites and $\phi_q^\dagger = \left[a_{1q}^\dagger, ...a_{mq}^\dagger, b_{1,-q}, ...b_{m,-q}\right]$. The first index μ in $a_{\mu q}$ and $b_{\mu q}$ is the sublattice index. μ can have values 1 to m where m is the number of sites per unit cell ($m = 3$ for the $(0,0), (\pi,0)$ *Ansätze* and $m = 6$ for *cuboc1 Ansatz*) and N_q is a $2m \times 2m$ matrix.

This N_q matrix can be diagonalised by Bogoliubov transformation $\phi_q = M_q \xi_q$, where $\xi_q^\dagger = \left[\alpha_{1q}^\dagger, ...\alpha_{mq}^\dagger, \beta_{1,-q}, ...\beta_{m,-q}\right]$. The transformation matrix must satisfy $M_q \tau M_q^\dagger = \tau$ where $\tau = \sigma_3 \otimes I_m$. We must find M_q such that $M_q^\dagger N_q M_q = \Omega_q$ where $\Omega_q = \mathrm{diag}(\omega_{\mu q}^\alpha ....., \omega_{\mu,-q}^\beta)$. The form of the M_q-matrix is given by $M_q = \begin{bmatrix} U_q & X_q \\ V_q & Y_q \end{bmatrix}$ where U_q, V_q, X_q and Y_q are the $m \times m$ matrix.

The diagonalised hamiltonian is given by

$$H_{\mathrm{MF}} = \sum_{q} \sum_{\mu} \left(\omega_{\mu q}^\alpha \alpha_{\mu q}^\dagger \alpha_{\mu q} + \omega_{\mu q}^\beta \beta_{\mu q} \beta_{\mu q}^\dagger\right) + N\left[\lambda(2S+1) + 2(\mathcal{A}^2 - \mathcal{B}^2)\right] \tag{3.6}$$

where $\omega_{\mu q}^\alpha$ and $\omega_{\mu q}^\beta$ are the excitation energies of $2m$ spinon modes. Note that for chiral *Ansatz* $\omega_{\mu q}^\alpha \neq \omega_{\mu q}^\beta$. The ground state energy is given by

$$E = \sum_{q,\mu} \omega_{\mu q}^\beta + N\left[\lambda(2S+1) + 2(\mathcal{A}^2 - \mathcal{B}^2)\right] \tag{3.7}$$

Bogolioubov matrix is computed using the procedure outlined in Ref. [108]. The mean field parameters $\mathcal{A}, \mathcal{B}, \lambda$, and ϕ are found by extremizing the ground state energy E. The positive definiteness of the Hamiltonian puts several conditions on the domain of these parameters. The method used for searching the saddle points is outlined in the next section. The complex link variables $\mathcal{A}_{ij}$ and $\mathcal{B}_{ij}$ satisfies the

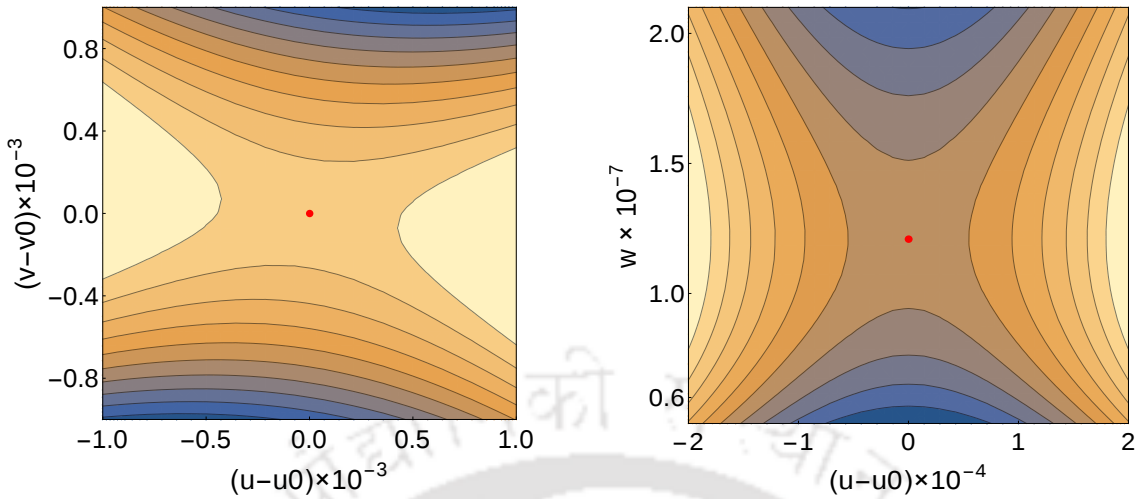

Figure 3.3: Optimum points $(u0, v0, w0)$ in the rotated frame (u, v, w) for *Ansatz* $(\pi, 0)$ at $S = 0.366$ and $\theta = 0.21$

self consistency equations

$$\mathcal{A}_{ij} = \langle \hat{\mathcal{A}}_{ij} \rangle \quad \& \quad \mathcal{B}_{ij} = \langle \hat{\mathcal{B}}_{ij} \rangle \tag{3.8}$$

which are equivalent to extremization of free energy as

$$\frac{\partial E}{\partial \mathcal{A}} = \frac{\partial E}{\partial \mathcal{B}} = \frac{\partial E}{\partial \phi} = \frac{\partial E}{\partial \lambda} = 0 \tag{3.9}$$

3.3 Numerical search for saddle points

The bosonic mean field Hamiltonian is diagonalizable if N_q is positive definite for all q. We begin the search by finding the valid domain in parameter space $\{\mathcal{A}, \mathcal{B}, \lambda\}$ where this conditions is true. The gapless LRO phases emerge as the corresponding saddle point approaches the boundaries, thus closing the gap in the spinon spectrum. These points are difficult to find since the eigenvalues of the Hessian has drastic varying magnitudes at the saddle point(see Fig. 3.3). As an example we have given the Hessian matrix of *Ansatz* $(\pi, 0)$ at $S = 0.366, \theta = 0.21$ and $N = 20$

$$h = \begin{pmatrix} 0.9230 & -0.5794 & -1.0186 \\ -0.5794 & -3.6344 & -0.3558 \\ -1.0186 & -0.3558 & -9.9997 \times 10^{11} \end{pmatrix}$$

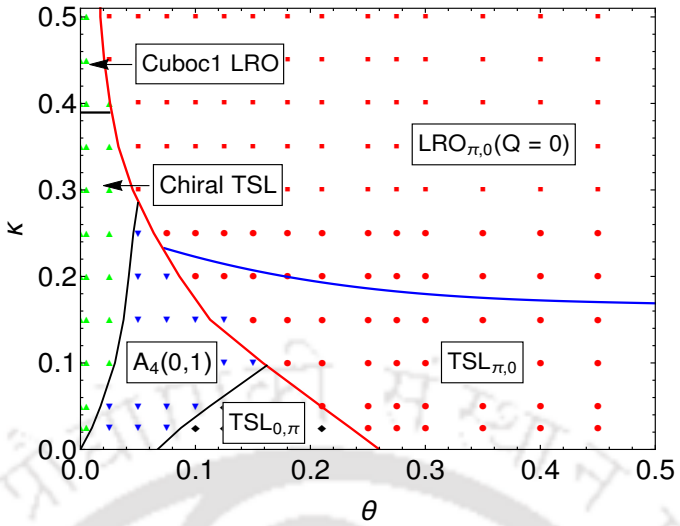

Figure 3.4: Ground state phase diagram

The eigenvalues of h are given by $\{-9.9997 \times 10^{11}, -3.7069, 0.9955\}$. Thus in LRO phases, we rotate co-ordinate axes which are nearly parallel to the eigenvectors of the Hessian, two of which are parallel to the boundary surface. The main hurdle in this procedure is to finding boundary surfaces. However these can be guessed by examining the classical orders. Thus analyzing eigenvalues of N_q at few high symmetry points in reciprocal lattice is enough. For $\sqrt{3} \times \sqrt{3}$ phase, the boundary plane is given by

$$\sqrt{3}|\cos\theta|\mathcal{A} + \mathcal{B} + \lambda = 0 \tag{3.10}$$

The boundary surfaces in *cuboc1* state are not planner but then it is still possible to search for saddle point along the surfaces and then perpendicular direction. This way we have been able to achieve much better accuracy where the sum of squares of gradients is of the order of 10^{-14}

3.4 Properties and the phase diagram

We have computed energies for various values of κ (0 to 0.5) and θ (0 to $\pi/6$) for all *Ansätze*. Based on the energy and the gap in the spinon spectrum, our proposed ground state phase diagram is shown in the Fig. 3.4. As expected, for low values of κ and also small strengths of DM interaction, the phases are gapped spin liquids. For $\theta \lesssim 0.5$, the gap in the spinon spectrum closes at about $\kappa = 0.39$ indicating a second ordered transition from gapped liquid phase to gap-less cuboctahedral LRO. For large strength of DM interaction, that is for $\theta > 0.2$, the system enters $\mathbf{Q} = 0$

LRO phase at $\theta \gtrsim 0.2$. Fig. 3.5 shows that the gap closes at $\kappa = 0.18$ for $\theta = 0.3$. To illustrate the nature of various phases we also have calculated static spin structure factor

$$S^{\alpha\alpha}(\mathbf{Q}) = \frac{3}{4N}\sum_{i,j} q^{i\mathbf{Q}\cdot(\mathbf{R}_i-\mathbf{R}_j)}\langle 0|S_i^\alpha S_j^\alpha|0\rangle$$

where $\alpha = x, y, z$, $\mathbf{R}_i$ and $\mathbf{R}_j$ are the positions of the site i and j. Due to DM interaction, the global spin rotation symmetry is reduced to $U(1)$, and hence one must calculate both S^{xx} and S^{zz}. The expression for XX-component of static spin structure factor is given by

$$\begin{aligned} S^{xx}(\mathbf{Q}) &= \frac{3}{16N}\sum_{q,\mu\nu}\Big[[X^*_{\mathbf{Q}+q}Y^T_{\mathbf{Q}+q}]_{\mu\nu}[Y^*_{-q}X^T_{-q}]_{\mu\nu} + [X^*_{\mathbf{Q}+q}X^T_{\mathbf{Q}+q}]_{\mu\nu}[Y^*_{-q}Y^T_{-q}]_{\mu\nu} \\ &+ [V_qU_q^\dagger]_{\mu\nu}[U_{-\mathbf{Q}-q}V^\dagger_{-\mathbf{Q}-q}]_{\mu\nu} + [V_{-\mathbf{Q}-q}V^\dagger_{-\mathbf{Q}-q}]_{\mu\nu}[U_qU_q^\dagger]_{\mu\nu}\Big] \end{aligned} \tag{3.11}$$

The ZZ- component of structure factor has the form

$$\begin{aligned} S^{zz}(\mathbf{Q}) &= \frac{3}{16N}\sum_{q,\mu,\nu}\Big[[X^*_{\mathbf{Q}+q}X^T_{\mathbf{Q}+q}]_{\mu\nu}[U_qU_q^\dagger]_{\mu\nu}\Big] + [V_{-\mathbf{Q}-q}V^\dagger_{-\mathbf{Q}-q}]_{\mu\nu}[X^*_{-q}X^T_{-q}]_{\mu\nu} \\ &- [X^*_{\mathbf{Q}+q}Y^T_{\mathbf{Q}+q}]_{\mu\nu}[U_qV_q^\dagger]_{\mu\nu} - [V_{-\mathbf{Q}-q}U^\dagger_{-\mathbf{Q}-q}]_{\mu\nu}[Y^*_{-q}X^T_{-q}]_{\mu\nu} \end{aligned} \tag{3.12}$$

where μ, ν are the sublattice index.

3.4.1 Spin liquid phases

The phases of the isotropic Heisenberg model ($\theta = 0$) have been studied by Messio and our results are matching with them. For $\kappa > 0.39$, the spinon spectrum is gapless at $\mathbf{Q} = \frac{3}{2}\mathbf{K}$. At $\kappa \leq 0.39$, the gap opens up and the system enters chiral spin liquid phase and remains in this phase down to $\kappa = 0$. Fig. 3.5 shows the variation of energy gap as a function of κ. However it is interesting to note that the short range correlations are cuboctahedral near the phase transition but as κ is decreased the peak in static structure factor becomes broad but also shift towards $\mathbf{K}$ point (Fig. 3.7(a)) before flattening out at $\kappa = 0.1$. Thus the short range correlations become more like $\sqrt{3}\times\sqrt{3}$ type as κ is decreased which is consistent with $q_1 = -q_2$ spin liquid state obtained by Sachdev [75].

For small values of boson density, $\kappa(< 0.15)$, the quantum fluctuations prevent any sort of long range order in the system even in presence of strong DM interaction. For very small values of θ, the system persists in *cuboc1* spin liquid phase before

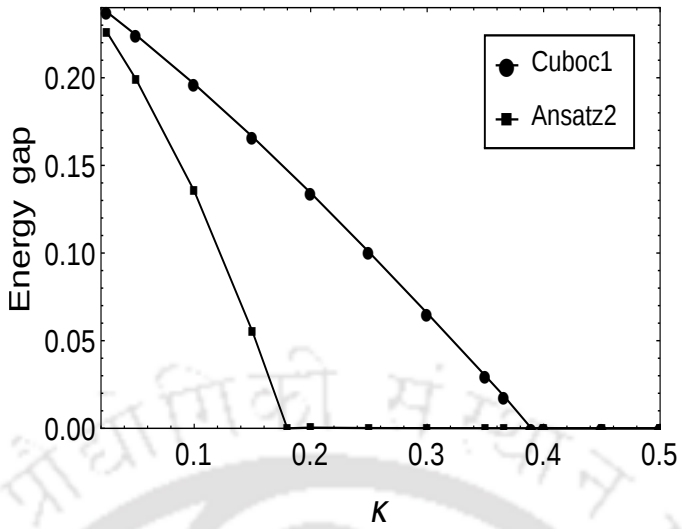

Figure 3.5: Variation of energy gap with κ for *cuboc1 Ansatz* at $\theta = 0$ and $(0, \pi)$ *Ansatz* at $\theta = 0.30$

making a first order transition to $(0, \pi)$ spin liquid phase. In this phase, the static structure factor again shows a very broad peak at $\mathbf{K}$ point. As the strength of the DM interaction is further increased the system enters $(\pi, 0)$ spin liquid phase with the short range correlations of type $\boldsymbol{Q} = 0$ showing a broad peak in spin structure factor at $\mathbf{M}_e$ point. Comparison with the phase diagram obtained by Messio, this transition occurs at much smaller values of DM interaction. This indicates the inclusion of $\mathcal{B}$ fields helps stabilizing $(\pi, 0)$ spin liquid against $(0, \pi)$ phase. We have also found a new time reversal symmetry breaking phase $A_4(0, 1)$, which is stable in small κ and in the small θ region of the phase diagram sandwiched between the chiral spin liquid and $\text{TSL}_{(0,\pi)}$ phase. In a recent work by Messio et al. showed that Its low energy excitations reproduce the inelastic neutron scattering measurements on Herbertsmithite [118]

3.4.2 Neel ordered phases

For very small values of DM interaction and $\kappa > 0.39$, all three *Ansätze* $(0, 0)$, $(0, \pi)$ and *cuboc1* are all in gapless phases corresponding to classical orders $\sqrt{3} \times \sqrt{3}$, $\boldsymbol{Q} = 0$ and cuboctahedral respectively [119]. However the lowest energy in *cuboc1 Ansatz*. In this phase, the soft modes in spinon spectrum are at $\frac{3}{4}\mathbf{K}$ points in extended Brillouin zone. Even though the *Ansatz* is still symmetric, the mechanism of symmetry breaking leading to emergence long range order through bose condensation is well understood and is described in Sachdev [59] and Messio [104]. The

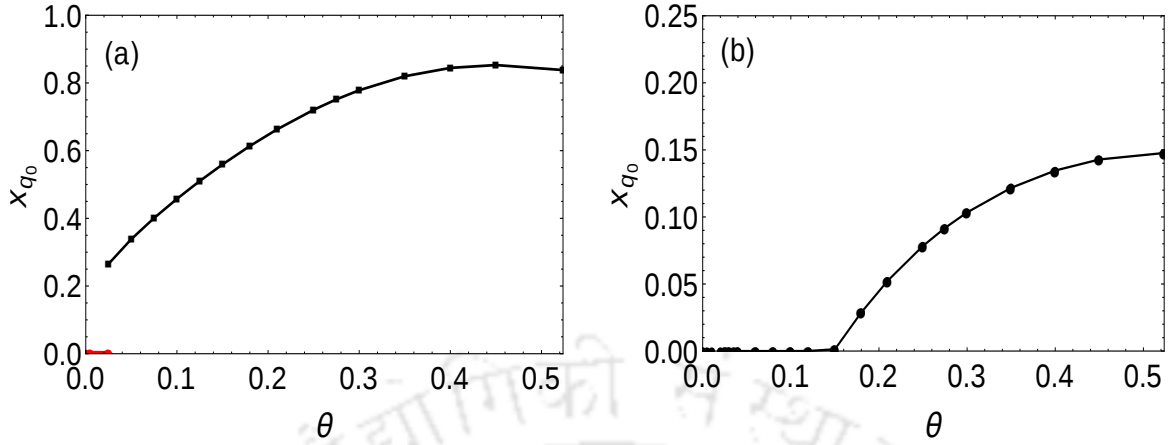

Figure 3.6: Condensate fraction x_{q_0} as a function of θ (a) at $\kappa = 0.366$ the red points shows *cuboc1 Ansatz* and black points shows $(\pi, 0)$ *Ansatz* (b) for $(\pi, 0)$ *Ansatz* at $S = 0.2$

spin structure factor in this phase shows strong peaks at $\frac{3}{2}\mathbf{K}$ point which confirms the *cuboc1* LRO phase (see Fig. 3.7(c)). At $\kappa = \frac{1}{2}$, the system is in *cuboc1* LRO phase for $\theta < 0.0173$ and then enters $\boldsymbol{Q} = 0$ phase with a first order phase transition. This width of *cuboc1* LRO decreases as $\kappa \to \infty$ where even infinitesimal DM interaction immediately orders the system in planar configuration. For $\theta > 0.1$, the $(\pi, 0)$ spin liquid shares a phase boundary with the $\mathbf{Q} = 0$ phase, which is favored by DM interaction. Across this boundary, the gap closes at $Q = 0$. The signature sharp peaks in static structure factor at $\mathbf{M}_e$ point. The condensate fraction x_0 in soft mode at q_0 can be computed using

$$\frac{1}{2S}\sum_i \langle n_i \rangle = x_{q_0} N + \sum_{\substack{j, i \neq i_0 \\ q \neq q_0}} \frac{|V_{ij}(q)|^2}{S}.$$

Fig. 3.6(a) shows the emergence of the condensate fraction as a function of θ along the $\kappa = 0.366$ horizontal line in the phase diagram. condensate fraction is zero in the *cuboc1 Ansatz* and becomes nonzero for the $(\pi, 0)$ *Ansatz* via first order phase transition at $\theta \approx 0.03$. In the Fig. 3.6(b), for $S = 0.2$ the second order phase transition occurs near $\theta = 0.15$ for $(\pi, 0)$ *Ansatz*.

3.4.3 Discussion

The ground-state phase diagram obtained here is qualitatively similar to that of Messio [76] except that the *cuboc1 Ansatz* replaces the $(0, 0)$ *Ansatz* in the phase diagram. The results obtained at $\kappa = 1/2$, however, are not in agreement with

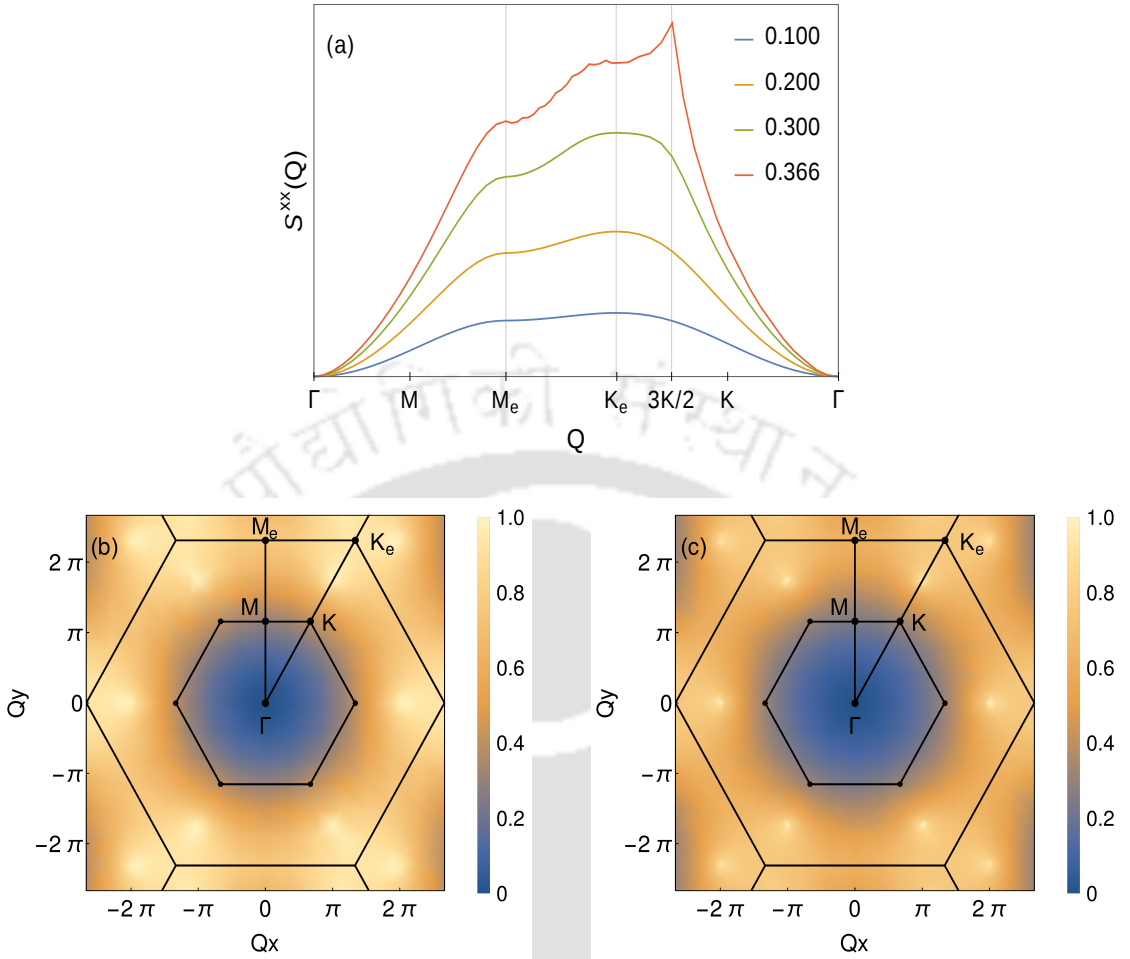

Figure 3.7: (a) XX component of static structure factor along the high-symmetry line $\Gamma - M_e - K_e - \Gamma$ for the *cuboc*1*Ansatz* for different values of κ at $\theta = 0$. The XX component of the static structure factor for the *cuboc1 Ansatz* at (b) $\kappa = 0.366$ and $\theta = 0$, and (c) $\kappa = 0.5$ and $\theta = 0$

earlier studies for spin 1/2 system [74, 75, 120] which predict a moment-free phase for small values of θ and a second ordered phase transition to $\mathbf{Q} = 0$ phase. However, the nature of the short-range correlations in the liquid phase is unclear. Cepas et al. argue that short-range correlations of type $\mathbf{Q} = 0$, whereas Huh et al. showed it to be of $\sqrt{3} \times \sqrt{3}$ type. However, Messio [72] has argued that, in SBMFT, since $n_i = 2S$ constraint is implemented only in an average sense, spin 1/2 system may not be correctly represented by $\kappa = 1/2$. Due to the fluctuations in n_i, the $\langle \boldsymbol{S}_i^2 \rangle$ is overestimated to be $\frac{3}{2}S(S+1)$ at $\theta = 0$. If we treat $\langle \boldsymbol{S}_i^2 \rangle$ to be a good quantum number, then the spin 1/2 system is approximated by the bosonic system at $\kappa = 0.366$. At this value of κ, our proposal shows that the system is $\mathbb{Z}_2$ chiral

spin liquid till $\theta < 0.03$ with short-range correlations of a cuboctahedral kind. For $\theta > 0.03$, the DM interaction forces the spins to be in planar arrangement with $\boldsymbol{Q} = 0$ long-range order.

It is also possible that the best representation may be at smaller values of κ, where we have noted that the short range correlations tend to be more like $\sqrt{3} \times \sqrt{3}$ type as argued by Messio et al. Even though at $\kappa = 0.366$ shows a first order transition from spin liquid to $\mathbf{Q} = 0$ LRO, it may not be adequate in reconciling with the experimental results. The strength of the DM interaction is estimated to be $0.08J$ in $ZnCu_3(OH)_6Cl_3$. This compound does not exhibit freezing of magnetic moments to very low temperatures [84]. In the present mean field theory, at $\kappa = 0.366$, the critical $D_c = 0.03J$. The optimized value of mean field parameters and energy for $S = 0.366$ is as given in the table below.

Ansatz	θ	$\mathcal{A}$	$\mathcal{B}$	λ	ϕ	energy
cuboc1	0	0.4036	0.1185	-0.5803	1.9847	-0.2976
$(\pi, 0)$	0.21	0.4226	0.1340	-0.6700	-	-0.3213

Table 3.1: Optimized values and energies for different *Ansätze*

3.5 Dynamical spin structure factor

Since in neutron scattering experiment the inelastic neutron scattering cross section is proportional to the dynamical spin structure factor, we have calculated the dynamical spin structure factor defined by

$$S^{\alpha\alpha}(\mathbf{Q}, \omega) = \int_{-\infty}^{\infty} \langle 0 | S^{\alpha}_{-\mathbf{Q}}(t) S^{\alpha}_{\mathbf{Q}}(0) | 0 \rangle e^{i\omega t} dt \tag{3.13}$$

where $\alpha = x, y, z$ and $|0\rangle$ is the ground state of the system .The expression for XX-component of dynamical spin structure factor is given by

$$\begin{aligned} S^{xx}(\mathbf{Q}, \omega) &= 2\pi \sum_{q} \sum_{\mu\nu} \Big[|[U_q^{\dagger} V^{*}_{-q-\mathbf{Q}}]_{\mu\nu} + [U^{\dagger}_{-q-\mathbf{Q}} V^{*}_{q}]_{\nu\mu}|^2 \\ &+ |[Y^{T}_{-q} X_{q+\mathbf{Q}}]_{\mu\nu} + [Y^{T}_{\mathbf{Q}+q} X_{-q}]_{\nu\mu}|^2 \Big] \times \delta(\omega - \omega_p) \end{aligned} \tag{3.14}$$

where μ, ν are the sublattice index. The expression for ZZ-component of dynamical spin structure factor reduces to

$$S^{zz}(\mathbf{Q}, \omega) = 2\pi \sum_{q} \sum_{\mu\nu} |\left[U_q^{\dagger} X_{\mathbf{Q}+q}\right]_{\mu\nu} - \left[V_q^{\dagger} Y_{\mathbf{Q}+q}\right]_{\mu\nu}|^2 \times \delta(\omega - \omega_p) \tag{3.15}$$

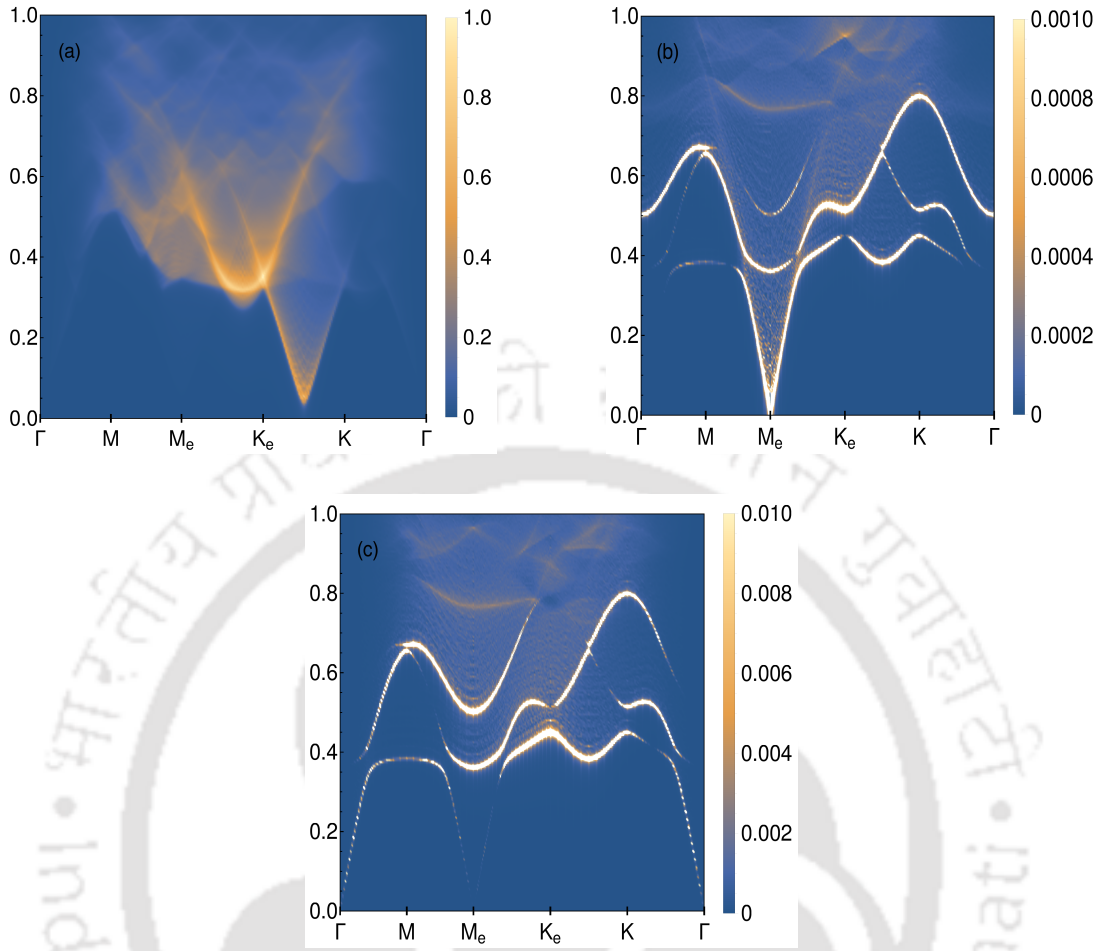

Figure 3.8: XX-component of dynamical structure factor for (a) *cuboc*1 *Ansatz* at $S = 0.366$ and $\theta = 0$ (b) $(\pi, 0)$ *Ansatz* at $S = 0.366$ with $\theta = 0.21$ (c) ZZ-component of dynamical structure factor for $(\pi, 0)$ *Ansatz* at $S = 0.366$ and $\theta = 0.21$. In LRO phase we choose scale to be very small such that the spinon continuum is visible.

where $\omega_p = \omega_q + \omega_{-\mathbf{Q}-q}$. At $\mathbf{Q} = 0$ the ZZ component will straight way will give zero because it is just the dot product of the two columns of the M-matrix(para orthogonalization), consistent with the figure. For numerical purpose, the delta function is approximated by Lorentzian function. The results are qualitatively similar to the results obtained by Messio. In Fig. 3.8, we illustrate the evolution of the dynamical structure factor across the phase transition from spin liquid to LRO phase for $\kappa = 0.366$. The dynamical structure factor is shown along the high symmetry line $\mathbf{\Gamma} - \mathbf{M}_e - \mathbf{K}_e - \mathbf{\Gamma}$. The dynamical structure factor of *cuboc1 Ansatz* at $\theta = 0$ in Fig. 3.8(a) shows sharp onset of spinon continuum at $\frac{3}{2}\mathbf{K}$ with very small gap. This is due to the proximity of critical point at $\kappa = 0.39$ beyond which there is *cuboc1*

long range order.

Since the DM interaction reduces the global spin rotation symmetry from $SU(2)$ to $U(1)$, there is notable difference between XX and ZZ component of dynamical structure factor. In Fig. 3.8(b) and Fig. 3.8(c), we show the dynamical structure factor of *Ansatz* $(0, \pi)$ at $\theta = 0.21$ which is $\mathbf{Q} = 0$ LRO phase. In the XX-component of dynamical structure factor, the magnon branches are quite strong, and in the density plot, it is visible as three lines of bright dots corresponding to three magnon branches. These magnon branches are obtained by considering the pair of spinons, one in the soft modes, and another one from the excited state. The elastic peak (along $\omega = 0$ line) appears with largest intensity at $\mathbf{M}_e$ point which is the $\mathbf{\Gamma}$ point of the next Wigner- Seitz cell. In the ZZ-component of dynamical structure factor the magnon branches are of very low intensity and suppressed, as the spins are forced to lie in the XY plane due to the DM interaction.

3.6 Conclusion

We have computed the ground-state phase diagram of Heisenberg Kagome antiferromagnet with DM interaction using the SBMFT approach. We have included the time-reversal symmetry breaking chiral *Ansatz* proposed by Messio [72]and also considered hopping mean-field $\mathcal{B}$. For large S, even with small DM interaction, the spins are forced to in-plane and in $\mathbf{Q} = 0$ long-range order. For small S, the quantum fluctuations induce a series of spin liquid phases with increasing DM interaction. In this region, the inclusion of the hopping field seems to stabilize $(\pi, 0)$ spin liquid phase over $(0, \pi)$ spin liquid.

Since the constraint of boson density is implemented strictly, $\langle \mathbf{S}_i^2 \rangle = \frac{1}{2}$ at $\kappa = 0.366$ due to the fluctuations in boson density. We find that, at $\kappa = 0.366$, the model shows a first ordered phase transition from chiral *cuboc1* spin liquid to $\mathbf{Q} = 0$ Neel phase at $D = 0.03J$. Even though this result is qualitatively in agreement with other studies, it is not adequate in explaining the moment free phase of Herbertsmithite [84] since the estimated DM strength is $0.08J$. Probably, one may need to consider even smaller values of κ to obtain better numerical agreement with other studies and experiments. We have also calculated the static and dynamical structure factor at the representative $\kappa = 0.366$ point.

Chapter 4

Regular Magnetic Order in Triangular and Kagome Lattice

4.1 Introduction

Finding the ground state of different frustrated magnets is a long-sought goal in condensed matter physics. The interest is triggered by the possibility of disordered state and their relationship to high-temperature superconductivity [121]. Each of those disordered phases is interesting in their own way and appears with different types of order and excitations associated with unusual quantum numbers. But, it turns out that the magnetic structure of the ordered phases of such magnets becomes non-trivial. For example, the classical ground of many such frustrated spin systems has "accidental degeneracies" which are lifted by quantum fluctuations. In those cases, quantum fluctuations induce magnetic order in the spin system, known as "order from disorder" [8–10].

In general, finding the classical ground state of such a spin system is a challenging problem to solve. For instance, there exists no general method to figure out the ground state spin configuration of a non-Bravais lattice described by simple Heisenberg Hamiltonian with $O(3)$ symmetry given by

$$H = \sum_{ij} J(|\vec{R}_i - \vec{R}_j|)\vec{S}_i \cdot \vec{S}_j \tag{4.1}$$

where J is the exchange integral. $\vec{S}_i$ and $\vec{S}_j$ are the classical spin vectors at i-th and j-th site, respectively.

In this chapter, we construct a family of spin configurations that respect all the lattice symmetries of a given lattice modulo global spin transformations. Such spin

configurations are dubbed as the *regular magnetic order*(RMO). The most simple example is the Neel state in one dimension. In that case, any lattice transformation can be compensated by appropriate spin rotations.

By construction, the family of RMOs only depends on the symmetries of the model, i.e., lattice symmetries and spin transformations(rotations and spin flips), and does not rely on the strength of the couplings present in the model. These RMOs become very interesting in case of frustrated magnets, as these are the good variational candidates for many spin models. For example, for Heisenberg spins on kagome lattice, the ground state is found to possess non-coplanar spin structures with first, second, and third neighbor exchange interactions. [119]. Apart from that, these RMOs can provide useful insights into the experimental data of magnetic materials where the information about the lattice is known, but the values of the couplings present in the material are unknown. In that case, the magnetic correlation can be directly compared to these states, and if these two correlation matches, we can extract some useful information about the couplings present in the material.

In this chapter, we mainly focus on the Heisenberg model, and we treat each spin as a three-dimensional unit vector. We use a simple group theoretical approach to investigate the possible regular magnetic order in triangular and kagome lattice. So, we have considered the wallpaper groups, which includes the triangular and kagome geometry. There is a total of seventeen wallpaper groups in 2-dimension. Among them, there are five wallpaper groups that include the triangular and kagome geometry. The wallpaper group $p6m$ is already done by Messio et al. [119]. We have extended their work and mainly focused on the rest of the four wallpaper groups $p6, p3, p3m1$ and $p31m$ in Hermann-Mauguin notations. We will consider each of them separately and list all the possible regular magnetic orders for each of those groups.

4.2 Notations and definitions

Let us denote the lattice by $\mathcal{L}$ which contains a pattern of sites. In mathematics, the lattice in $\mathbb{E}^2$ is defined as $\{m\vec{a} + n\vec{b} \mid m, n \in \mathbb{Z}\}$ and $\vec{a}, \vec{b}$ are two non-colinear vectors. Here $\mathcal{L}$ is a lattice with basis as commonly defined by physicists. Now, we denote the group of transformation $\mathcal{G}_\mathcal{L}$ on $\mathcal{L}$ as $\mathcal{G}_\mathcal{L} = \{\sigma : \mathcal{L} \to \mathcal{L}\}$. Let $\mathcal{H}$ be the spin configuration space that is $\mathcal{H} = \{\phi | \phi : \mathcal{L} \to \mathbb{E}^3\}$. There are two types of transformation on the $\mathcal{H}$.

(i) **Lattice transformation** : For each $\sigma \in \mathcal{G}_\mathcal{L}$, there is $O_\sigma : \mathcal{H} \to \mathcal{H}$ such that

$O_\sigma\phi(i) = \phi(\sigma^{-1}(i))$. Since this group is isomorphic to $\mathcal{G}_\mathcal{L}$, we will refer to this group as $\mathcal{G}_\mathcal{L}$ hoping that there is no confusion.

(ii) **Spin rotations** : There can be two types of spin rotations; local and global. For each $g \in O(3)$, we have $R_g : \mathcal{H} \to \mathcal{H}$ such that $(R_g\phi)(i) = g\phi(i)$. We will refer to this group of global spin rotations by the same symbol $O(3)$.

The group of transformations $\mathcal{G}$ on $\mathcal{H}$, is a direct product of $\mathcal{G}_\mathcal{L} \times O(3)$.

4.2.1 Stabilizer group of spin transformation

Let ϕ be a spin configuration. The set of all transformation that leave the spin configuration ϕ invariant is denoted by G_ϕ. So, $G_\phi = \{g \in \mathcal{G} \mid g\phi = \phi\}$. Then G_ϕ is a subgroup of $\mathcal{G}$ and is called the *stabilizer* group of the spin configuration ϕ. Let $G^S_\phi = O(3) \cap G_\phi$ that is the G^S_ϕ is a subgroup of $O(3)$ that leaves the spin configuration ϕ invariant.

Example : To illustrate the concept, let us consider the 1D lattice as shown in Fig. 4.1. The group of transformation $\mathcal{G}_\mathcal{L}$ is generated by translation $\tau : i \mapsto i + 1$ and mirror $m : i \mapsto -i$ where i is the site index.

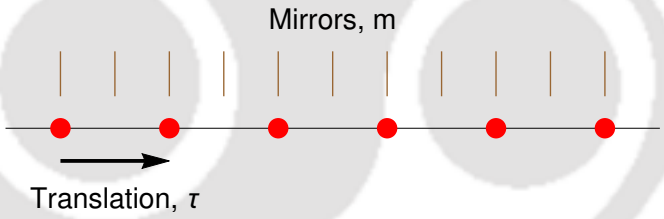

Figure 4.1: Group of transformations in 1D lattice

(a) Let $\phi(i) = \hat{n}\ \forall\ i$ as shown in Fig. 4.2(a)

- Lattice transformation : ϕ is invariant under all transformation in $\mathcal{G}_\mathcal{L}$.
- Global spin rotations : ϕ is invariant under $O(2)$ (rotations about $\hat{n}$ and mirrors containing $\hat{n}$).
- Stabilizer group : Then $G_\phi = \mathcal{G}_\mathcal{L} \times O(2)$.

(b) Let $\phi(i) = (-1)^i\ \hat{n} \quad \forall\ i$ as shown in Fig. 4.2(b)

- Lattice transformation : ϕ is invariant under translations τ^{2k} where $k \in \mathbb{Z}$ and mirrors passing through the sites i.
- Global spin rotations : ϕ is invariant under $O(2)$. Therefore $G^s_\phi = O(2)$

- Stabilizer group : It is the direct product of lattice transformation and global spin rotations. The group G_ϕ also contains elements like $g\tau^{2k+1}$ where $g \in O(3)$ and $g(\hat{n}) = -\hat{n}$ (all π rotations about any axis $\perp \hat{n}$, all mirrors $\perp \hat{n}$ and inversion multiplied by G^s_ϕ), also the mirrors passing through the mid point between the neighboring sites.

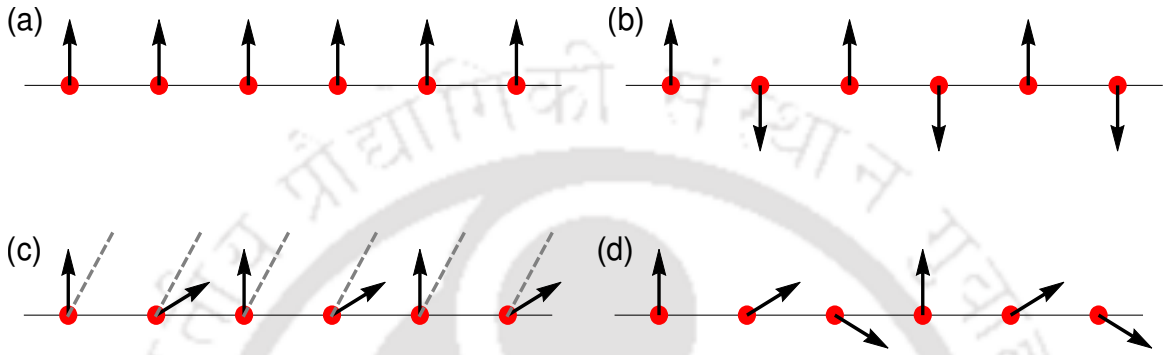

Figure 4.2: Examples for symmetry group of configurations

(c) Let $\phi(i) = \hat{z}$ if i is even and $\phi(i) = \frac{1}{2}\hat{z} + \frac{\sqrt{3}}{2}\hat{x}$ as shown in Fig. 4.2(c)

- Lattice transformation : ϕ is invariant under translations τ^{2k} where $k \in \mathbb{Z}$ and mirrors passing through the sites i.
- Global spin rotations : $G^s_\phi = \{I, M_{xz}\}$ where M_{xz} is a mirror operation in the xz plane.
- Stabilizer group : Let $\hat{n} = \frac{1}{2}\hat{z} + \frac{\sqrt{3}}{2}\hat{x}$. Then ϕ is invariant under $\tau^{2k+1}R_{\hat{n}}(\pi)$ and $\tau^{2k+1}M$ where mirror M contains $\hat{n}$ and $\hat{y}$. (same for mirrors passing through the midpoint between neighboring sites)

(d) Let ϕ be a spin configuration as shown in Fig. 4.2(d)

- Lattice transformation : ϕ is invariant under translations τ^{3k} where $k \in \mathbb{Z}$.
- Global spin rotations : $G^s_\phi = \{I, M_{xz}\}$ where M_{xz} is a mirror operation in the xz plane.
- Stabilizer group : ϕ is not invariant under τ or τ^2 and any global rotations.

4.2.2 Regular structures

Definition : A spin configuration $\phi \in \mathcal{H}$ is called *regular* if for every $\sigma \in \mathcal{G}_\mathcal{L}$, there is $g_\sigma \in O(3)$ such that $g_\sigma(\sigma(\phi)) = \phi$

Example : To illustrate the concept, let us consider the case of 1D lattice

(a) This spin configuration is regular because it is anyway invariant under $\mathcal{G}_{\mathcal{L}}$.

(b) This spin configuration is not invariant under τ but it is invariant under $M\tau$ where M is the mirror in the xy plane. (infinitely many possibilities instead of M)

(c) This case is similar to (b) but only two choices for $g\tau$.

(d) This spin configuration is not regular since $\tau \in \mathcal{G}_{\mathcal{L}}$, there is no $g \in O(3)$ such that $g\tau(\phi) = \phi$

For a regular structure, we can prove the following theorem which states that

Theorem : *If a spin configuration ϕ is regular then the group $\mathcal{G}_\phi/\mathcal{G}^s_\phi$ is isomorphic to $\mathcal{G}_{\mathcal{L}}$.*

The proof is given in the appendix. This theorem is central to the idea of the algebraic symmetry group presented in the next section. It is difficult to list out all the RMOs of a system. However, we can find all RMOs by using a systematic procedure based on algebraic symmetry groups.

4.2.3 Algebraic symmetry groups

Definition : A subgroup of $O(3) \times \mathcal{G}_{\mathcal{L}}$ that is homomorphic to $\mathcal{G}_{\mathcal{L}}$ is called an *algebraic symmetry group.*

If ϕ is a regular structure, then it has one of the algebraic symmetry groups. The idea is to find the entire list of such groups. However, if ϕ is regular then for any $g \in O(3)$, $g\phi$ is also regular and $G_{g\phi} = gG_\phi g^{-1}$. Then $G_{g\phi}/G^s_{g\phi}$ is isomorphic to G_ϕ/G^s_ϕ. Then we only need to list the equivalence classes of algebraic symmetry groups, and loosely we will call the equivalence classes also by the same name.

Let us consider three elements σ_1, σ_2 and σ_3 of $\mathcal{G}_{\mathcal{L}}$ with the algebraic relation $\sigma_1\sigma_2 = \sigma_3$. The algebraic constraint imposes constraints on $g_\sigma \in O(3)$ for each $\sigma \in \mathcal{G}_{\mathcal{L}}$. To begin with, we will assume that there exist a compatible spin configuration ϕ corresponding to each mapping. Then by construction, if G_{σ_1} be the image of σ_1, we must have $G_{\sigma_1}\sigma_1 \in G^s_\phi$. Similarly, $G_{\sigma_1}\sigma_1 G_{\sigma_2}\sigma_2 \in G^s_\phi$. This implies that $G_{\sigma_1}\sigma_1 G_{\sigma_2}\sigma_2\sigma_3^{-1}G^{-1}_{\sigma_3} \in G^s_\phi$

$$G_{\sigma_1}\sigma_1 G_{\sigma_2}\sigma_2\sigma_3^{-1}G_{\sigma_3} \in G^s_\phi, \quad \forall\ \sigma_1, \sigma_2\ \in\ \mathcal{G}_{\mathcal{L}} \tag{4.2}$$

Since the elements of $\mathcal{G}_{\mathcal{L}}$ and g_σ commutes, we have

$$\begin{aligned} G_{\sigma_1} G_{\sigma_2} \sigma_1 \sigma_2 \sigma_3^{-1} G_{\sigma_3}^{-1} &\in G_\phi^s \\ G_{\sigma_1} G_{\sigma_2} G_{\sigma_3}^{-1} &\in G_\phi^s \\ G_{\sigma_1} G_{\sigma_2} G_{\sigma_1\sigma_2}^{-1} &\in G_\phi^s \end{aligned}$$

So, we have started with the algebraic relation between the elements of $\mathcal{G}_\mathcal{L}$ and we end up with a pure spin transformation. If the above condition is not satisfied, then the mapping must be excluded from the algebraic symmetry group as it will not result in a RMO.

We must mention that the algebraic symmetry group only depends on the spin rotation group, the subgroup G_ϕ^s, and the algebraic relation between the generators of the $\mathcal{G}_\mathcal{L}$ but there is no direct dependence on the lattice $\mathcal{L}$.

4.2.4 Compatible states

An algebraic symmetry group G is compatible with a spin configuration ϕ if $G\,\phi = \phi$. Now, the next step is to find all the compatible states corresponding to each of the algebraic symmetry groups. This step is explicitly dependent on the lattice $\mathcal{L}$. To construct the compatible states with a given algebraic symmetry group, we first fix the direction of the spin at site i. Then we apply all the elements of lattice symmetry group $\mathcal{G}_\mathcal{L}$ to extract the spin arrangement of all other sites. Here we must mention that two elements of lattice symmetry group $X, Y \in \mathcal{G}_\mathcal{L}$ leads to the same site i i.e $X(i) = Y(i)$, then we must have $G_X(i) = G_Y(i)$. This will result in a constraint on the direction of the spin at site i or indicate that there exist no compatible sates for the given mapping.

4.2.5 Construction of regular magnetic order

To construct the regular magnetic orders, we have the following steps. First, we fix the spin symmetry group G_ϕ^s. Then we look for the algebraic relation between the generators of the $\mathcal{G}_\mathcal{L}$. These algebraic relation imposes constraint on $g_\sigma \in O(3)$ for each $\sigma \in \mathcal{G}_\mathcal{L}$. In the second step, we have to determine the spin configuration compatible with each of the algebraic symmetry group if there exist at all.

The spin rotation group for Heisenberg spins is $O(3)$ group. Now the possible unbroken spin symmetric group $G_\phi^s = \{I\}$ can be isomorphic to any of the group $\{I\}, \mathbb{Z}_2$ and $O(2)$ which leads to the non-coplanar, coplanar and collinear spin configuration respectively. The first case, $G_\phi^s = \{I\}$ is the most interesting one and will consider for each of the wallpaper group $p6, p3, p31m$ and $p3m1$.

4.3 $p6$ group

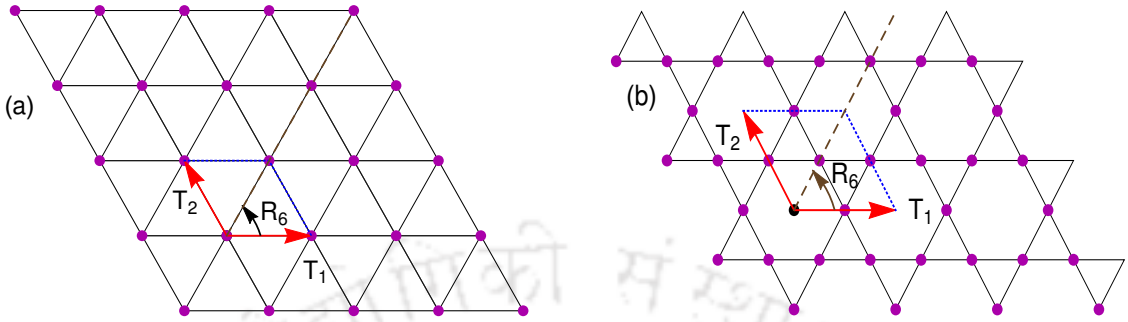

Figure 4.3: Generators of p_6 wallpaper group. (a) Triangular lattice (b) Kagome lattice

Let us denote the lattice by $\mathcal{L}$ and (r_1, r_2) be the oblique co-ordinates with respect to the basis $\vec{a} = (1, 0)$ and $\vec{b} = (\frac{1}{2}, \frac{-\sqrt{3}}{2})$. The lattice symmetry group $\mathcal{G}_\mathcal{L}$ is generated by the three generators T_1, T_2 and R_6 where T_1, T_2 are two translations, R_6 is the six fold rotation about the origin as shown in the Fig. 4.3. The action of each of the generators on the lattice sites is given by

$$T_1 : (r_1, r_2) \rightarrow (r_1 + 1, r_2) \tag{4.3a}$$
$$T_2 : (r_1, r_2) \rightarrow (r_1, r_2 + 1) \tag{4.3b}$$
$$R_6 : (r_1, r_2) \rightarrow (r_1 - r_2, r_1) \tag{4.3c}$$

Let us consider the mapping G from $\mathcal{G}_\mathcal{L}$ to g_σ that is compatible with some spin configuration ϕ.The mapping G can be constructed from the images of the generators of $\mathcal{G}_\mathcal{L}$ using Eq. 4.2. Since, different combinations of the generators of $\mathcal{G}_\mathcal{L}$ may lead to the same element of lattice symmetry group $\mathcal{G}_\mathcal{L}$, the images by G of the generators of the lattice symmetry group must satisfy the same algebraic constraints. Now, we can write product of generators in the following form $R_6^r T_1^{t_1} T_2^{t_2}$ where $r = 0, 1, 2, 3, 4, 5$ and $t_1, t_2 \in \mathbb{Z}_2$. The relation between the generators of $p6$ group are following

$$T_1 T_2 = T_2 T_1 \tag{4.4a}$$
$$T_1 R_6 T_2 = R_6 \tag{4.4b}$$
$$R_6 T_1 T_2 = T_2 R_6 \tag{4.4c}$$
$$R_6^6 = I \tag{4.4d}$$

Now, the images by G of the generators of the lattice symmetry group must satisfy

the same algebraic constraints. So, we have the following equations.

$$G_1G_2 = G_2G_1 \tag{4.5}$$
$$G_1G_6G_2 = G_6 \tag{4.6}$$
$$G_2G_6 = G_6G_1G_2 \tag{4.7}$$
$$G_6^6 = I \tag{4.8}$$

Each element G_X, corresponding to the elements $X \in \mathcal{G}_\mathcal{L}$ is characterized by its determinant $\epsilon_X = \pm 1$ and a rotation $R_{\hat{n}_X\theta_X}$ by an angle $\theta_X \in [0, \pi]$ about an axis $\hat{n}_X$ such that $G_X = \epsilon_X R_{\hat{n}_X\theta_X}$. For the $p6$ group we get total twelve solutions as given below

(i) $G_{T_1} = I, G_{T_2} = I,$ and $G_{R_6} = \epsilon_{R_6} I$ (4.9a)

(ii) $G_{T_1} = I, G_{T_2} = I,$ and $G_{R_6} = \epsilon_{R_6} R(\hat{n}, \frac{\pi}{3})$ (4.9b)

(iii) $G_{T_1} = I, G_{T_2} = I,$ and $G_{R_6} = \epsilon_{R_6} R(\hat{n}, \frac{2\pi}{3})$ (4.9c)

(iv) $G_{T_1} = I, G_{T_2} = I,$ and $G_{R_6} = \epsilon_{R_6} R(\hat{n}, \pi)$ (4.9d)

(v) $G_{T_1} = G_{T_2} = R(\hat{n}, \frac{2\pi}{3}),$ and $G_{R_6} = \epsilon_{R_6} R(\hat{n}_6, \pi), n_6 \perp n$ (4.9e)

(vi) $G_{T_1} = R(\hat{x}, \pi), G_{T_2} = R(\hat{y}, \pi)$ and $G_{R_6} = \epsilon_{R_6} R(\hat{n}, \frac{2\pi}{3}), \hat{n} = (1, 1, 1)$ (4.9f)

where ϵ_{R_6} can take values ± 1.

4.3.1 RMOs in triangular lattice

The position vector for any arbitrary point is given by $\vec{r} = m\vec{a} + n\vec{b}$ where $m, n \in \mathbb{Z}$. Let us consider that the spin configuration at starting point is $\phi(0, 0)$. So, the spin configuration at any arbitrary site is given by

$$\phi(m, n) = G_{T_1}^m G_{T_2}^n \phi(0, 0) \tag{4.10}$$

Under 6-fold rotation, we must have,

$$\phi(m, n) = G_{R_6} \phi(n, n - m) \tag{4.11}$$

After some manipulation we get,

$$G_{T_1}^m G_{T_2}^n \phi(0, 0) = G_{T_1}^m G_{T_2}^n G_{R_6} \phi(0, 0) \tag{4.12}$$

This implies that $\phi(0,0)$ must be an eigenvector of G_{R_6} with an eigenvalue $+1$. Now we can list all the possible RMOs corresponding to each of the mapping given in Eq, 4.9 for the triangular lattice.

(i) This is the trivial case where all the symmetry elements are identity. For $\epsilon_{R_6} = +1$, all the eigenvalues of G_{R_6} are positive. So, any linear combination of the eigenvectors can be taken as $\phi(0,0)$. The resulting RMO is the well known ferromagnetic state, as shown in Fig. 4.7.

For $\epsilon_{R_6} = -1$, all the eigenvalues of G_{R_6} are negative. So, there is no RMO possible for this mapping.

(ii) In this case, we choose $\hat{n}$ to be in the $(1,1,1)$ direction. For $\epsilon_{R_6} = +1$ case, the positive eigenvalue of G_{R_6} appears with the eigenvector $(1,1,1)$. So, $\phi(0,0)$ can be taken as $(1,1,1)$. The resulting RMO is ferromagnetic state.

For $\epsilon_{R_6} = -1$, all the eigenvalues of G_{R_6} are negative. So, there is no RMO possible for this case.

(iii) Here too, we choose $\hat{n}$ to be in the $(1,1,1)$ direction. For $\epsilon_{R_6} = +1$ case, the positive eigenvalue of G_{R_6} is associated with the eigenvector $(1,1,1)$. The resulting RMO is ferromagnetic state.

For $\epsilon_{R_6} = -1$, all the eigenvalues of G_{R_6} are negative. So, there is no RMO possible for this case.

(iv) This is also similar to the previous case. Here for both the case $\epsilon_{R_6} = \pm 1$ we get the ferromagnetic state.

(v) Since in this case $\hat{n}_6 \perp \hat{n}$, we choose $\hat{n} = (1,1,1)$ and $\hat{n}_6 = (1,-1,0)$. For $\epsilon_{R_6} = +1$ case, the positive eigenvalue of G_{R_6} appears with the eigen vector $(-1,1,0)$. So, the $\phi(0,0)$ can be taken as $(-1,1,0)$ and the resulting RMO is a planar structure, containing three sub-lattices, as shown in the Fig. 4.8.

For $\epsilon_{R_6} = -1$ case, we have two eigenvalues of G_{R_6} which are positive and the associated eigenvectors are $(1,1,0)$ and $(0,0,1)$. So, any linear combination of these two vectors can be taken as $\phi(0,0)$. In this case, we get a non-coplanar structure with three sub-lattices, as shown in Fig. 4.9.

(vi) Here, $\hat{n}$ is taken in the $(-1,-1,-1)$ direction. For $\epsilon_{R_6} = +1$, positive eigenvalue of G_{R_6} appears with the eigenvectors $(1,1,1)$ and hence $\phi(0,0)$ can be taken as $(1,1,1)$. In this case the RMO obtained is tetrahedral which has four sub-lattices as shown in the Fig. 4.10.

For $\epsilon_{R_6} = -1$, all the eigenvalues of G_{R_6} is negative. So, there will be no RMO

corresponding to this algebraic symmetry group.

4.3.2 RMOs in kagome lattice

Since, the lattice symmetry group $\mathcal{G}_{\mathcal{L}}$ of kagome lattice is isomorphic to the lattice symmetry group of triangular lattice, the algebraic solutions remains same for both the lattice. Let the three sublattices A, B and C are located at $\frac{1}{2}\vec{a}$, $\frac{1}{2}\vec{b}$ and $-\frac{1}{2}(\vec{a}+\vec{b})$. Consider a lattice point of sublattice index μ in a unit cell with left bottom corner at $m\vec{a}+n\vec{b}$. Clearly

$$\phi(m,n,B) = G_{R_6}^2\phi(n-m,-m,A) \tag{4.13}$$

After few steps of algebra we get,

$$G_1^m G_2^n \phi(0,0,B) = G_1^m G_2^n G_{R_6}^2 \phi(0,0,A) \tag{4.14}$$

Thus we get, the relation between the three sublattices,

$$\phi(0,0,A) = G_{R_6}^2\phi(0,0,C) = G_{R_6}^4\phi(0,0,B) = G_{R_6}^6\phi(0,0,A) \tag{4.15}$$

But we also have the condition that $\phi(0,0,A) = G_1G_6^3\phi(0,0,A)$. For each possibilities of RMO's , spins at each site must follow the above conditions. We can choose $\phi(0,0,A)$ as the eigenvector of $G_1G_{R_6}^3$ corresponding to the positive eigenvalue.

(i) This is the trivial case where all the symmetry operations are identity. For $\epsilon_{R_6} = +1$, all the eigenvalues of $G_1G_{R_6}^3$ are positive. So, any linear combination of the eigenvectors can be taken as $\phi(0,0,A)$. The resulting RMO is the well known ferromagnetic state, as shown in Fig. 4.11.

For $\epsilon_{R_6} = -1$, all the eigenvalues are negative. So, in this case there will not be any compatible RMO.

(ii) This case is very similar to the previous one. We choose $\hat{n}$ to be along $(1,1,1)$ direction. For $\epsilon_{R_6} = +1$ case, the positive eigenvalue of $G_1G_{R_6}^3$ appears with the eigenvectors $(1,1,1)$. The resulting RMO is ferromagnetic state.

For $\epsilon_{R_6} = -1$, there are two eigenvalues of $G_1G_{R_6}^3$ which are positive and the corresponding eigenvectors are $(-1,0,1)$ and $(-1,1,0)$. So we can take any linear combination of these two vectors as $\phi(0,0,A)$. In this case, the resulting RMO is $Q=0$ planar state, which is shown in the Fig. 4.12.

(iii) Here too, we choose $\hat{n}$ to be along $(1,1,1)$ direction. For $\epsilon_{R_6} = +1$ case, all the eigenvalue of $G_1 G_{R_6}^3$ appears with positive sign. So, any linear combination of the eigenvectors can be taken as $\phi(0,0,A)$, and the resulting RMO is a $Q = 0$ umbrella state as shown in Fig. 4.13.

For $\epsilon_{R_6} = -1$ case, all the eigenvalue of $G_1 G_{R_6}^3$ appears with a negative sign, so there will not be any compatible RMO for this mapping.

(iv) In this case, we choose $\hat{n}$ to be along $(1,1,1)$ direction. By looking at the positive eigenvalues of $G_1 G_{R_6}^3$ we choose $\phi(0,0,A)$. Here we get ferromagnetic state for both $\epsilon_{R_6} = \pm 1$.

(v) Since in this case $\hat{n}_6 \perp \hat{n}$, we choose $\hat{n} = (1,1,1)$ and $\hat{n}_6 = (1,-1,0)$. For $\epsilon_{R_6} = +1$ case, the positive eigenvalue appears with the eigen vector $(-1,0,1)$. So, $\phi(0,0,A)$. can be taken as $(-1,0,1)$ and we get $\sqrt{3} \times \sqrt{3}$ planar state with three sub-lattices as shown in Fig. 4.14.

For $\epsilon_{R_6} = -1$ case, the positive eigenvalues of $G_1 G_{R_6}^3$ appears with the eigenvectors $(1,0,1)$ and $(0,1,0)$. So we can take linear combination of these two vectors as $\phi(0,0,A)$. Here we get, non-coplanar $\sqrt{3} \times \sqrt{3}$ umbrella state with three sub-lattices as shown in the Fig. 4.15.

(vi) In this case $\hat{n}$ is taken to be $(-1,-1,-1)$. For $\epsilon_{R_6} = 1$ case, the positive eigenvalue of $G_1 G_{R_6}^3$ appears with the eigen vector $(1,0,0)$. So, $\phi(0,0,A)$ can be taken as $(1,0,0)$ and the resulting RMO is the octahedral state state which has six sub-lattices and the spins are pointing towards the corner of an octahedra as shown in the Fig. 4.16. The magnetic unit-cell contains 12 sites.

Now, $\epsilon_{R_6} = -1$ case is the most interesting one. Positive eigenvalues of $G_1 G_{R_6}^3$ appears with the eigenvectors $(0,0,1)$ and $(0,1,0)$. So, any linear combination of these two vector can be chosen as $\phi(0,0,A)$. Here, we choose $\phi(0,0,A) = (0, \cos(\pi c), \sin(\pi c))$ where c is a continuous parameter. As we increase the value of c, starting from -1 to $+1$, we get a series of regular structures. For $c = 0$, the RMO corresponds to octahedral state with six sub-lattices as shown in the Fig. 4.16. As we increase the value of c to $1/4$ we get cuboc1 state as shown in the Fig. 4.17. If we change the value of c further at $c = -1/4$ or $3/4$, we get the cuboc2 state, as shown in Fig. 4.18. If we change the value of c further and take $\phi(0,0,A) = (0, \cos(\Phi), \sin(\Phi))$ where Φ is the golden ratio, we get the icosahedron1 structure as shown in the Fig. 4.19. Now, if we change the value of c to $-\Phi/\pi$ or $1 - \Phi/\pi$, we have icosahedron2 structure as shown in the Fig. 4.20. Finally, at $c = 1/2$ and $c = 1$ the octahedral structure is restored. Now, we list all the possible

RMOs corresponding to each of the algebraic symmetry groups in case of triangular and kagome lattice for the wallpaper group $p6$. Details of these states are given in the Discussion section. ('×' mark implies there is no RMO corresponding to the algebraic symmetry group)

No.	G_1	G_2	G_6	$\hat{n}$	Triangular	Kagome
1	I	I	I	Any	F	F
			-I	Any	×	×
2	I	I	$R(\hat{n},\frac{\pi}{3})$	Any	F	F
			$-R(\hat{n},\frac{\pi}{3})$	Any	×	$Q=0$ (P)
3	I	I	$R(\hat{n},\frac{2\pi}{3})$	Any	F	$Q=0$(U), F
			$-R(\hat{n},\frac{2\pi}{3})$	Any	×	×
4	I	I	$R(\hat{n},\pi)$	Any	F	F
			$-R(\hat{n},\pi)$	Any	F	F
5	$R(\hat{n},\frac{2\pi}{3})$	$R(\hat{n},\frac{2\pi}{3})$	$R(\hat{n}_6,\pi)$	$\hat{n}_6\perp\hat{n}$	P	$\sqrt{3}\times\sqrt{3}$
			$-R(\hat{n}_6,\pi)$	$\hat{n}_6\perp\hat{n}$	U	$\sqrt{3}\times\sqrt{3}$ (U),F
6	$R(\hat{x},\pi)$	$R(\hat{y},\pi)$	$R(\hat{n},\pi)$	$\frac{-1}{\sqrt{3}}(1,1,1)$	T	O
			$-R(\hat{n},\pi)$	$\frac{-1}{\sqrt{3}}(1,1,1)$	×	O, C_1, I_1, C_2, I_2

Table 4.1: List of regular magnetic orders in $p6$ wallpaper group.

4.4 $p3$ group

For this wallpaper group, the lattice symmetry group $\mathcal{G}_\mathcal{L}$ is generated by the three generators given by T_1, T_2 and R_3 where T_1, T_2 are two translations, R_3 is the three fold rotation about the origin as shown in the Fig. 4.4. Like previous case the spin rotation group remains $O(3)$ and the unbroken spin symmetry group G^s_ϕ is also chosen to be $\{I\}$. The action of R_3 on lattice site (r_1, r_2) is given by

$$R_3 : (r_1, r_2) \;\rightarrow\; (-r_2, r_1 - r_2) \tag{4.16}$$

Now, we can write the product of generators in the following form $R_3^r T_1^{t_1} T_2^{t_2}$ where $r = 0, 1, 2$ and $t_1, t_2 \in \mathbb{Z}_2$.

$$T_1T_2 = T_2T_1 \tag{4.17}$$
$$R_3T_1 = T_2R_3 \tag{4.18}$$
$$R_3T_2 = T_2^{-1}T_1^{-1}R_3 \tag{4.19}$$
$$R_3^3 = I \tag{4.20}$$

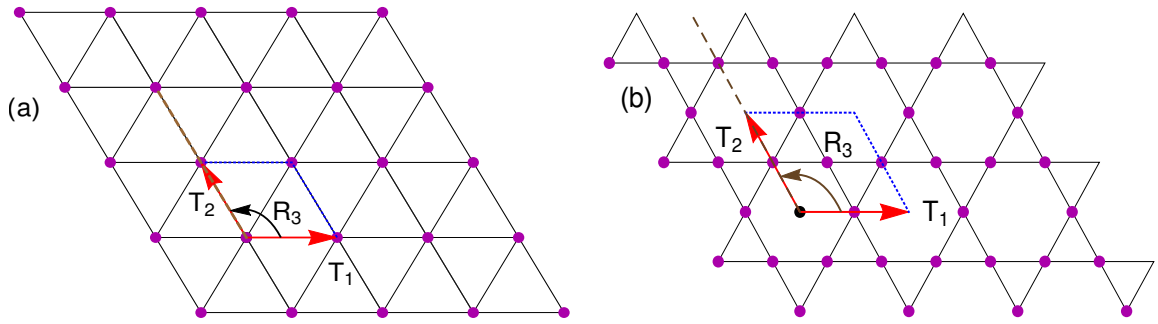

Figure 4.4: Generators of $p3$ wallpaper group. (a) Triangular lattice (b) Kagome lattice

Now, the images by $G \in \mathcal{G}^A$ of the generators of the lattice symmetry group must satisfy the same algebraic constraints. So, we have the following equations

$$G_{T_1}G_{T_2} = G_{T_2}G_{T_1} \tag{4.21a}$$
$$G_{R_3}G_{T_1} = G_{T_2}G_{R_3} \tag{4.21b}$$
$$G_{R_3}G_{T_2} = G_{T_2}^{-1}G_{T_1}^{-1}G_{R_3} \tag{4.21c}$$
$$G_{R_3}^3 = I \tag{4.21d}$$

Here ϵ_{R_3} can only be $+1$. Solving the above equations we get the following solutions

$$\text{(i)} \quad G_{T_1} = I, G_{T_2} = I, \quad \text{and} \quad G_{R_3} = I \tag{4.22a}$$
$$\text{(ii)} \quad G_{T_1} = I, G_{T_2} = I, \quad \text{and} \quad G_{R_3} = R(\hat{n}, \frac{2\pi}{3}) \tag{4.22b}$$
$$\text{(iii)} \quad G_{T_1} = R(\hat{n}, \frac{2\pi}{3}), G_{T_2} = R(\hat{n}, \frac{2\pi}{3}), \quad \text{and} \quad G_{R_3} = I \tag{4.22c}$$
$$\text{(iv)} \quad G_{T_1} = R(\hat{n}, \frac{2\pi}{3}), G_{T_2} = R(\hat{n}, \frac{2\pi}{3}), \quad \text{and} \quad G_{R_3} = R(\hat{n}, \frac{2\pi}{3}) \tag{4.22d}$$
$$\text{(v)} \quad G_{T_1} = R(\hat{n}, \frac{2\pi}{3}), G_{T_2} = R(\hat{n}, \frac{2\pi}{3}), \quad \text{and} \quad G_{R_3} = R(-\hat{n}, \frac{2\pi}{3}) \tag{4.22e}$$
$$\text{(vi)} \quad G_{T_1} = R(\hat{x}, \pi), G_{T_2} = R(\hat{y}, \pi) \text{ and } G_{R_3} = R(\hat{n}, \frac{2\pi}{3}), \hat{n} = (1,1,1) \tag{4.22f}$$

4.4.1 RMOs in triangular lattice

Let us consider that the spin configuration at starting point is $\phi(0,0)$. So, the spin configuration at any arbitrary site with oblique co-ordinate (m,n) is given by

$$\phi(m,n) = G_{T_1}^m G_{T_2}^n \phi(0,0) \tag{4.23}$$

Under R_3 rotation, we must have,

$$\phi(m,n) = G_{R_3}\phi(n-m,-m) \tag{4.24}$$

After some algebra we get the following condition

$$G_{T_1}^m G_{T_2}^n \phi(0,0) = G_{T_1}^m G_{T_2}^n G_{R_3}\phi(0,0) \tag{4.25}$$

In the last step we have used the fact that $G_{R_3}G_{T_1}G_{R_3}^{-1} = G_{T_2}$ and $G_{R_3}G_{R_2}G_{R_3}^{1} = G_{T_1}^{-1}G_{T_2^{-1}}$. Thus $\phi(0,0)$ becomes the eigenvectors of G_{R_3} with eigenvalue $+1$. Now, we can list the possible RMOs for $p3$ group in case triangular lattice

(i) $G_{T_1} = G_{T_2} = G_{R_3} = I$. Then, $\phi(m,n) = \phi(0,0)\ \forall\ m,n \in \mathbb{Z}$, thus the spin arrangement is ferromagnetic. Because $G_{R_3} = I$, $\phi(0,0)$ can be any vector.

(ii) $G_{T_1} = G_{T_2} = I$. Then, $\phi(m,n) = \phi(0,0)\ \forall\ m,n \in \mathbb{Z}$, thus the spin arrangement is ferromagnetic. Because $G_{R_3} = R(\hat{n}, 2\pi/3)$, $\phi(0,0) = \pm\hat{n}$

(iii) $G_{T_1} = G_{T_2} = R(\hat{n}, 2\pi/3)$. Because $G_{R_3} = I$, $\phi(0,0)$ can be any vector. Let, $\phi(0,0) = p\hat{n} + q\hat{t}$ where $\hat{t} \perp \hat{n}$ then

$$\phi(m,n) = R(\hat{n}, 2\pi/3)^{m+n} \quad \phi(0,0) = p\hat{n} + qR(\hat{n}, 2\pi/3)^{m+n}\hat{t}$$

The resulting RMO is a umbrella state which also includes ferromagnetic state.

(iv) Since $G_{R_3} = R(\hat{n}, 2\pi/3)$, $\phi(0,0) = \pm\hat{n}$. Then

$$\phi(m,n) = R(\hat{n}, 2\pi/3)^{m+n} \quad \phi(0,0) = \pm\hat{n}$$

So, the spin arrangement must be ferromagnetic.

(v) This case is similar to the previous one. The spin arrangement must be ferromagnetic.

(vi) Since $G_{R_3} = R(\hat{w}, 2\pi/3)$, Thus $\phi(0,0) = \pm\hat{w}$. Then, $\phi(m,n) = R_x^m R_y^n \hat{w}$

$$\phi(m,n) = \begin{cases} \frac{1}{\sqrt{3}}(1,1,1) & \text{for } m,n \text{ even} \\ \frac{1}{\sqrt{3}}(-1,1,-1) & \text{for } m \text{ even } n \text{ odd} \\ \frac{1}{\sqrt{3}}(1,-1,-1) & \text{for } m \text{ odd } n \text{ even} \\ \frac{1}{\sqrt{3}}(-1,-1,1) & \text{for } m,n \text{ odd} \end{cases}$$

This implies tetrahedral spin arrangement.

4.4.2 RMOs in kagome lattice

Let us consider three sublattices A, B and C are located at $\frac{1}{2}\vec{a}$, $\frac{1}{2}\vec{b}$ and $-\frac{1}{2}(\vec{a}+\vec{b})$. Consider an arbitrary lattice point with sublattice index μ in a unit cell with left bottom corner at $m\vec{a}+n\vec{b}$. Clearly

$$\phi(m,n,B) = G_{R_3}\phi(n-m,-m,A) = G_{R_3}G_{T_1}^{n-m}G_{T_2}^{-m}\phi(0,0,A) \tag{4.26}$$

After doing some algebra we get,

$$G_{T_2}^{n}G_{T_1}^{m}\phi(0,0,B) = G_{T_2}^{n}G_{T_1}^{m}G_{R_3}\phi(0,0,A) \tag{4.27}$$

Thus we get,

$$\phi(0,0,A) = G_{R_3}\phi(0,0,C) = G_{R_3}^{2}\phi(0,0,B) = G_{R_3}^{3}\phi(0,0,A) \tag{4.28}$$

This implies that $\phi(0,0,A)$ must be an eigenvector of $G_{R_3}^3$, which is identity in all cases. Therefore there is no restriction on $\phi(0,0,\mu)$. Using this, we can calculate the spin arrangement for the entire lattice.
(i) $G_{T_1} = G_{T_2} = G_{R_3} = I$. Then, $\phi(m,n,\mu) = \phi(0,0,A)\ \forall\ m,n,\mu \in \mathbb{Z}$ where μ is the sub-lattice index, thus the spin arrangement is ferromagnetic as shown in Fig. 4.11.
(ii) $G_{T_1} = G_{T_2} = I$. Then, $\phi(m,n,\mu) = \phi(0,0,A)\ \forall\ m,n,\mu \in \mathbb{Z}$

$$\begin{aligned}
\phi(m,n,A) &= \phi(0,0,A)\\
\phi(m,n,B) &= R(\hat{n},\frac{2\pi}{3})\phi(0,0,A)\\
\phi(m,n,c) &= R(\hat{n},\frac{2\pi}{3})\phi(0,0,B)
\end{aligned}$$

$\forall\ m,n \in \mathbb{Z}$ thus arrangement is $Q=0$ umbrella state which includes ferromagnetic and planar combinations.
(iii) $G_{T_1} = G_{T_2} = R(\hat{n},\frac{2\pi}{3})$. As $G_{R_3} = I$, $\phi(0,0,A) = \phi(0,0,B) = \phi(0,0,C)$ can be any vector. Let, $\phi(0,0) = p\hat{n} + q\hat{t}$ where $\hat{t} \perp \hat{n}$ then

$$\phi(m,n,\mu) = R(\hat{n},2\pi/3)^{m+n}\phi(0,0,\mu)$$

This gives rise to $\sqrt{3}\times\sqrt{3}$ umbrella state which includes the planar state and as well as ferromagnetic state.
(iv) $G_{T_1} = G_{T_2} = G_{R_3} = R(\hat{n},\frac{2\pi}{3})$. Here there is no restriction on $\phi(0,0,A)$, so we can choose any vector. In this case we found a new RMO, we call it type-I umrella

structure as shown in the Fig. 4.21.
(v) $G_{T_1} = G_{T_2} = G_{R_3} = R(-\hat{n}, \frac{2\pi}{3})$. Here also, there is no restriction on $\phi(0,0,A)$, so we can choose any vector. In this case we found a new RMO, we call it type-II umbrella structure as shown in the Fig. 4.22.
(vi) This case is most interesting. Lack of restriction on $\phi(0,0,A)$ results in a series of regular order in this case. For example, if we choose $\phi(0,0,A)$ to be along the $(1,0,0)$ direction, then the resulting RMO is Octahedral. For $(1,1,1)$ direction we have got tetrahedral. For $(0,1,1)$ case we have found cuboc1 whereas along $(1,1,0)$ direction we have got cuboc2 state. If we take $\phi(0,0,A) = (0, \cos(\Phi), \sin(\Phi))$ where Φ is the golden ratio, we get the icosahedron structure. We call it the icosahedron1 structure. As we discussed earlier in the case of p_6, if we change the sign of Φ, we get another kind of icosahedron state. We call it icosahedron2 state.

Finally, we list all the possible RMOs corresponding to each of the mapping $G \in \mathcal{G}^A$ in case of triangular and kagome lattice for the wallpaper group $p3$. Details of these states are given in the Discussion section.

No.	G_{T_1}	G_{T_2}	G_{R_3}	Direction	Triangular	Kagome
1	I	I	I	-	F	F
2	I	I	$R(\hat{n}, \frac{2\pi}{3})$	Any	F	F,U
3	$R(\hat{n}, \frac{2\pi}{3})$	$R(\hat{n}, \frac{2\pi}{3})$	I	Any	F,U	$\sqrt{3} \times \sqrt{3}$(U)
4	$R(\hat{n}, \frac{2\pi}{3})$	$R(\hat{n}, \frac{2\pi}{3})$	$R(\hat{n}, \frac{2\pi}{3})$	Any	F	U_1
5	$R(\hat{n}, \frac{2\pi}{3})$	$R(\hat{n}, \frac{2\pi}{3})$	$R(-\hat{n}, \frac{2\pi}{3})$	Any	F	U_2
6	$R(\hat{x}, \pi)$	$R(\hat{y}, \pi)$	$R(\hat{w}, \frac{2\pi}{3})$	$\hat{w} = (1,1,1)$	T	T, O, C_1, C_2, I_1, I_2

Table 4.2: List of regular magnetic orders in $p3$ wallpaper group

4.5 $p3m1$ group

In this wallpaper group, the lattice symmetry group $\mathcal{G}_\mathcal{L}$ is generated by four generators T_1, T_2, R_3 and σ where T_1, T_2 are two translations, R_3 is the three fold rotation about the origin as shown in the Fig. 4.5 and σ is the reflection about plane which is at 30^o with respect to T_2 axis. Like previous case the spin rotation group remains $O(3)$ and the unbroken spin symmetry group G^s_ϕ is also chosen to be $\{I\}$. The action of σ on lattice site (r_1, r_2) is given by

$$\sigma : (r_1, r_2) \quad \rightarrow \quad (r_1, r_1 - r_2) \tag{4.29}$$

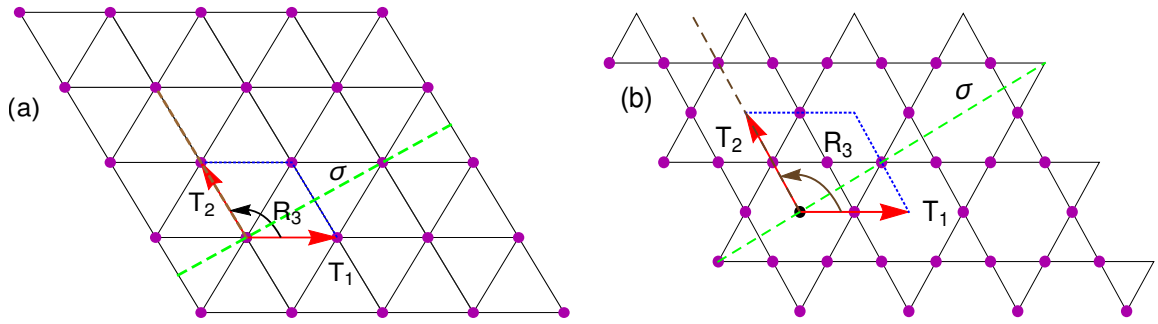

Figure 4.5: Generators of $p3m1$ wallpaper group. (a) Triangular lattice (b) Kagome lattice

Now, we can write product of generators in the following form $\sigma^s R_3^r T_1^{t_1} T_2^{t_2}$ where $r = 0, 1, 2$, $s = 0, 1$ and $t_1, t_2 \in \mathbb{Z}_2$. The relations between the generators are

$$T_1T_2 = T_2T_1 \tag{4.30a}$$
$$T_1R_3 = R_3R_1^{-1}R_2^{-1} \tag{4.30b}$$
$$T_2R_3 = R_3T_1 \tag{4.30c}$$
$$T_2\sigma = \sigma T_2^{-1} \tag{4.30d}$$
$$T_1\sigma = \sigma T_1T_2 \tag{4.30e}$$
$$R_3\sigma = \sigma R_3^2 \tag{4.30f}$$
$$R_3^3 = I \tag{4.30g}$$
$$\sigma^2 = I \tag{4.30h}$$

Now, the images by $G \in \mathcal{G}^A$ of the generators of the lattice symmetry group must satisfy the same algebraic constraints. So, we have following equations

$$G_1G_2 = G_2G_1 \tag{4.31a}$$
$$G_1G_3 = G_3G_1^{-1}G_2^{-1} \tag{4.31b}$$
$$G_2G_3 = G_3G_1 \tag{4.31c}$$
$$G_2G_\sigma = G_\sigma G_2^{-1} \tag{4.31d}$$
$$G_1G_\sigma = G_\sigma G_1G_2 \tag{4.31e}$$
$$G_3G_\sigma = G_\sigma G_3^2 \tag{4.31f}$$
$$G_3^3 = I \tag{4.31g}$$
$$G_\sigma^2 = I \tag{4.31h}$$

Here, we see that ϵ_σ can take values ± 1. In this case we get the following solutions

(i) $G_{T_1} = I, G_{T_2} = I, G_{R_3} = I$ and $G_\sigma = \epsilon_\sigma I$ (4.32a)

(ii) $G_{T_1} = I, G_{T_2} = I, G_{R_3} = I$ and $G_\sigma = \epsilon_\sigma R(\hat{n}_\sigma, \pi)$ (4.32b)

(iii) $G_{T_1} = I, G_{T_2} = I, G_{R_3} = I$ and $G_\sigma = \epsilon_\sigma R(\hat{n}_\sigma, \pi)$ (4.32c)

(iv) $G_{T_1} = G_{T_2} = R(\hat{n}, \frac{2\pi}{3}), G_{R_3} = I$ and $G_\sigma = \epsilon_\sigma R(\hat{n}_\sigma, \pi)$ where $\hat{n}_\sigma \perp \hat{n}$ (4.32d)

(v) $G_{T_1} = R(\hat{x}, \pi), G_{T_2} = R(\hat{y}, \pi), G_{R_3} = R(\hat{w}, \frac{2\pi}{3})$ and $G_\sigma = \epsilon_\sigma R(\hat{n}, \pi)$, (4.32e)
where $\hat{n} = (-1, 0, 1)$ and $\hat{w} = (1, 1, 1)$

4.5.1 RMOs in triangular lattice

Like previous cases, we can show that $\phi(0, 0)$ must be an eigenvector of not only G_{R_3} but also G_σ corresponding to the positive of eigenvalue. If the eigenvector does not match, then there will not be any RMO. As prescribed in case of $p6$ and $p3$, here we obtained ferromagnetic state, planar state, umbrella state and tetrahedral state for different algebraic symmetry groups as shown in the Table. 4.3.

4.5.2 RMOs in kagome lattice

In case of kagome lattice we can show that $\phi(0, 0, A)$ must be an eigenvector of $G_{T_1} G_\sigma G_{R_3}^2$ associated with positive eigenvalue.
It is easy to see that Case(i) and case(ii) leads to the ferromagnetic state except for the case(i) with $G_\sigma = -I$ where all the eigenvalues of $G_{T_1} G_\sigma G_{R_3}^2$ are negative.
(iii) In this case, we choose $\hat{n}$ along the $(1, 1, 1)$ direction. Now as $\hat{n} \perp \hat{n}_\sigma$, we choose $\hat{n}_\sigma$ along (0,1,-1) direction. For $\epsilon_\sigma = +1$, positive eigenvalue of $G_{T_1} G_\sigma G_{R_3}^2$ associated with the eigenvector (-1,1,0). So, we can take $\phi(0, 0, A)$along the direction (-1,1,0). So, the resulting RMO is $\sqrt{3} \times \sqrt{3}$ state and it is planar containing three sub-lattices.

For $\epsilon_\sigma = -1$, we get two eigenvectors of $G_{T_1} G_\sigma G_{R_3}^2$ with positive eigenvalues. The eigenvectors are $(0, 0, 1)$ and $(1, 1, 0)$. Any linear combination of these two vectors can be taken as $\phi(0, 0, A)$. The resulting RMO is the $\sqrt{3} \times \sqrt{3}$ umbrella state which also contains planar spin configuration and also ferromagnetic state.
(iv) In this case, we take $\hat{w}$ to be along $(1, 1, 1)$ direction and $\hat{n}$ along the $(-1, 0, 1)$ direction. So, for $\epsilon_\sigma = +1$, we get positive eigenvalue of $G_{T_1} G_\sigma G_{R_3}^2$ matrix with eigenvector $(0, 1, 1)$. So, $\phi(0, 0, A)$ can be taken along $(0, 1, 1)$ direction. In this case the resulting RMO is the cuboc1 state.

Now, $\epsilon_\sigma = -1$ case is the most interesting one. Here the positive eigenvalues of $G_{T_1}G_\sigma G_{R_3}^2$ appears with the eigenvectors $(0,-1,1)$ and $(1,0,0)$. So, any linear combination of these vectors can be taken as $\phi(0,0,A)$. In this case, we take $\phi(0,0,A) = \{\cos(\pi c), -\sin(\pi c)/\sqrt{2}, \sin(\pi c)/\sqrt{2}\}$. Depending on the values of c, we get a series of regular structures. For example, $c = -1, 0$ and 1 we get octahedral state with six sub-lattices. For $c = -1/2$, and $1/2$ we get cuboc2 state where the neighboring spins are at an angle $\pi/3$ to each other. For $c = \tan^{-1}(\phi)/\pi$ we get icosahedron1 state and for $c = -\tan^{-1}(\phi)/\pi$ we get icosahedron2 state, where Φ is the golden ratio. For $c = \tan^{-1}(\sqrt{2})/\pi$ we have type-I extended tetrahedral state with 4 sub-lattice and For $c = -\tan^{-1}(\sqrt{2})/\pi$ we have type-II extended tetrahedral state with 4 sub-lattice. Each of these structure has 12 site unit cell and each of the sub-lattice is pointing towards the corner of tetrahedron.

Finally, we list all the possible regular magnetic order corresponding to each of the algebraic symmetry group for $p3m1$ group. Details of these states are given in the Discussion section. ('×' mark implies there is no RMO corresponding to the algebraic symmetry group)

No.	G_1	G_2	G_3	G_σ	$\hat{n}$	Triangular	Kagome
1	I	I	I	I	-	F	F
				-I	-	×	×
2	I	I	I	$R(\hat{n},\pi)$	Any	F	F
				-$R(\hat{n},\pi)$	Any	F	F
3	$R(\hat{n},\frac{2\pi}{3})$	$R(\hat{n},\frac{2\pi}{3})$	I	$R(\hat{n}_\sigma,\pi)$	$\hat{n}_\sigma \perp \hat{n}$	P	$\sqrt{3}\times\sqrt{3}$(p)
				-$R(\hat{n}_\sigma,\pi)$	$\hat{n}_\sigma \perp \hat{n}$	U	$\sqrt{3}\times\sqrt{3}$ (U),F
4	$R(\hat{x},\pi)$	$R(\hat{y},\pi)$	$R(\hat{w},\frac{2\pi}{3})$	$R(\hat{n},\pi)$	(-1,0,1)	×	C_1
				-$R(\hat{n},\pi)$	(-1,0,1)	T	$O, I_1, T_1, I_2, T_2, C_2$

Table 4.3: List of regular magnetic orders in $p3m1$ wallpaper group

4.6 $p31m$ group

In this wallpaper group the lattice symmetry group S_L is generated by four generators T_1, T_2, R_3 and σ, where T_1, T_2 are the translation, R_3 is the 3-fold rotation and σ is a mirror plane parallel to T_1 axis as shown in the Fig, 4.6. Here too, the spin rotation group remains $O(3)$ and the unbroken spin symmetry group G_ϕ^s is also chosen to be $\{I\}$.The action of σ on lattice site (r_1, r_2) is given by

$$\sigma : (r_1, r_2) \quad \rightarrow \quad (r_1 - r_2, -r_2) \tag{4.33}$$

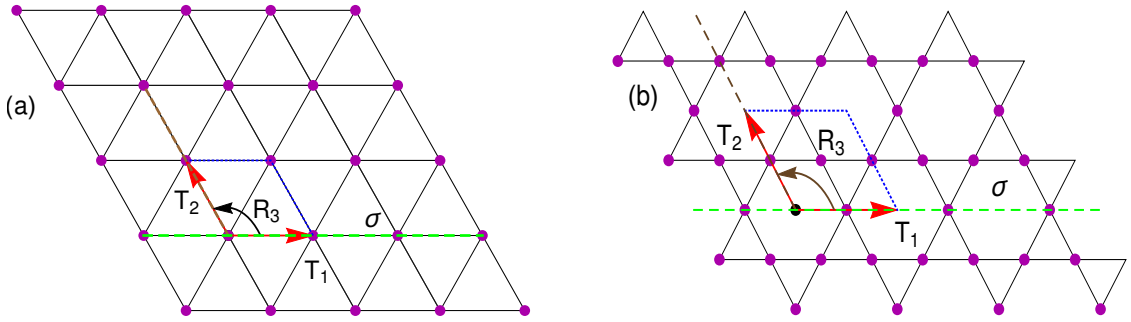

Figure 4.6: Generators of $p31m$ wallpaper group. (a) Triangular lattice (b) Kagome lattice

Now, we can write product of generators in the following form $\sigma^s R_3^r T_1^{t_1} T_2^{t_2}$ where $r = 0, 1, 2$, $s = 0, 1$ and $t_1, t_2 \in \mathbb{Z}_2$. The relation between the generators are given by the following equations

$$T_1T_2 = T_2T_1 \tag{4.34a}$$
$$T_1T_3 = R_3T_1^{-1}T_2^{-1} \tag{4.34b}$$
$$T_2R_3 = R_3T_1 \tag{4.34c}$$
$$T_2\sigma = \sigma T_1^{-1}T_2^{-1} \tag{4.34d}$$
$$T_1\sigma = \sigma T_1 \tag{4.34e}$$
$$R_3\sigma = \sigma R_3^2 \tag{4.34f}$$
$$R_3^3 = I \tag{4.34g}$$
$$\sigma^2 = I \tag{4.34h}$$

Now, the images by $G \in \mathcal{G}^A$ of the generators of the lattice symmetry group must satisfy the same algebraic constraints. So, we have following equations

$$G_1G_2 = G_2G_1 \tag{4.35a}$$
$$G_1G_3 = G_3G_1^{-1}G_2^{-1} \tag{4.35b}$$
$$G_2G_3 = G_3G_1 \tag{4.35c}$$
$$G_2G_\sigma = G_\sigma G_1^{-1}G_2^{-1} \tag{4.35d}$$
$$G_1G_\sigma = G_\sigma G_1 \tag{4.35e}$$
$$G_3G_\sigma = G_\sigma G_3^2 \tag{4.35f}$$
$$G_3^3 = I \tag{4.35g}$$
$$G_\sigma^2 = I \tag{4.35h}$$

Here, we see that ϵ_σ can take values ± 1. For $p31m$ group we get the following solutions

$$\text{(i)} \quad G_{T_1} = I, G_{T_2} = I, G_{R_3} = I \quad \text{and} \quad G_\sigma = \epsilon_\sigma I \tag{4.36a}$$

$$\text{(ii)} \quad G_{T_1} = I, G_{T_2} = I, G_{R_3} = I \quad \text{and} \quad G_\sigma = \epsilon_\sigma R(\hat{n}_\sigma, \pi) \tag{4.36b}$$

$$\text{(iii)} \quad G_{T_1} = I, G_{T_2} = I, G_{R_3} = I \quad \text{and} \quad G_\sigma = \epsilon_\sigma R(\hat{n}_\sigma, \pi) \tag{4.36c}$$

$$\text{(iv)} \quad G_{T_1} = R(\hat{n}, \frac{2\pi}{3}), G_{T_2} = R(\hat{n}, \frac{2\pi}{3}), G_{R_3} = I \quad \text{and} \quad G_\sigma = \epsilon_\sigma R(\hat{n}_\sigma, \pi), \quad \text{where} \quad \hat{n}_\sigma = \hat{n} \tag{4.36d}$$

$$\text{(v)} \quad G_{T_1} = R(\hat{x}, \pi), G_{T_2} = R(\hat{y}, \pi), G_{R_3} = R(\hat{w}, \frac{2\pi}{3}) \text{ and } G_\sigma = \epsilon_\sigma R(\hat{n}, \pi), \quad \text{where} \quad \hat{n} = (0, -1, 1) \quad \text{and} \quad \hat{w} = (1, 1, 1) \tag{4.36e}$$

4.6.1 RMOs in triangular lattice

Like previous cases, we can show that $\phi(0, 0)$ must be an eigenvector or linear combination of the eigenvectors of not only G_{R_3} but also G_σ corresponding to the positive eigenvalues. If there are no common eigenvector between them, then there will not be any RMO. For this $p3m1$ group, we obtained Ferromagnetic, umbrella state, which includes planar structure as well as the ferromagnetic and tetrahedral state for different algebraic symmetry groups as shown in the Table. 4.4

4.6.2 RMOs in kagome lattice

For kagome lattice we can show that $\phi(0, 0, A)$ can be chosen as the eigenvector of $G^2_{R_3} G_\sigma G^{-1}_{R_3}$ corresponding to the positive eigenvalue.
It is easy to see that case(i), and case(ii) will lead to ferromagnetic spin arrangement except for the first case where $G_\sigma = -I$.
(iii) In this case we choose, $\hat{n}$ along $(1, 1, 1)$ direction. Since G_{R_3} and G_σ both are identity, all the eigenvalues of $G^2_{R_3} G_\sigma G^{-1}_{R_3}$ are positive for $\epsilon_\sigma = +1$. In this case, we obtain the $\sqrt{3} \times \sqrt{3}$ umbrella state with planar spin configuration and also ferromagnetic state.

Similarly, for $\epsilon_\sigma = -1$, all the eigenvalues of $G^2_{R_3} G_\sigma G^{-1}_{R_3}$ are negative. In this there will not be any RMO.
(iv) Here, for $\epsilon_\sigma = +1$, positive eigenvalue of $G^2_{R_3} G_\sigma G^{-1}_{R_3}$ appears with the eigenvectors $(1, 1, 1)$. The resulting RMO is ferromagnetic state.

For $\epsilon_\sigma = -1$, positive eigenvalue of $G^2_{R_3} G_\sigma G^{-1}_{R_3}$ appears with two eigenvectors

$(0,1,1)$ and $(1,0,0)$. So, any linear combination of these two vectors can be taken as the $\phi(0,0,A)$. Here we get $\sqrt{3}\times\sqrt{3}$ umbrella state with planar spin configuration and ferromagnetic state.
(v) In this case, $\epsilon_\sigma = +1$, positive eigenvalue of $G^2_{R_3} G_\sigma G^{-1}_{R_3}$ appears with the eigenvectors $(0,-1,1)$. The resulting RMO is cuboc2 state.

For $\epsilon_\sigma = -1$, positive eigenvalues of $G^2_{R_3} G_\sigma G^{-1}_{R_3}$ are associated with the eigenvectors $(0,1,1)$ and $(1,0,0)$. So we take the linear combination of these two vectors as $\phi(0,0,A)$. So, we take $\phi(0,0,A) = \{\cos(\pi c), \sin(\pi c)/\sqrt{2}, \sin(\pi c)/\sqrt{2}\}$. Depending on the values of c, we get a series of regular structures. For $c = -1, 0$ and 1 we get the octahedral state. For $c = \tan^{-1}(\sqrt{2})/\pi$ we have tetrahedral state with four sub-lattices. Again for $c = 1/2$ and $-1/2$ we get cuboc1 state with 12 sub-lattices. Finally, For $c = \tan^{-1}(\Phi)/\pi$ we get icosahedron1 state and for $c = -\tan^{-1}(\Phi)/\pi$ we get icosahedron2 state, where Φ is the golden ratio.

Finally, we list all the possible regular magnetic order corresponding to each of the algebraic symmetry group for $p31m$ group.Details of these states are given in the Discussion section. ('$\times$' mark implies there is no RMO corresponding to the algebraic symmetry group)

No.	G_1	G_2	G_3	G_σ	$\hat{n}$	Triangular	Kagome
1	I	I	I	I	-	F	F
				-I	-	$\times$	$\times$
2	I	I	I	$R(\hat{n},\pi)$	Any	F	F
				-$R(\hat{n},\pi)$	Any	F	F
3	$R(\hat{n},\frac{2\pi}{3})$	$R(\hat{n},\frac{2\pi}{3})$	I	I	Any	U	$\sqrt{3}\times\sqrt{3}$ (U),F
				-I	Any	$\times$	$\times$
4	$R(\hat{n},\frac{2\pi}{3})$	$R(\hat{n},\frac{2\pi}{3})$	I	$R(\hat{n}_\sigma,\pi)$	$\hat{n}_\sigma = \hat{n}$	$\times$	F
				-$R(\hat{n}_\sigma,\pi)$	$\hat{n}_\sigma = \hat{n}$	U	$\sqrt{3}\times\sqrt{3}$ (U),F
5	$R(\hat{x},\pi)$	$R(\hat{y},\pi)$	$R(\hat{w},\frac{2\pi}{3})$	$R(\hat{n},\pi)$	$(0,-1,1)$	$\times$	C_2
				-$R(\hat{n},\pi)$	$(0,-1,1)$	T	O, C_1, I_1, T, I_2

Table 4.4: List of regular magnetic orders in $p31m$ wallpaper group

4.7 Discussion

In this section, we will discuss the details of each of the states, found in all of the wallpaper groups as presented earlier.

4.7.1 Triangular lattice :

For triangular lattice, we have found the following states

(i) Ferromagnetic(F) state : In ferromagnetic state, all the spins are pointing in the same direction as shown in Fig. 4.7. The unit cell contains one site.

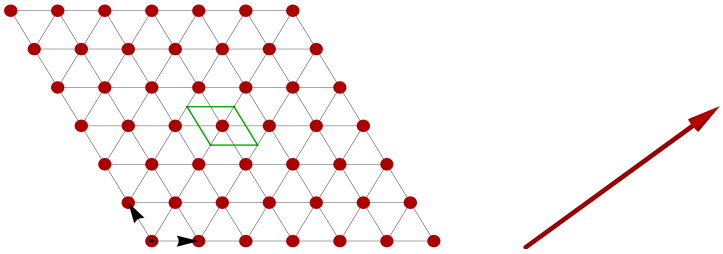

Figure 4.7: Ferromagnetic(F) state

(ii) Coplanar state : This state contains three sub-lattices and in each triangle, the spins are at an angel 120^o to each other lying in a plane as shown in the Fig. 4.8. Each of the sub-lattices are shown by different colors in the diagram and the unit cell contains three sites as shown by the green line.

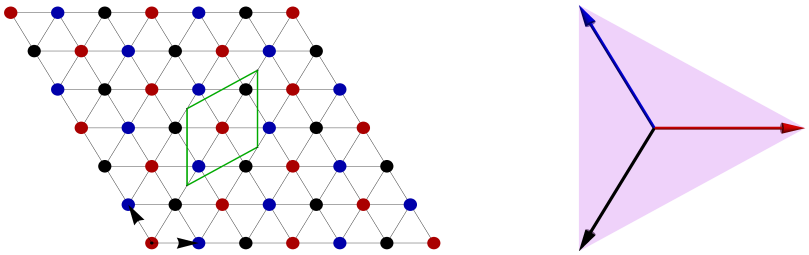

Figure 4.8: Coplanar state.

(iii) F umbrella state : This is a non-coplanar structure with three sub-lattices, where the relative angle between the spins are the same and also $\leq 120^o$. In this case, the spin arrangements interpolate between the ferromagnetic state and the coplanar state. Some intermediate state is shown in Fig. 4.9.

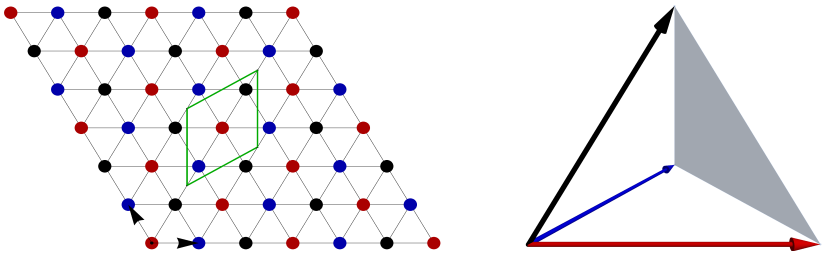

Figure 4.9: F umbrella state.

(iii) Tetrahedral(T) state : The tetrahedral has four sub-lattices, pointing towards the corner of a tetrahedron and the sub-lattices are shown by four different

colors in the Fig. 4.10. The sign of $\phi(0,0) = \pm(1,1,1)/\sqrt{3}$ determines the chirality of the spin configuration.

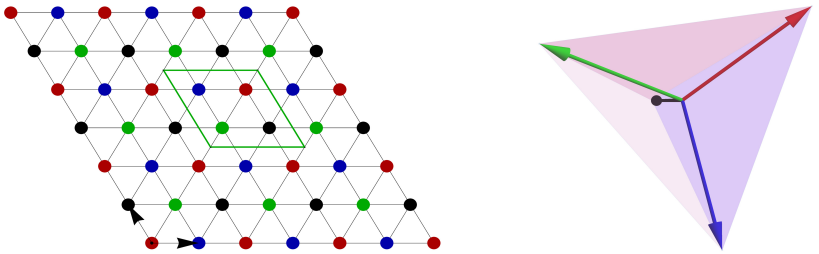

Figure 4.10: Tetrahedral state.

4.7.2 Kagome lattice :

For kagome lattice we have got the following states

(i) Ferromagnetic(F) state : In ferromagnetic state, all the spins are pointing in the same direction as shown in Fig. 4.11. The unit cell contains three sites, as shown by the green line in the diagram.

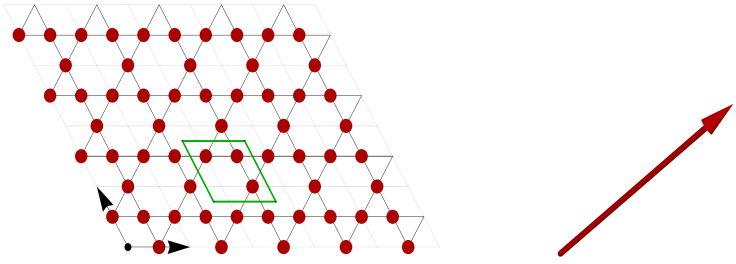

Figure 4.11: Ferromagnetic(F) state

(ii) $Q = 0$(P) state : $Q = 0$ planar state has three sub-lattices, and the spins are at an angle $2\pi/3$ to each other as shown in the Fig. 4.12. The unit-cell contains three sites, and the spins lie in the kagome plane. The unit cell is shown by the green lines in the diagram.

(iii) $Q = 0$(U) state : $Q = 0$ umbrella state has three sub-lattices and the relative angle between spins are identical. The angle varies from 0 to $2\pi/3$. If the relative angle between the spins is zero, it becomes ferromagnetic, whereas it becomes $Q = 0$ planar when the angle becomes $2\pi/3$. Some intermediate state is shown in Fig. 4.13. Here too, the unit-cell contains three sites, shown by three different colors.

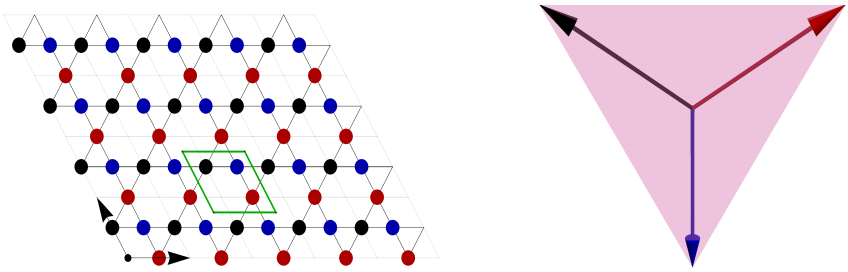

Figure 4.12: $Q = 0$ planar state

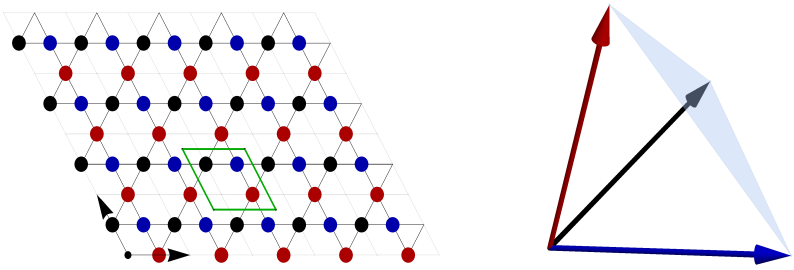

Figure 4.13: $Q = 0$ umbrella state

(iv) $\sqrt{3} \times \sqrt{3}$ (P) state : $\sqrt{3} \times \sqrt{3}$ planar state has three sub-lattices and the relative angle between the spins is $2\pi/3$. The unit cell contains nine sites as shown by green lines in Fig. 4.14.

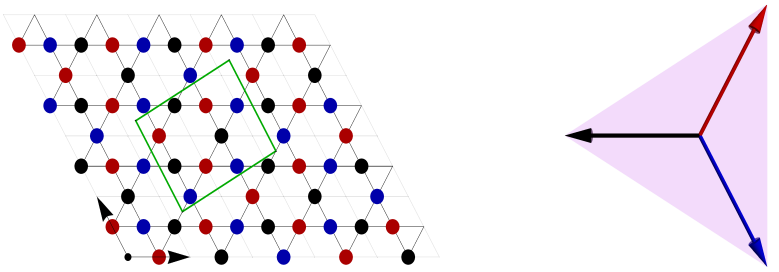

Figure 4.14: $\sqrt{3} \times \sqrt{3}$ planar state

(v) $\sqrt{3} \times \sqrt{3}$(U) state : This state is non-coplanar $\sqrt{3} \times \sqrt{3}$ with three sub-lattices. The unit cell contains nine sub-lattices as shown in the Fig. 4.15. In this case, the spin arrangements interpolates between the ferromagnetic state and the co-planar $\sqrt{3} \times \sqrt{3}$ state. Some intermediate state is shown in the Fig. 4.15.

(vi) Octahedral(O) state : The has six sub-lattices and the spins are pointing towards the corner of an octahedra. The unit cell contains tweleve sites and it is shown by green lines in the Fig. 4.16

(vii) Cuboc1(C_1) state : Cuboc1 state which has 12 sub-lattices and the spins

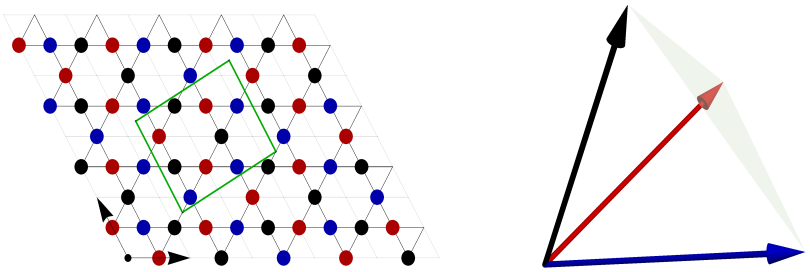

Figure 4.15: $\sqrt{3} \times \sqrt{3}$ umbrella state

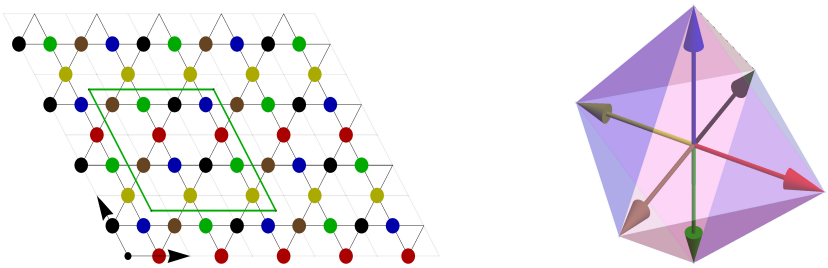

Figure 4.16: Octahedral state

are pointing towards the corner of a cuboctahedron as shown in the Fig. 4.17. In this case the relative angle between the neighboring spins are 120^o and the magnetic unit cell contains twelve sites. The sub-lattices are shown by different colors and the unit cell is shown by green lines in the diagram.

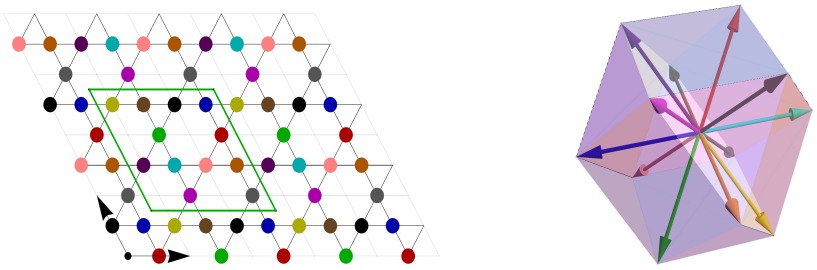

Figure 4.17: Cuboc1 state

(viii) Cuboc2(C_2) state : Cuboc2 state which has 12 sub-lattices and the spins are pointing towards the corner of a cuboctahedron as shown in the Fig. 4.18. In this case the relative angle between the neighboring spins are 60^o in contrast to cuboc1 state. The magnetic unit cell contains twelve sites.

(ix) Icosahedron1(I_1) state : The icosahedron1 state has 12 sub-lattices, and the spins are pointing towards the corner of an icosahedron. The unit-cell also contains 12 sites. The neighboring spins make an angle of 116.565^o to each other. It has 30

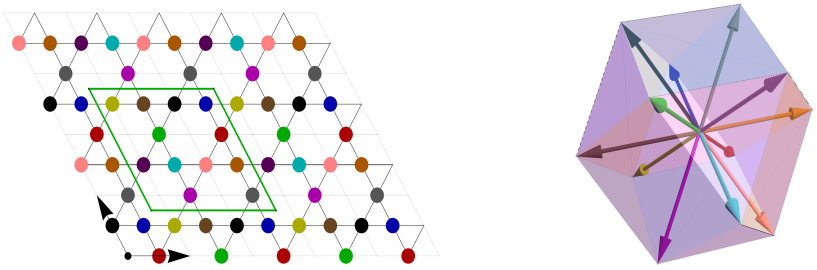

Figure 4.18: Cuboc2 state

edges, and 20 equilateral triangle faces with five triangles sharing a common vertex as shown in the Fig. 4.19

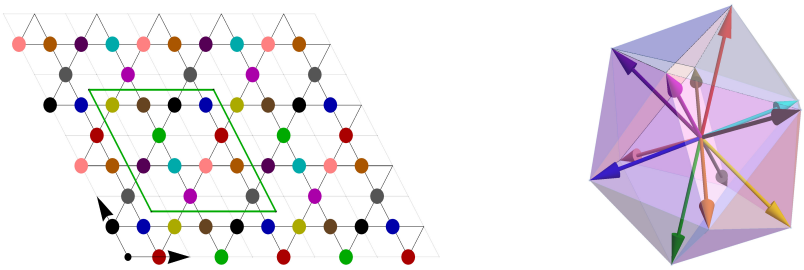

Figure 4.19: Icosahedron1 state

(x) Icosahedron2(I_2) state : In icosahedron2 structure, the neighboring spins are at 63.435^o to each other. Here, too the unit cell contains 12 sites and all the spins are pointing towards the corner of an icosahedron as shown in the Fig. 4.20

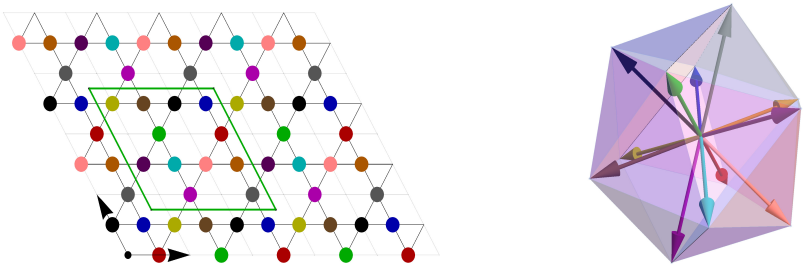

Figure 4.20: Icosahedron2 state

(xi) Type-I umbrella(U_1) state : This state has three sub-lattices and umbrella kind of structure which includes planar structure and ferromagnetic state. The relative angle between spins are identical, the angle varies from 0 to $2\pi/3$. Each of the sub-lattices occupy an up triangle as shown by different color in the Fig. 4.21. The unit cell is quite large which contains 27 sites and shown by green lines in the diagram.

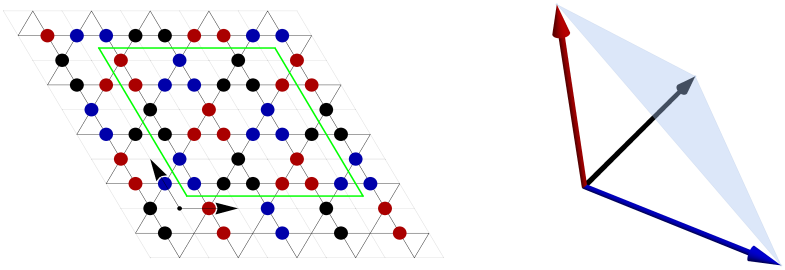

Figure 4.21: Type-I umbrella state

(xii) Type-II umbrella(U_2) state : This state is similar to the type-I umbrella state. Here each of the sub-lattices occupy an down triangle as shown by different color in the Fig. 4.22

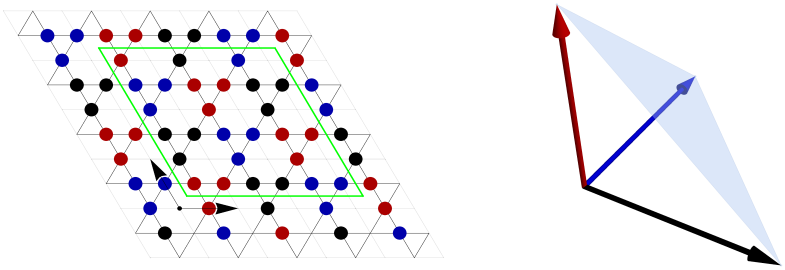

Figure 4.22: Type-II umbrella state

(xiii) Tetrahedral(T) state : This state has four sub-lattices and the spins are pointing towards the corner of a tetrahedron. The unit cell contains 12 sub-lattices as shown in the Fig. 4.23

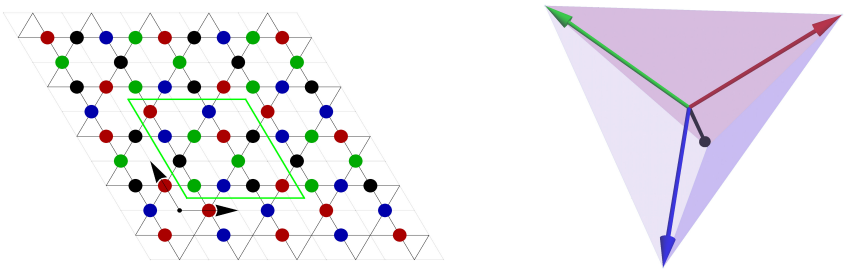

Figure 4.23: Tetrahedral state

(xiv) Type-I extended tetrahedral(T_1) state : This state has four sub-lattices. Each of the sub-lattices occupy an up triangle as shown by different color in the Fig. 4.24. The unit cell is quite large which contains 12 sites and shown by green lines in the diagram.

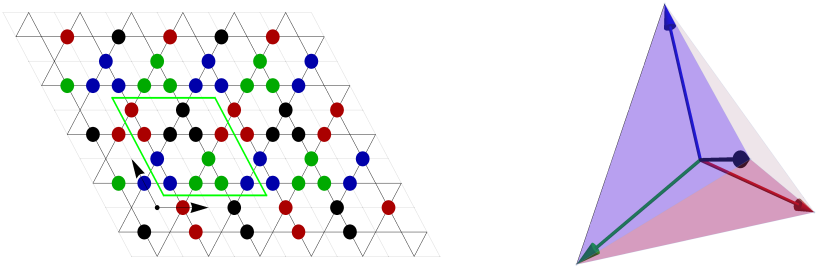

Figure 4.24: Type-I extended tetrahedral state

(xv) Type-II extended tetrahedral($\mathbf{T}_2$) state : This state is similar to type-II extended tetrahedral state. Here, each of the sub-lattices occupy an down triangle as shown by different color in the Fig. 4.25.

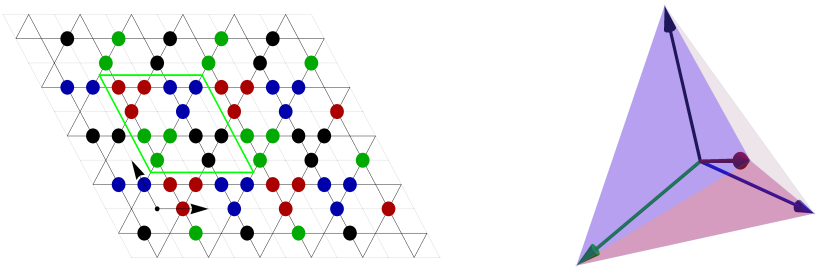

Figure 4.25: Type-II extended tetrahedral state

In this work, we have started with the unbroken symmetry group H_C^S as $\{I\}$ but other possibilities like $H_C^S = \mathbb{Z}_2$ or $O(2)$ which leads to the co-planar state and ferromagnetic state, is also included. So, one can easily do the exercise for other choices of H_c^S, but that would not lead to any other new RMOs.

In our study, we have considered the manifold $\mathcal{A} = S_2$ i.e., and the spins are treated as three-dimensional unit vectors. But, in the same footing, one can study other manifolds. For example nematic orders can be studied using the manifold $\mathcal{A} = S_2/\mathbb{Z}_2$ with spin symmetry group $S_S = O(3)$.

4.8 Conclusion

Based on the group theoretical approach, we have constructed a family of classical magnetic orders, termed as regular magnetic order in kagome and triangular lattice. This approach is introduced by Messio et al. [119] and is analogous to the Wen's classification of quantum spin liquids based on projective symmetry group [5]. Such RMOs can be constructed for any models on any lattice and hence a general method

to construct classical magnetic orders. It turns out that these states are a good candidate as a variational state to study the ground-state phase diagram for many spin systems. It also provides useful insights to the couplings present in a magnetic material by comparing the magnetic correlation where the range or strength of the interactions is not known.

In this study, we have extended the work of Messio et al [5] for other wallpaper groups, which includes kagome and triangular geometry. We have obtained a few new classical orders which are not reported earlier. The realization of these states as a ground state of specific spin models is the subject of future study.

4.9 Appendix

Theorem : *If a spin configuration ϕ is regular then the group $\mathcal{G}_\phi/\mathcal{G}_\phi^s$ is isomorphic to $\mathcal{G}_\mathcal{L}$.*

Proof : There are several steps in the proof.

(i) *Define mapping :* Let $\sigma \in \mathcal{G}_\mathcal{L}$ then, $\exists\ g\ \in O(3)$ such that $g\sigma \in G_\phi$. Define a mapping $\xi : \mathcal{G}_\mathcal{L} \to G_\phi/G_\phi^s$ such that

$$\xi : \sigma \mapsto (g\sigma)\ G_\phi^s \tag{4.37}$$

This is well defined mapping since if there are another $g_1 \in O(3)$ such that $g_1\sigma \in G_\phi$ then, $g_1\sigma \in (g\sigma)G_\phi^s$. To show this, note that $(g_1\sigma)^{-1} \in G_\phi$ and hence $(g_1\sigma)^{-1}g_1\sigma = g_1^{-1}g_1 \in G_\phi^s$. Thus, $g_1\sigma = \sigma g\ (g_1 g^{-1})$. Thus $g_1\sigma \in (g\sigma)\ G_\phi^s$

(ii) *To show that ξ is a homomorphism :* If σ_1 and σ_2 are two elements of $\mathcal{G}_\mathcal{L}$. Thus if $g_1\sigma_1 \in G_\phi$ and $g_2\sigma_2 \in G_\phi$, then clearly $(g_1\sigma_1)\ (g_2\sigma_2) \in G_\phi$. Thus clearly, ξ preserves the multiplication and hence it a homomorphism.

(iii) *To show that ξ is one to one :* If σ_1 and σ_2 are two elements of $\mathcal{G}_\mathcal{L}$ and if

$$\begin{aligned}(g_1\sigma_1)G_\phi^s &= (g_2\sigma_2)G_\phi^s \\ g_1\sigma_1 &= g_2\sigma_2 g \\ (g_1 g g_2^{-1})(\sigma_1\sigma_2^{-1}) &= e\end{aligned}$$

This can only happen when $\sigma_1 = \sigma_2$ and then $g_2^{-1}g$ must be in G_ϕ^s.

Chapter 5

$Q = 0$ Order in KHAF : A SBMFT Study

5.1 Introduction

Geometrically frustrated magnets are the potential candidate to host exotic ground states like quantum spin liquids, a state with fractional excitations, high entanglement, and without any broken symmetries even at $T = 0$ [1, 2, 109, 122]. The most promising candidate to possess spin liquid ground state is the spin 1/2 kagome lattice with vertex sharing triangles. Antiferromagnetic ordering of the spins on a kagome lattice is frustrated by the nature of the geometry of the lattice. The key features which make it suitable for the spin liquid ground state are its low dimensionality and a higher degree of frustration. The low value of spin leads to the large quantum fluctuation, hence preventing the ordered ground state [48, 55, 65, 110]. However, in search of material realizing quantum spin liquid ground state, materials tend to deviate from the perfect kagome structure due to the presence of disorder, structural distortion, Dzyaloshinskii-Moriya interaction(DMI) or other long-range interactions. However, a theoretical study reveals that the presence of minute perturbation may have a deep impact on the ground state manifold [73]. One of such perturbation which is very sensitive to the low-temperature magnetic structure of this frustrated magnets is DMI [6, 7]. DMI appears in a lattice where there is a lack of inversion symmetry between the two magnetic sites, was first introduced to explain the weak ferromagnetism in α-Fe_2O_3 [6]. The interaction term is of the form $H'_{ij} = \vec{D}_{ij} \cdot (\vec{\mathbf{S}}_i \times \vec{\mathbf{S}}_j)$ where $\vec{D}_{ij}$ is the Dzyaloshinskii-Moriya(DM) vector, the strength of the coupling and i, j are the site index. The DM vector $\vec{D}_{ij}$ lies on a mirror plane bisecting the bond joining the two magnetic sites i and j

In the experimental side, several materials were thought to be potential candidates for the kagome antiferromagnet (KAFM) to host a quantum spin liquid ground state like herbertsmithite [18], volborthite [95] and vesignieite [19]. Among all these, the mineral Herbertsmithite is found to be a geometrically perfect description of quantum kagome Heisenberg antiferromagnet(KHAF), which has been studied intensively [123]. This material does not show any sign of ordering down to 50 mk, which is 3000 times lower than the characteristic exchange energy. Herbertsmithite is strongly suspected of hosting a quantum spin liquid ground state with spinon excitations. [47, 84] Form ESR data, the measured value of the in-plane component of DMI, comes out as $0.01J$, whereas the out-of-plane of DMI is much larger $0.06J$ [112, 124]. Exact diagonal results predict that there may be quantum critical point $D_c = 0.1J$, at the one side $D < D_c$ there is moment free phase and on the other side $D > D_c$ there is Neel ordered phase. [74]

Unlike herbertsmithite, vesignieite shows a magnetic transition to $Q = 0$ magnetic order with the in-plane moments on the three sublattices oriented at 120^o with each other, at a surprisingly high temperature $T_N = 9K$. [19, 92, 93] ESR spectra reveal the presence of large DMI anistropy [125]. So, it is expected that the large value of DMI may lead to the $Q = 0$ magnetic structure i.e., the other side of the quantum critical point [91]. In contrast to herbertsmithite, the dominant anisotropy is the in-plane component of DMI. For vesignieite, the measured value of the in-plane component is found to be $0.19J$, and the out-of-plane component is $0.07J$, as indicated by ESR data analysis.

Apart from herbertsmithite, vesignieite, the compound $Nd_3Sb_3Mg_2O_{12}$ is also of much interest since it shows large canting angle $\eta = 30.6^o$ indicating the presence of large in-plane DMI, $D_p = 0.8J$ as predicted by Scheie et. al. [126]. However Laurell et al. [127] argued that the predicted value should be $D_p > 1.5$ to reproduce such a large canting angle. There are also interesting cases with even larger DMI as predicted from first principle calculation [128].

In this work, we study the ground state of the nearest neighbor Heisenberg model with added Dzyaloshinskii-Moriya interaction using the Schwinger boson mean-field theory(SBMFT) framework and numerically using exact diagonalization(ED) method up to cluster size $N = 30$. There are several SBMFT studies as well as an exact diagonalization study, which only focuses on the out-of-plane component od DMI [74, 76, 118, 129, 130]. In the present study, we consider the in-plane and the out-of-plane component of DMI both to study the ground-state phase diagram. We have compared the results obtained from these two different approaches.

The layout of this chapter is as follows. In sec. II, we discuss the model Hamiltonian and the orientation of the DM vector. In sec. III, we briefly describe the classical ground state of this model. In sec. IV, we present the Schwinger boson formalism. In sec. IV, we present the result obtained from the SBMFT approach. In sec. V, we discuss the exact diagonalization results of the proposed model. In sec. VI, we compare the results obtained from these two distinct approaches and discuss their relevance in the experiment. Finally, in sec. VII, we make the concluding remarks.

5.2 Model Hamiltonian

In this work, we have explored the model Hamiltonian of vesignieite, as obtained in the Ref. [93]. For vesignieite, they found that the strength of symmetric anisotropic exchange(AE) is comparable to the Dzyaloshinskii-Moriya interaction term and argued that since DMI results form the first order correction of J in the spin-orbit coupling where as AE is the second order correction. Naturally DMI is supposed to be more influential on the low temperature magnetic structure [93]. So, the effective spin Hamiltonian for vesignieite is given by

$$H = \sum_{\langle ij \rangle} [J_{ij} \vec{\mathbf{S}}_i \cdot \vec{\mathbf{S}}_j + \vec{\mathbf{D}}_{ij} \cdot (\vec{\mathbf{S}}_i \times \vec{\mathbf{S}}_j)] \tag{5.1}$$

where the isotropic exchange interaction strength $J_{ij} = J$ for the nearest-neighbour pairs. The Dzyaloshinskii-Moriya vector, $\vec{\mathbf{D}}_{ij}$ has D_p and D_z as the strengths of the in-plane and out-of-plane components of DMI. $\langle ij \rangle$ indicates the interactions are restricted to nearest neighbor only. The order of the cross product between i-th and j- th site for given $\vec{\mathbf{D}}_{ij}$ are denoted by arrows as shown in the Fig. 5.1(a) .The lattice vectors are $\vec{a} = a(1, 0)$ and $\vec{b} = a(\frac{1}{2}, \frac{\sqrt{3}}{2})$. The DM vector is given by

$$\begin{aligned} \vec{D}_{31} &= D_p \hat{j} + D_z \hat{k} \\ \vec{D}_{12} &= \hat{R}(\hat{k}, -\frac{2\pi}{3}) \vec{D}_{31} \\ \vec{D}_{23} &= \hat{R}(\hat{k}, -\frac{4\pi}{3}) \vec{D}_{31} \end{aligned} \tag{5.2}$$

where $\hat{R}(\hat{k}, \theta)$ is the rotation operator that rotates a vector by an angle θ about the axis $\hat{k}$. The orientation of the out-of-plane and in-plane components of DMI are shown in the Fig. 5.1(a).

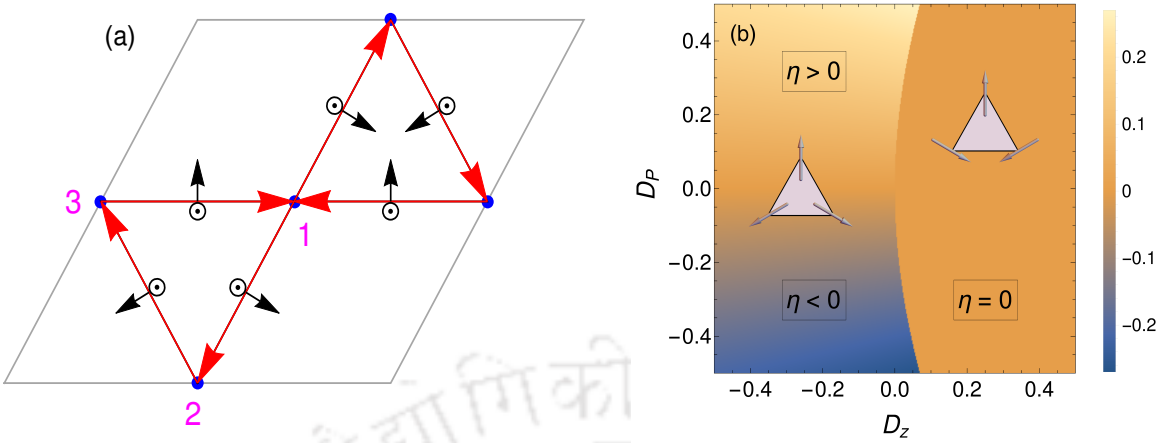

Figure 5.1: (a) The orientation of DM vector, in-plane component D_p is shown by the black arrow and the out-of-plane component D_z is uniform along $\hat{z}$. (b) Classical ground state phase diagram for spin-1/2

The introduction of DMI reduces the symmetries of the isotropic Heisenberg model. When $\vec{\mathbf{D}}_{ij} = D_z\hat{\mathbf{k}}$, that is when $D_p = 0$, then the global spin rotation symmetry reduces to $U(1)$ from $SU(2)$ but the wallpaper group remains $p6m$. When $D_p \neq 0$, then there are global spin rotation symmetries, and the wallpaper group reduces to $p3m1$.

5.3 Classical ground state

The classical ground state was discussed by Elhajal et al. [73]. We introduce their results since it is relevant to the SBMFT used in the later sections. First, consider the pure isotropic case i.e., the absence of Dzyaloshinskii-Moriya interaction. Based on the projective symmetry group(PSG) analysis, Messio et al. [119] showed that there is eight possible classical magnetic structure in a kagome lattice, termed as regular magnetic order(RMO). They suggested that these states can be good variational candidates to compute the ground-state phase diagram in the mean-field approach. The states are given by (i) Ferromagnetic state (ii) $Q = 0$ state (iii) $\sqrt{3} \times \sqrt{3}$ states (iv) octahedral states (v) cuboc1 state (vi) cuboc2 state (vii) $Q = 0$ umbrella state and (viii) $\sqrt{3} \times \sqrt{3}$ umbrella states. Classical energies and the structure factor for these states can be found in Ref. [119].

Motivated by the experimental result of vesignieite that there is a strong presence of DMI and the ground state is found to be $Q = 0$ long-range order(LRO) state. In the following, we discuss the $Q = 0$ classical ground state of KHAF with DMI. The

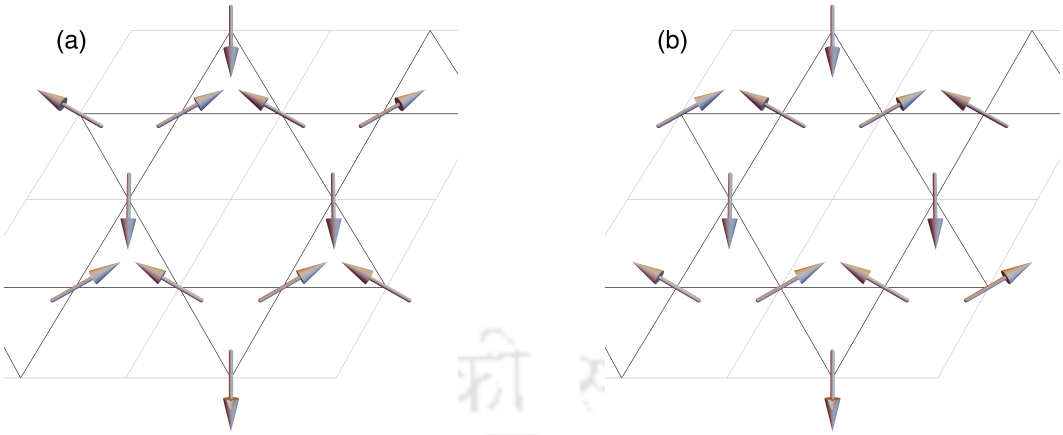

Figure 5.2: (a) Positive chirality as $D_z < 0$ and (b) Negative chiralty as $D_z > 0$

classical ground state of kagome Heisenberg antiferromagnet is highly degenerate. All the possible states, where the three spins respect the angle $2\pi/3$ with each other to minimize the ground state energy. With the introduction of the DMI, the symmetry is lowered, though the ground state is non-coplanar $Q = 0$ LRO with planar components of the spins making $2\pi/3$ angle with each other.

With lowered symmetries, the spin arrangements can now be classified using the notion of chirality, which is the angle between the spins in a given triangle of kagome lattice. If $\vec{S}_1, \vec{S}_2$ and $\vec{S}_3$ are three spins in a given triangle located in a counter-clockwise direction, then we define the spin chirality as

$$\chi_z = \left[\vec{S}_1 \times \vec{S}_2 + \vec{S}_2 \times \vec{S}_3 + \vec{S}_3 \times \vec{S}_1\right] \cdot \hat{\mathbf{k}} \tag{5.3}$$

In addition, the spins are non-coplanar, all the spins make a canting angle of η with the plane of the lattice. The energies for these spin configurations are given by

$$\begin{aligned} \frac{E_+}{N} &= \frac{J}{2}[1 - 3\cos(2\eta)] - \sqrt{3}(D_z \cos^2\eta + D_p \sin(2\eta)\cos\phi) \\ \frac{E_-}{N} &= \frac{J}{2}[1 - 3\cos(2\eta)] + \sqrt{3} D_z \cos^2\eta \end{aligned} \tag{5.4}$$

where N is the total number of sites and $E_+(E_-)$ is the energy of the configuration(as shown in the Fig. 5.2) with positive(negative) chirality, and ϕ is the angle azimuthal angle of $\vec{S}_1$.

From the energy expressions, we can describe the ground state spin configuration. In the absence of in-plane component, the Hamiltonian is invariant under rotation around the z-axis. The spins are forced to lie in the lattice plane with positive or

negative chirality depending on the sign of D_z. In a more interesting case, when both in-plane and out-of-plane are present; there are two phases distinguished by chirality. For large positive D_z, the spins remain coplanar with negative chirality irrespective of the value of D_p. For negative D_z, the spins have positive chirality but make a canting angle

$$\eta = \frac{1}{2}\tan^{-1}\left[\frac{2D_p}{\sqrt{3}J + D_z}\right] \tag{5.5}$$

giving rise to weak ferromagnetism.

The complete phase diagram is shown in Fig. 5.1(b). The two phases are separated by a first-order transition. For negative D_z, the canting angle continues to grow with the value of D_p, as shown by the color map in the phase diagram.

5.4 Schwinger boson formalism

One of the advantages of SBMFT formalism is that this approach can address both the long-range ordered and the spin liquid state. Unlike the fermionic approach, long-range order appears due to the condensation of the Schwinger bosons, and hence the spin liquid states will have gapped bosonic spinons.

The model Hamiltonian Eq. 5.1 can be mapped to a simpler model with $U(1)$ symmetry up to terms second order in D_p. This is due to the fact that the vector sum of the in-plane components of DMI is zero in a triangle. So, for small values of in-plane components of DMI, we can rotate the spins in such a way that the $U(1)$ symmetry is restored [74]. However, when the strength of the in-plane component of DMI is comparable to or greater than the strength of the out-of-plane component of DMI, then the above rotation will not work. In this case, we do the following.

We rotate the spins at i-th and j-th site by an angle θ_i and θ_j with $\theta_j = -\theta_i$ about an axis $\hat{\mathbf{d}}_{ij}$ i.e along the $\vec{\mathbf{D}}_{ij}$ vector. The rotated spin at site i and j is given by $\mathbf{S}'_i = R(\hat{\mathbf{d}}_{ij}, \theta_{ij})\mathbf{S}_i$ and $\mathbf{S}'_j = R(\hat{\mathbf{d}}_{ij}, -\theta_{ij})\mathbf{S}_j$. Applying this rotation [117], we can write the above Hamiltonian in the following form

$$H = J\sum_{\langle ij\rangle} \vec{\mathbf{S}}'_i \cdot \vec{\mathbf{S}}'_j \tag{5.6}$$

where $\theta_{ij} = \sqrt{(D^p_{ij})^2 + (D^z_{ij})^2}/2J$. We have used the assumptions that quadratic terms in D_p and D_z are very small. The derrivation of Eq. 5.6 is given in the Appendix. Now, if we fix the model parameters D_p and D_z, then θ is automatically

fixed as θ depends only on the magnitude of D_p and D_z. So, θ_{ij} can be taken as θ throughout the calculation. Also note that $\vec{\mathbf{S}}'_i$ is not same for each bond $\langle ij \rangle$ but for each bond it differs since the rotation axis $\hat{\mathbf{d}}_{ij}$ depends on the bond.

In Schwinger boson formalism, the spin operator at each site is represented by two bosonic operators a and b, given by

$$\mathbf{S} = \mathbf{\Phi}^\dagger \cdot \sigma \cdot \mathbf{\Phi} \tag{5.7}$$

with $\mathbf{\Phi}^T \equiv (a, b)$ be the bosonic spinor and σ be the vector of Pauli matrices. The component of spin along an arbitrary direction $\hat{n}$ is given by

$$\mathbf{S}_{\hat{n}} \mapsto \frac{1}{2}\mathbf{\Phi}^\dagger(\hat{n} \cdot \sigma)\mathbf{\Phi}$$

In Schwinger boson formalism there is an emergent $U(1)$ gauge symmetry as $a_i \to e^{i\phi(i)}a_i$ and $b_i \to e^{i\phi(i)}b_i$. The boson operators obeys the typical bosonic commutation relations $[\Phi_{i\alpha}, \Phi^\dagger_{j\beta}] = \delta_{ij}\delta_{\alpha\beta}$. This representation enlarges the Hilbert space. So, to remain within the physical space, the total number of Schwinger boson at a particular is constrained to be $2S$. In the standard mean field treatment the constraint is implemented by taking the ground state average and a Lagrange multiplier λ is introduced which can be thought as chemical potential. Now we define two bond operator in the following way

$$A_{ij} = \frac{i}{2}\mathbf{\Phi}_i^T \sigma_y \mathbf{\Phi}_j \quad \text{and} \quad B^\dagger_{ij} = \frac{1}{2}\mathbf{\Phi}_i^\dagger \mathbf{\Phi}_j \tag{5.8}$$

The bond operator $A^\dagger_{ij}$ creates a singlet at the bond ij where as B_{ij} helps the Schwinger boson to hop from site i to site j. Since the form of Hamiltonian in Eq. 5.6 is invariant under global spin rotation, we can always decouple the Hamiltonian in terms of two bond operator as given by

$$\mathbf{S}'_i \cdot \mathbf{S}'_j =: B'^\dagger_{ij} B'_{ij} : -A'^\dagger_{ij} A'_{ij} \tag{5.9}$$

:: indicates the normal ordered product. The rotated bond operators can be written in terms of unrotated bond operators as following

$$B'^\dagger_{ij} = \cos\theta B^\dagger_{ij} + \sin\theta C^\dagger_{ij} \quad \text{and} \quad A'^\dagger_{ij} = \cos\theta A^\dagger_{ij} - \sin\theta D^\dagger_{ij} \tag{5.10}$$

with two additional bond operators, given by

$$C_{ij}^{\dagger} = \frac{1}{2}\mathbf{\Phi}_i^{\dagger}(i\hat{\mathbf{d}}_{ij}\cdot\sigma)\mathbf{\Phi}_j \quad \text{and} \quad D_{ij}^{\dagger} = \frac{1}{2}\mathbf{\Phi}_i^{T}(\sigma_y\hat{\mathbf{d}}_{ij}\cdot\sigma)\mathbf{\Phi}_j \tag{5.11}$$

With this bond operators we can identify two identities

$$\begin{aligned}\hat{\mathbf{d}}_{ij}\cdot(\vec{\mathbf{S}}_i\times\vec{\mathbf{S}}_j) &= \frac{1}{2}(:B_{ij}^{\dagger}C_{ij}+C_{ij}^{\dagger}B_{ij}:+A_{ij}^{\dagger}D_{ij}+D_{ij}^{\dagger}A_{ij})\\ 2(\hat{\mathbf{d}}_{ij}\cdot\vec{S}_i)(\hat{\mathbf{d}}_{ij}\cdot\vec{S}_j) &- \vec{S}\cdot\vec{S}_j = (:C_{ij}^{\dagger}C_{ij}:-D_{ij}^{\dagger}D_{ij})\end{aligned}$$

The model Hamiltonian in terms of bond operators can be cast in the following way

$$H = \sum_{\langle ij\rangle} J(\hat{B}_{ij}^{\prime\dagger}\hat{B}_{ij}^{\prime} - \hat{A}_{ij}^{\prime\dagger}\hat{A}_{ij}^{\prime}) \tag{5.12}$$

We can decouple the quadratic field Hamiltonian in terms of bilinear operators using standard mean-field decoupling scheme. The form of the mean-field Hamiltonian is as following.

$$H_{\mathrm{MF}} = \sum_{\langle ij\rangle} J\Big[(\hat{B}_{ij}^{\prime\dagger}\mathbf{B}_{ij}^{\prime} - \hat{A}_{ij}^{\prime\dagger}\mathbf{A}_{ij}^{\prime}) + \text{H. C}\Big] - \sum_i \lambda_i\hat{n}_i + \epsilon_0 \tag{5.13}$$

with the mean fields corresponding to the bond operators is given by

$$\begin{aligned}\langle\hat{B}_{ij}^{\prime}\rangle &= \mathbf{B}_{ij}^{\prime} \quad \text{and} \quad \langle\hat{B}_{ij}^{\prime\dagger}\rangle = \mathbf{B}_{ij}^{\prime *}\\ \langle\hat{A}_{ij}^{\prime}\rangle &= \mathbf{A}_{ij}^{\prime} \quad \text{and} \quad \langle\hat{A}_{ij}^{\prime\dagger}\rangle = \mathbf{A}_{ij}^{\prime *}\end{aligned}$$

with ϵ_0 is constant which depends on the mean fields and λ given by $\epsilon_0 = \sum_{\langle ij\rangle}[|\mathbf{A}_{ij}^{\prime}|^2 - |\mathbf{B}_{ij}^{\prime}|^2 + 2S\sum_i\lambda_i$. Let $\vec{\delta}$ be the neighbor vectors, then the mean field Hamiltonian is given by

$$H_{\mathrm{MF}} = \sum_{i,\delta}\Big[[\cos\theta\hat{B}_{i,i+\delta}^{\dagger}\mathbf{B}^{\prime}(\delta)+\sin\theta\hat{C}_{i,i+\delta}^{\dagger}\mathbf{B}^{\prime}(\delta)-\cos\theta\hat{A}_{i,i+\delta}^{\dagger}\mathbf{A}^{\prime}(\delta)+\sin\theta\hat{D}_{i,i+\delta}^{\dagger}\mathbf{A}^{\prime}(\delta)]+\text{H.C.}\Big]+\epsilon_0$$

We define the Fourier transformation $\Phi_i = \frac{1}{\sqrt{N}}\sum_k e^{-ik\cdot r_i}\xi_{k,\mu_i}$ where $\xi_{k,\mu_i} = \begin{pmatrix}\alpha_{k\mu_i}\\ \beta_{k\mu_i}\end{pmatrix}$ with sub-lattice index μ_i and N be the total number of sites. Then above mean field Hamiltonian reduces to a compact form, given by

$$H_{\mathrm{MF}} = \sum_{k>0}\psi_k^{\dagger}D_k\psi_k + \epsilon_0 \tag{5.14}$$

We define $\Psi_k^T = \left(\xi_{k,1}, \xi_{-k,1}^\dagger, \xi_{k,2}, \xi_{-k,2}^\dagger, \xi_{k,3}, \xi_{-k,3}^\dagger\right)$ and the D_k matrix is given by

$$D_k = \begin{pmatrix} -\lambda & 0 & Y_{12}(k) & X_{12}(k) & Y_{31}^\dagger(k) & X_{31}^T(-k) \\ 0 & -\lambda & X_{12}(-k)^{\dagger T} & Y_{12}(-k)^{T\dagger} & X_{31}(k)^\dagger & Y_{31}(-k)^T \\ Y_{12}(k)^\dagger & X_{12}(-k)^T & -\lambda & 0 & Y_{23}(k) & X_{23}(k) \\ X_{12}(k)^\dagger & Y_{12}(-k)^T & 0 & -\lambda & X_{23}(-k)^{\dagger T} & Y_{23}(-k)^{T\dagger} \\ Y_{31}(k) & X_{31}(k) & Y_{23}(k)^\dagger & X_{23}(-k)^T & -\lambda & 0 \\ X_{31}(-k)^{\dagger T} & Y_{31}(-k)^{T\dagger} & X_{23}(k)^\dagger & Y_{23}(-k)^T & 0 & -\lambda \end{pmatrix}$$

where $X_{ij}(k)$ and $Y_{ij}(k)$ are are 2×2 matrix, given by

$$X_{ij}(k) = \tfrac{i}{2}\left(\mathbf{A}'_{ij}e^{-ikr_{ij}} + \mathbf{A}'_{i+3,j+3}e^{-ikr_{i+3,j+3}}\right)\sigma_y\left(\cos\theta - i\sin\theta\hat{\mathbf{d}_{ij}}\cdot\sigma\right) \quad (5.15)$$

$$Y_{ij}(k) = \tfrac{1}{2}\left(\mathbf{B}'_{ij}e^{-ikr_{ij}} + \mathbf{B}'_{i+3,j+3}e^{-ikr_{i+3,j+3}}\right)\left(\cos\theta + i\sin\theta\hat{\mathbf{d}_{ij}}\cdot\sigma\right) \quad (5.16)$$

The structure of the D_k matrix is slightly different at the special points Γ, M and K. Using the standard Bigoliouubov transfromation we can diagonalize the mean field Hamiltonian $\psi_k = M\tilde{\psi}_k$ where M is the Bigoliouubov matrix of the form $M = \begin{pmatrix} U & V \\ X & Y \end{pmatrix}$ and $\tilde{\Psi}_k^T = \left(\tilde{\xi}_{k,1}, \tilde{\xi}_{-k,1}^\dagger, \tilde{\xi}_{k,2}, \tilde{\xi}_{-k,2}^\dagger, \tilde{\xi}_{k,3}, \tilde{\xi}_{-k,3}^\dagger\right)$ and $\tilde{\xi}_K = \begin{pmatrix} \tilde{\alpha}_k \\ \tilde{\beta}_k \end{pmatrix}$

The mean field energy is given by

$$E_{\text{MF}} = \sum_{\mu,k>0}\left[\omega_{k\mu}(\tilde{\alpha}_{k\mu}^\dagger\tilde{\alpha}_{k\mu} + \tilde{\beta}_{k\mu}^\dagger\tilde{\beta}_{k\mu}) + (2S+1)N\lambda + 2(\mathbf{A}'^2 - \mathbf{B}'^2)\right] \quad (5.17)$$

where $\omega_{k\mu}$ is the dispersion relation of the $\mu = 1, ..., 2m$ spinon modes with m be the number sites within the unit cell. The ground state $|\tilde{0}\rangle$ is the vacuum of the Bogoliubov bosons.

Choice of mean fields : In the large S limit the SBMFT result should mimic the classical ground state i.e the $Q = 0$ umbrella state. In the classical limit we define

$$\begin{aligned} \langle a\rangle &= r_1 e^{i\theta_1} \\ \langle b\rangle &= r_2 e^{i\theta_2} \end{aligned} \quad (5.18)$$

where r_1, r_2 is the modulus and θ_1, θ_2 be the argument of the average values of two flavors of bosonic operator a and b in the classical limit. To obtain the $Q = 0$ spin

configuration, we must have

$$\langle a_i \rangle = \sqrt{2S}\cos\left(\frac{\xi}{2}\right) \quad \text{and} \quad \langle b_i \rangle = \sqrt{2S}\sin\left(\frac{\xi}{2}\right) e^{i\beta_i}$$

where $\beta_1 = \frac{7\pi}{6}, \beta_2 = \frac{\pi}{2}$, and $\beta_3 = -\frac{\pi}{6}$ and $\xi = \pi/2 - \eta$. The mean fields we obtain using these are summarized in Table. 5.1

Mean-fields		Bond-(1,2)	Bond-(2,3)	Bond-(3,1)	After Gauge
A	$\lvert\cdot\rvert$	$\frac{S}{2}\sqrt{3}\sin(\xi)$			-
	Phase	$\frac{\pi}{3}$	$-\frac{\pi}{3}$	π	0
D	$\lvert\cdot\rvert$	$\frac{S}{2}\left(2D_p\cos(\xi) + D_z\sin(\xi)\right)$			-
	Phase	$\pi + \frac{\pi}{3}$	$\pi - \frac{\pi}{3}$	$\pi - \pi$	π
B	$\lvert\cdot\rvert$	$\frac{S}{2}\sqrt{3\cos^2(\xi) + 1}$			-
	Phase	Φ_B	Φ_B	Φ_B	$\Phi_B + \frac{4\pi}{3}$
C	$\lvert\cdot\rvert$	$\sqrt{\left(D_z\cos(\xi) - 2D_p\sin(\xi)\right)^2 + 3D_z^2}$			-
	Phase	Φ_C	Φ_C	Φ_C	$\Phi_C + \frac{4\pi}{3}$

Table 5.1: Phases and the magnitude(denoted by $|.|$) of different bond operators

One can immediately notice that a gauge transformation by angles $\left\{\frac{5\pi}{6}, -\frac{\pi}{2}, \frac{\pi}{6}\right\}$ at three sublattices will make both A and D fields real. At the same time, B and C fields will acquire a constant phase of $4\pi/3$. Thus, in the final calculation, we can take $\mathbf{A}'$ as a real number and $\mathbf{B}'$ as a complex number. However, the optimization of the mean-field parameters shows that for the symmetry of the spiral order, we must have $\mathbf{B}' = 0$. We are left to optimize $\mathbf{A}'$ field and λ.

The mean field parameters can be obtained by extrimizing the mean field energy with respect to the mean field parameters which is equivalent to the solve the self-consistency equations.

$$\frac{\partial E}{\partial \mathbf{A}'} = 0 \quad \text{and} \quad \frac{\partial E}{\partial \lambda} = 0 \tag{5.19}$$

Few optimized values of the mean field parameters and energies are given in Table 5.2

S	D_p	D_z	$\mathbf{A}'$	λ	Energy
0.20	0.2	0.05	0.26429	-0.46458	-0.13970
0.50	0.2	0.05	0.52736	-0.92482	-0.55622

Table 5.2: Optimized values of the mean field parameters and energies for $N = 1200$

5.5 SBMFT results

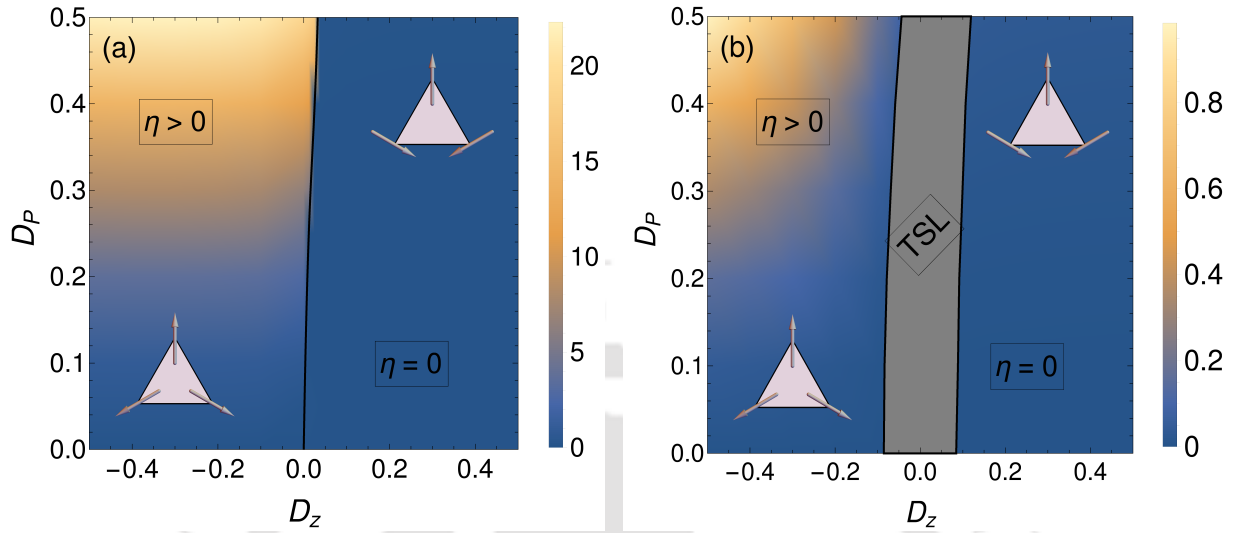

Figure 5.3: Ground state phase diagram for (a) $S = 0.5$ and (b) $S = 0.2$

We have computed the zero-temperature ground state phase diagram for this model in the parameter space of $0 \leq D_p \leq 0.5$ and $-0.5 \leq D_z \leq 0.5$ based on chirality, the ZZ correlation at Γ point and also the gap in the thermodynamic limit for various values of S. Our proposed ground state phase diagram for $S = 0.5$ is quite similar to the classical phase diagram and is, as shown in Fig. 5.3(a). In the phase diagram for $S = 0.5$, we found $Q = 0$ structure with two chiralities. The boundary between two phases obtained from the chirality is shown by a black line. The boundary obtained from SBMFT is not the same as obtained from the classical case, but the qualitative features remain the same as shown in Fig. 5.3(a). The boundary line is curved into the first quadrant of the phase diagram; that is, the chirality changes at positive values of D_z for a given larger D_p, as shown in Fig. 5.4(b). This is a result of the fact that the chirality selected by these two components is not the same, and hence there is a competition between these two. In the negative chirality phase, the spins are forced to lie in the kagome plane, resulting in $S^z = 0$, whereas for the positive chirality, the spins are canted and the canting angle is shown by the color gradient. If we change the sign the in-plane component, the effect of D_p is to change the canting angle from positive to negative.

As the value of S is lowered, a gapped spin liquid phase opens up at the boundary line at a critical value of S, which is very close to 0.2, and the spin-liquid phase becomes wider with decreasing value of S. The ground-state phase diagram for

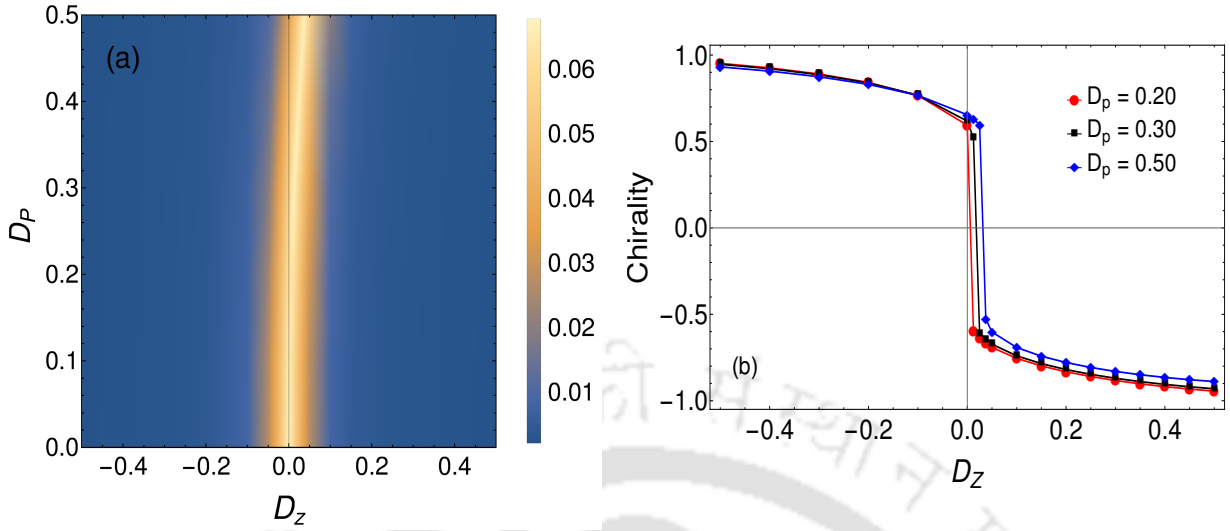

Figure 5.4: (a) Gap as a function of D_p and D_z for $S = 0.2$. (b) Chirality as a function of D_z for $S = 1/2$ for different values of D_p

$S = 0.2$ is shown in the Fig. 5.3(b) At this value of S, the gapped spin liquid phase is sandwiched between two $Q = 0$ LRO phases with two different chirality. The boundary between the QSL and the LRO is obtained from the extrapolation of the gap data. Gap as a function of D_p and D_z is shown in the density plot in Fig. 5.4(a).

Fig. 5.5 shows the quasi particle dispersion relations along the high symmetry line Γ - M - K -Γ, where $\Gamma = (0, 0), M = (0, 2\pi/\sqrt{3}), M_e = (0, 4\pi/\sqrt{3})$ and $K = (1, \sqrt{3})2\pi/3, K_e = (1, \sqrt{3})4\pi/3$. In Fig. 5.5(a) the spinon spectrum is shown at $S = 0.05$ with $D_p = 0.05$ and $D_z = 0.3$. The spectrum is gapped indicating the ground state is in the spin liquid state. The spectrum for $S = 0.2$ with $D_p = 0.2$ and $D_z = 0.05$ is as shown in the Fig. 5.5(b) where the spectrum is still gapped. In Fig. 5.5(c) the spinon spectrum is shown for $S = 0.5$ with $D_p = 0.05$ and $D_z = 0.1$ which is gapless at Γ indicating the ground state has acquired LRO. To investigate the long range magnetic order, we calculate the static structure factor which is defined as

$$S^{\alpha\beta}(Q) = \frac{3}{4N} \sum_{ij} e^{i[Q\cdot(R_i - R_j)]} \langle 0|S_i^\alpha S_j^\beta|0\rangle \tag{5.20}$$

where R_i and R_j is the site index and $\alpha, \beta \in \{x, y, z\}$. A magnetic long order state produces a sharp discrete Bragg peak, whereas QSL produces continuous, diffusive scattering spectra. Here, we have calculated both the transverse component and ZZ component of the static structure factor for different points in the parameter space to examine the magnetic structure. The XX-component of static structure factor

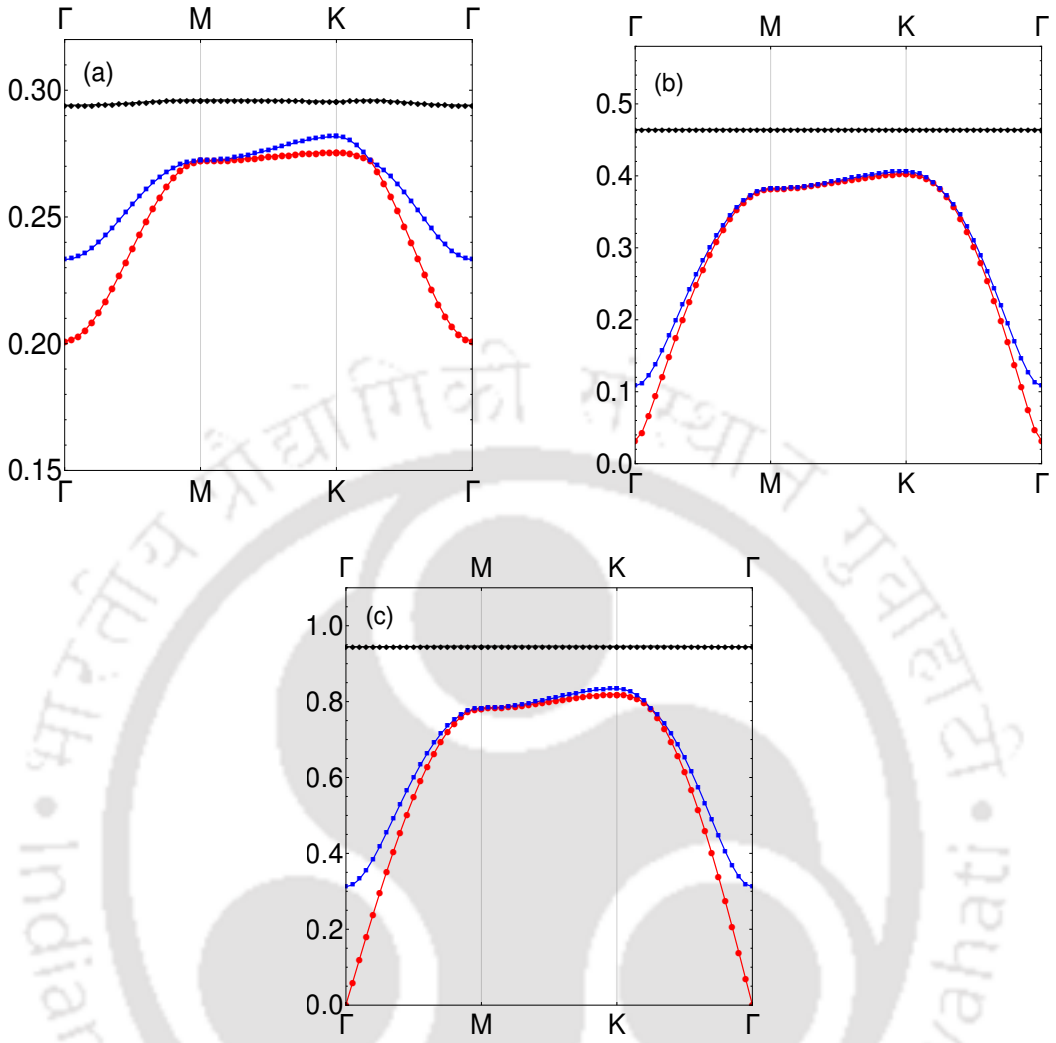

Figure 5.5: Spinon spectrum in the spin liquid region (a) at $S = 0.05$ with $D_p = 0.05$ and $D_z = 0.3$ and (b) at $S = 0.2$ with $D_p = 0.2$ and $D_z = 0.05$ (c) in the LRO region $S = 0.5$ with $D_p = 0.05$ and $D_z = 0.1$

for $S = 0.20$ at $D_p = 0.05$ and $D_z = 0.05$ is shown in the Fig. 5.6(a). This is a representative point in the QSL region of the phase diagram. There is a broad peak at M_e supports the conclusion that the ground state is in the spin-liquid state. To illustrate the canting of the spins, we show the static structure factor for $S = 0.5$ with $D_z = 0$ and $D_p = 0.5$ in Fig. 5.6(b). Sharp peaks appear at the M_e point, indicating a magnetic LRO of $Q = 0$ type. From Fig. 5.6(c), we see a peak at Γ point. This suggests that there is a ferromagnetic component along the z-direction, which is the result of the spins tilting away from the XY plane. The canting angle can also be estimated from this data.

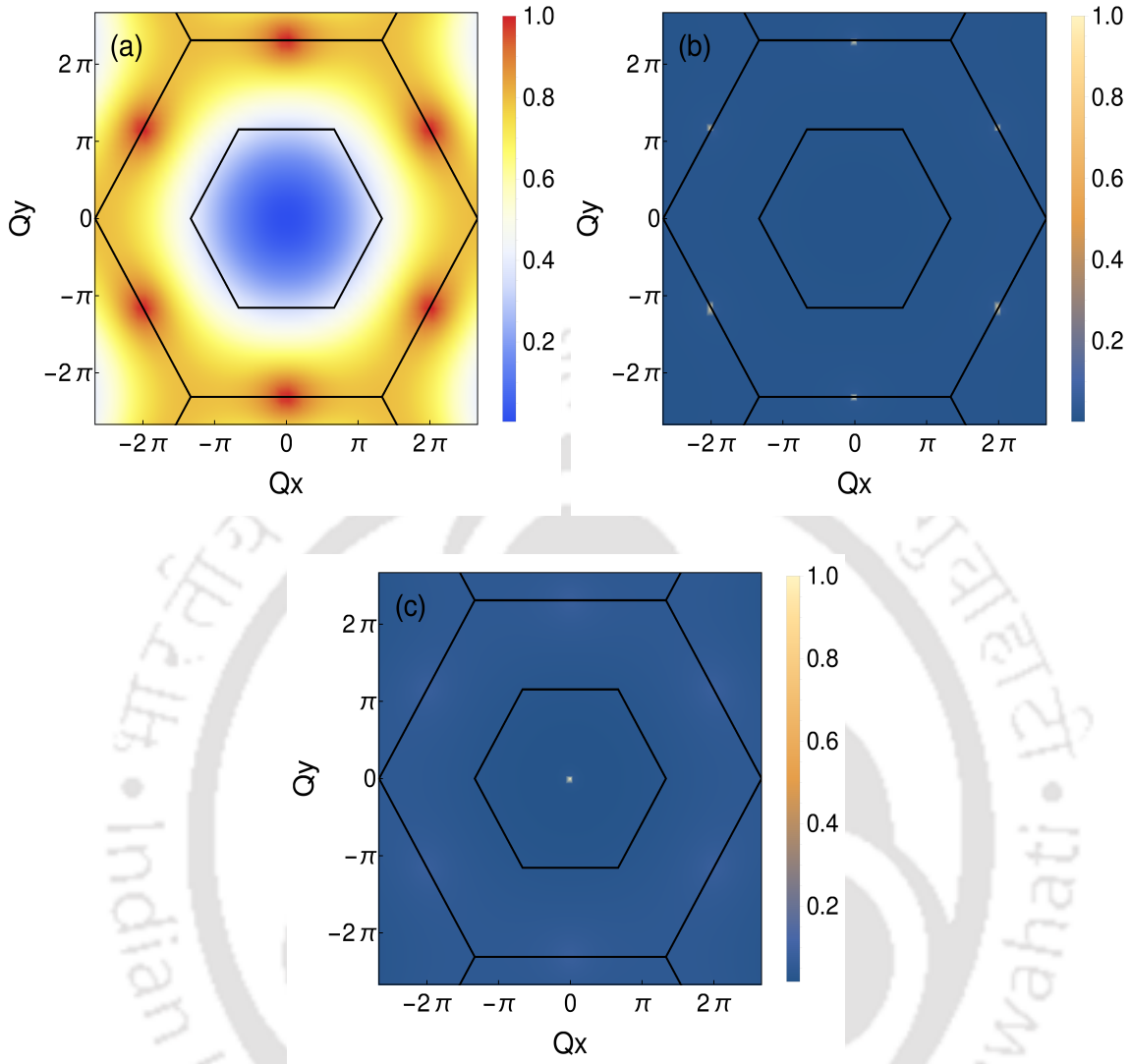

Figure 5.6: (a) XX-component of SSF at $S = 0.2$ with $D_p = 0.05$ and $D_z = 0.05$ (b) XX-component of SSF at $S = 0.5$ with $D_p = 0.5$ and $D_z = 0$ (c) ZZ-component of SSF at $S = 0.5$ with $D_p = 0.5$ and $D_z = 0$

5.6 Discussion

For vesignieite, the measured value of in-plane component $D_p = 0.19J$ and the out-of-plane component $D_z = 0.07J$ [93] which are the two dominant term compared to other anisotropies like isotropic exchange anisotropy. The ground state is expected to be influenced by both in-plane as well as the out-of-plane component of DMI. In the classical limit, any small amount of D_z will force the spin to lie in the kagome plane. In the absence of the in-plane component, the critical value $D_c = 0.1J$ predicted by ED result, there is a disordered state at one side and ordered state on

the other. So, we expect that the presence of in-plane component D_p will affect this critical value. The presence of the in-plane component of DMI is responsible for the tilting of the spins towards the z-axis. The measured value of the canting angle for vesignieite is found to be $3^o < \phi < 9^o$, as obtained from NMR data analysis.

Since, in the previous SBMFT studies, it was argued that lower values of spin (S = 0.366) is found to be a better description of the spin-1/2 case due to the fact that the constraint $n_i = 2S$ is not implemented exactly rather implemented as an average [72]. However, even at $S = 0.366$, the ground state is also in the magnetic LRO region for all values of D_p and D_z. It seems the canted LRO nature of the ground state of vesignieite is dictated by the presence of DM interaction with the dominant component in the kagome plane.

5.7 Conclusion

We study the effect of in-plane and the out-of-plane component of Dzyaloshinskii-Moriya interaction on the ground state of spin-1/2 kagome antiferromagnet using Schwinger Boson mean-field theory. We found two chiralities of $q = 0$ structure in the phase diagram for the spin-1/2 case in both the approaches. In the case of SBMFT, for the lower values of S, the spin liquid phase is sandwiched between the above two chiralities. We also found that this spin-liquid region shrinks to the phase boundary between the two chiralities in the large S limit. In the classical limit, our SBMFT result is in agreement with the result obtained from the classical phase diagram.

5.8 Appendix

Here, we provide the proof for Eq. 5.6. Let us consider the triangle $\Delta \equiv (123)$ as shown in the Fig. 5.1(a). So, the Hamiltonian for this part is given by

$$H_\Delta = H_{12} + H_{23} + H_{31} \tag{5.21}$$

where H_{12} has the following form

$$H_{12} = J\vec{S}_1 \cdot \vec{S}_2 + \vec{D}^P_{12} \cdot (\vec{S}_1 \times \vec{S}_2) + \vec{D}^z_{12} \cdot (\vec{S}_1 \times \vec{S}_2) \tag{5.22}$$

Similarly, we can write the expressions for the other two bonds. Now, consider the bond-12. We treat each of the spins as a three dimensional classical unit vectors. Then, we rotate the spins by θ_{12} and $-\theta_{12}$ around the axis $\hat{d}_{12}$ where, $\theta_{12} = \frac{\sqrt{(D^P_{12})^2+(D^z_{12})^2}}{2J}$. For small values of θ_{12}, the relation between the rotated and unrotated spins is as given below

$$\begin{aligned} \vec{S}_1 &= \vec{S}'_1 + \theta_{12}\ (\vec{S}'_1 \times \hat{d}_{12}) \\ \vec{S}_2 &= \vec{S}'_2 - \theta_{12}\ (\vec{S}'_2 \times \hat{d}_{12}) \end{aligned}$$

where, $\vec{S}'_1$ and $\vec{S}'_2$ be the rotated spins and $\hat{d}_{12} = \frac{1}{\sqrt{(D^P_{12})^2+(D^z_{12})^2}}\left[D^P_{12}\ \hat{j} + D^z_{12}\ \hat{k}\right]$. Then we can also write $\hat{d}_{12} = \frac{1}{2\theta J}\left[D^P_{12}\ \hat{j} + D^z_{12}\ \hat{k}\right]$. Now, if we neglect θ^2_{12} term, then the Heienberg term for the bond-12 reduces to

$$\vec{S}_1 \cdot \vec{S}_2 = \vec{S}'_1 \cdot \vec{S}'_2 + 2\ \theta_{12}\ \hat{d}_{12} \cdot (\vec{S}'_2 \times \vec{S}'_1) \tag{5.23}$$

The cross product of the DM interaction term in Eq. 5.22 reduces to

$$\vec{S}_1 \times \vec{S}_2 = \vec{S}'_1 \times \vec{S}'_2 + \theta_{12}\ \left[2\ \hat{d}_{12}\ (\vec{S}'_1 \cdot \vec{S}'_2) - \vec{S}'_1\ (\hat{d}_{12} \cdot \vec{S}'_2) - \vec{S}'_2\ (\hat{d}_{12} \cdot \vec{S}'_1)\right] \tag{5.24}$$

Using Eq. 5.23 and Eq. 5.24 in Eq. 5.22 we get,

$$H_{12} = J\ \vec{S}'_1 \cdot \vec{S}'_2 + (2\theta^2_{12} J \hat{d}_{12}) \cdot \left[2\ \hat{d}_{12}\ (\vec{S}'_1 \cdot \vec{S}'_2) - \vec{S}'_1\ (\hat{d}_{12} \cdot \vec{S}'_2) - \vec{S}'_2\ (\hat{d}_{12} \cdot \vec{S}'_1)\right]$$

The second term in the RHS is second order in θ_{12} and hence, can be neglected. So, we finally have

$$H_{12} = J\ \vec{S}'_1 \cdot \vec{S}'_2 \tag{5.25}$$

Similar excercise can be done for bond-23 and bond-31 to get the following form

$$H_\Delta = J\left[\vec{S}'_1 \cdot \vec{S}'_2 + \vec{S}''_2 \cdot \vec{S}''_3 + \vec{S}'''_3 \cdot \vec{S}'''_1\right] \tag{5.26}$$

Chapter 6

$Q = 0$ Order in KHAF : An Exact Diagonalization Study

6.1 Introduction

In the last chapter, we studied the Heisenberg antiferromagnet on kagome lattice with DM interaction using the Schwinger boson mean-field theory. The main focus was to study the effect of a large planar component of DM interaction. While SBMFT is a great tool for extracting qualitative features of spin systems, the constraint of boson number per site can not be implemented. Usually, this constraint is enforced at an average level, leading to fluctuations of boson number at each site. This makes the qualitative results at $S = 0.5$ untenable.

To obtain a better insight into this problem, we have employed the method of exact diagonalization of finite size systems. As the name suggests, the method is exact but for finite systems only. Despite its exactness, the technique suffers from other drawbacks. First, the finite size can not imitate the full symmetry group of the infinite system, and the results are shape-dependent and also depends on the boundary conditions. This makes the extrapolations harder if we don't have large enough systems. Since the dimension of Hilbert space grows exponentially, the system size is typically small. Especially in the 2D case, it is not possible to consider more than a few unit cells. Thus, one needs to be very careful while extrapolating and interpreting the results.

In this chapter, we use exact diagonalization to study the ground state of kagome Heisenberg antiferromagnet with added Dzyaloshinskii-Moriya interaction. We have computed the ground-state phase diagram and also the properties associated with each phase. We have compared the obtained results with the SBMFT results, as

discussed earlier in Chapter-5.

6.2 Implementation details

Exact diagonalization(ED) is a numerical tool to compute the ground state and first few excited states of a Hamiltonian matrix on a finite cluster of spins. The method exact diagonalization conceptually straight forward, involves the following steps.

- The first step is to identify the invariant subspaces of the Hamiltonian by taking into account the symmetries.
- Choosing the appropriate sub-spaces and corresponding basis. This requires considerations of computation cost and storage.
- Diagonalize the Hamiltonian numerically using some algorithms like conjugate gradient, Davidson algorithm, and Lanczos algorithm to obtain the ground state and few relevant excited states.
- Calculate various physical quantities using the obtained eigenvectors.

This method is exact and widely used to study the ground state of different frustrated magnets though it is limited by small system size due to the huge computational requirement. The estimation of the computational requirement for the present problem is given in the section below.

6.2.1 Estimation of computational resources

We know that the Hilbert space for a spin-1/2 particle is $\mathcal{H} = \mathbb{C}^2$, and for a many-body system containing N spin-1/2 particle, the Hilbert space will be $\mathbb{C}^{2^N}$. Therefore, the exponential scaling of the Hilbert space dimension turns out to be a big challenge. For an example, the basis for $N = 30$ spins has a size $2^{30} \sim 10^9$. So, a double complex vector needs a memory of $16GB$, which is a big requirement. The memory needed to represent the basis states, and the Hamiltonian matrix will quickly exceed the capacity. The Hamiltonian matrix we encounter in the spin system problems is sparse. We have at most $\mathcal{O}(N^2)$ terms in the Hamiltonian and thus only $\mathcal{O}(N^2)$ non-zero matrix elements per row and column.

Therefore the memory required to store the sparse matrix is still large $\mathcal{O}(N^2 2^N)$. The memory requirement for an exact diagonalization calculation without any symmetry for KHAF with DM interaction is given in Table. 6.1. Here, we have used

the package PARPACK to diagonalize the sparse Hamiltonian matrix. We have considered two states, the ground state and the first excited state, and hence the memory required for those associated with two eigenvectors is taken into account. c is the resulting column vector obtained from the matrix-vector product Ab. Details of the matrix-vector product are discussed in the section below.

No.	Spins	Hamiltonian	PARPACK	Eigenvectors	c	Total
1	24	36.875	3	0.5	0.25	40.625
2	27	331	24	4	2	361
3	30	2936	192	32	16	3176
4	33	25792	1536	256	128	27712
5	36	224768	12288	2048	1024	240128

Table 6.1: Memory estimation in GB for a typical exact diagonalization calculation for kagome Heisenberg anti-ferromagnet with Dzyaloshinskii-Moriya interaction

6.2.2 Parallelization and computational strategies

For parallel computation, to perform the matrix-vector multiplication $Ab = c$, one has to distribute the not only the matrix A but also the vector b and the resulting vector c. The vector elements can be copied and distributed to all the processors of the multiprocessor computer system. For a multiprocessor computer system consisting of n processors, any vector v can be distributed in such a way that $v = kn$, where each processor contains the continuous sequence of k-vector elements. To illustrate the concept, let us consider the algorithm matrix-vector product based on a row-wise block-striped decomposition scheme. To perform the multiplication, we have to ensure that each processor must contain the corresponding row of the original matrix A and the copy of vector b. The multiplication scheme is shown schematically for a 3×3 matrix A and column vector b with dimension 3×1, in the Fig. 6.1. The components of the resulting vector c are to be collected from each of the processors of the multiprocessor computer system. To collect the elements of the vector c, we have to perform the *all gather operation*(**MPI_Allgather**). This operation allows each processor to transfer its compound element of the resulting vector c to all the other processors.

To maximize the system size, which can be fit in the available memory, we need various strategies to handle the Hamiltonian matrix. The strategies are based on the fact that the Lanczos algorithm only requires the computation of matrix-vector products but not the entire matrix. We can generate the matrix elements on-the-fly

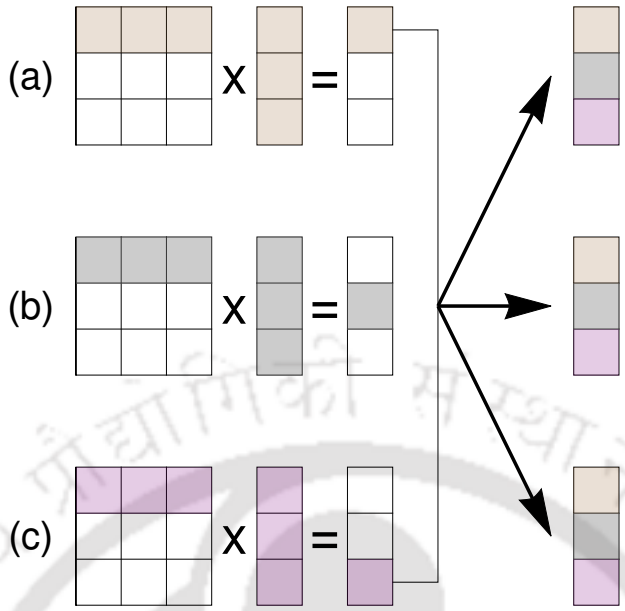

Figure 6.1: Pictorial representation of matrix-vector product in parallel computation

during multiplication. This way, we can maximize the system size at the cost of a much larger time of calculation.

6.2.3 Diagonalization

We have used the package PARPACK to diagonalize the sparse Hamiltonian matrix. Arnoldi's method is very much similar to the usual *Power method*, and the extremal eigenvalues converge first. The lowest eigenvalues converge to the ground state energy exponentially fast. We start from an initial random vector, which iteratively builds an orthonormal basis of the Hilbert space in which the given Hamiltonian becomes tri-diagonal. It turns out that the number iterations required to obtain the ground state energy are much much smaller than the Hilbert space dimension. Typically, the first two eigenvalues converge around 100-200 iterations for a sparse matrix of size 10^6.

Here we briefly describe the Arnoldi method for exact diagonalization [131, 132]. The method of Arnoldi was introduced to reduce the matrix into the Heisenberg form. But it turns out that we can get good approximate eigenvalues if we stop before completion. Let us consider a square matrix of order n, which is to be diagonalized. Now, after n steps of Arnoldi's method, we have an orthogonal reduction of Heisenberg form, i.e., $A\ V = V\ H$, where H is an upper Heisenberg matrix, and V is an orthogonal matrix. The matrices V and H are uniquely determined by the first

column of V, a unit vector $v = Ve_1$, called the initial vector. If Arnoldi's method fails after m steps for some initial vectors, then we have the condition

$$A\ V_m - V_m H_m = 0 \tag{6.1}$$

where H_m is the Heisenberg matrix of order m and V_m is a $n \times m$ matrix with orthogonal columns. Typically when the algorithm does not break down after m steps, we have the following relation

$$A\ V_m - V_m H_m = f e_m^* \tag{6.2}$$

where f is known as the residual of the m-step Arnoldi factorization. If the algorithm breaks down after m steps, then the residual is zero. However, this situation never appears in practice because of the finite precision of the arithmetic. In order to maintain the orthogonality, Gram-Schmidt orthogonalization is used iteratively. The computed basis vectors are the columns of V_m matrix, known as Arnoldi's vectors.

Now, by construction, $V_m^*\ f = 0$, then form from Eq. 6.2 we have

$$V_m^* A V_m = H_m \tag{6.3}$$

So, this H_m represents the orthogonal representation of A onto the Krylov subspace. Now we can use Rayleigh-Ritz approximation of the eigenpairs of A. Let (λ_i, y_i) be the eigenpairs of H_m, then the Ritz value λ_i and the Ritz vector $x_i = V_m y_i$ can be approximated to be an eigenpaiar of A. Typically only a small percentage of m turns out to be good.

In practice, to obtain a good approximation, we require a large number of steps m. So, the memory requirement and also the computational cost becomes an issue. For this reason, a restarted version of the algorithm is implemented. The basic idea is that once we calculate V_m for a fixed value of m, a new Arnoldi process is started. In the sequel, m denotes the maximum number of vectors allowed for the basis.

6.3 Application to KHAF with DMI

Here we explore the model Hamiltonian of vesignieite as discussed in Chapter-5. The effective spin Hamiltonian of vesignieite, consists of two term, first one is the Heisenberg term and the second one the Dzyaloshinskii-Moriya interaction term.

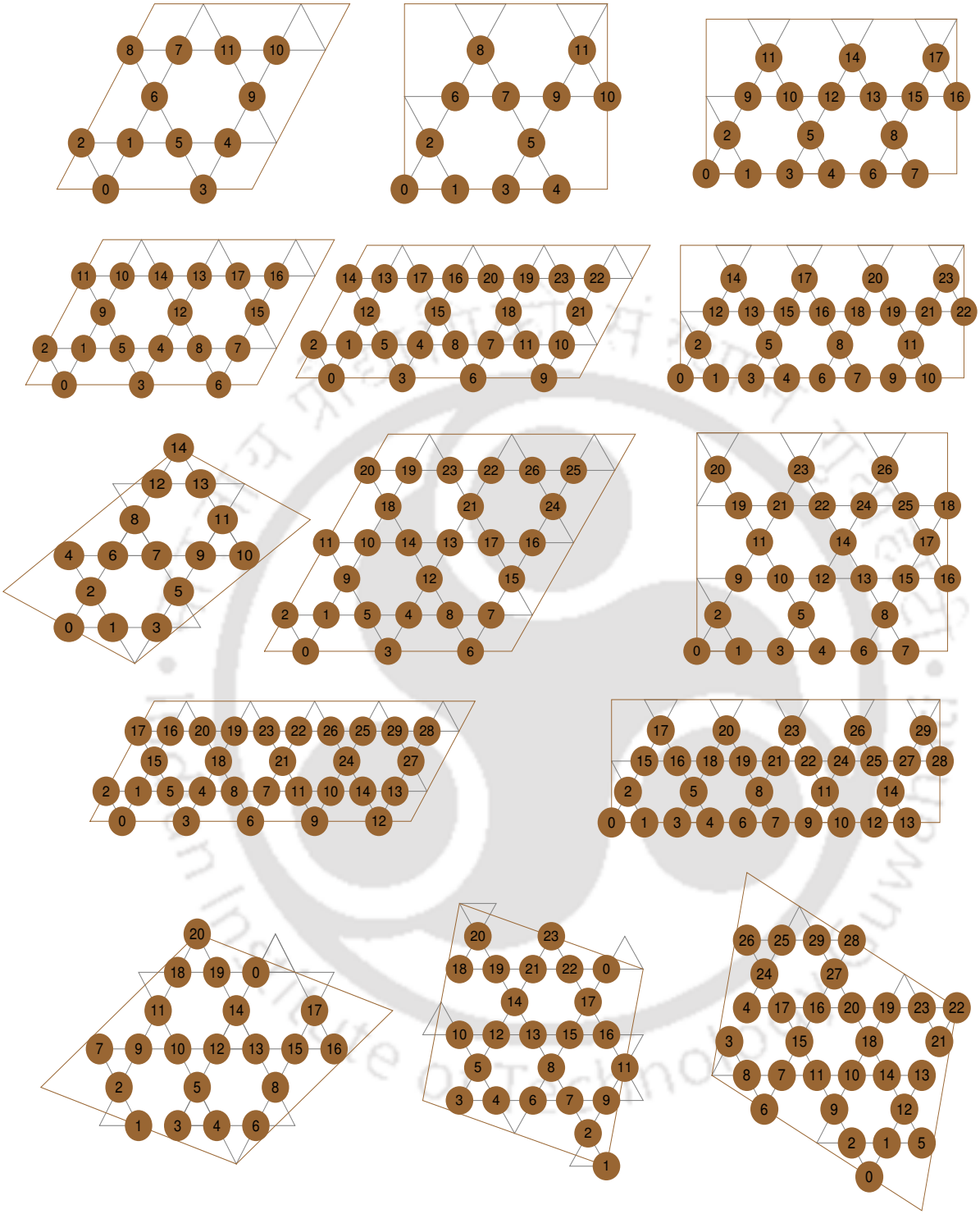

Figure 6.2: Kagome clusters of different sizes and shapes as implemented in the exact diagonalization calculation. The thick brown line is the boundary of the shapes. The maximum number encoded in the solid sphere of each of the shapes is the number spin.

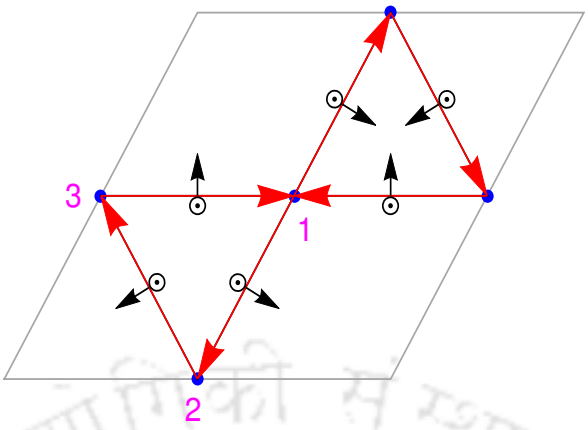

Figure 6.3: The orientation of DM vector, in-plane component D_p is shown by the black arrow and the out-of-plane component D_z is uniform along $\hat{z}$.

The model Hamiltonian is given by

$$H = \sum_{ij} \left[J_{ij} \vec{S}_i \cdot \vec{S}_j + \vec{D}_{ij} \cdot \vec{S}_i \times \vec{S}_j \right] \tag{6.4}$$

where J_{ij} is the strength of the exchange coupling, restricted to nearest neighbor only and $\vec{D}_{ij}$ is the DM vector with D_p and D_z be the strength of the in-plane and out-of-plane component. The orientation of the out-of-plane and in-plane components of DMI are shown in the Fig. 6.3(a). The DM vector is given by

$$\begin{aligned} \vec{D}_{31} &= D_p \hat{j} + D_z \hat{k} \\ \vec{D}_{12} &= \hat{R}(\hat{k}, -\frac{2\pi}{3}) \vec{D}_{31} \\ \vec{D}_{23} &= \hat{R}(\hat{k}, -\frac{4\pi}{3}) \vec{D}_{31} \end{aligned} \tag{6.5}$$

where $\hat{R}(\hat{k}, \theta)$ is the rotation operator that rotates a vector by an angle θ about the axis $\hat{k}$. The main focus of the study is to investigate the impact of a large planar component of DM interaction. We compute the ground-state phase diagram and various physical quantities to examine the magnetic structure of each of the phases present in the phase diagram of the above model. The absence of the global spin rotation symmetry, due to the presence of DM interaction, the Hilbert space could not be decomposed into the invariant sub-spaces, restricting the size of the system to 30. We have applied periodic boundary conditions to reduce the finite size effect. We consider different shapes with a total number of spins N is $12, 15, 18, 21, 24, 27, 30$ as shown in the Fig. 6.2. We have obtained the ground-state phase diagram of the

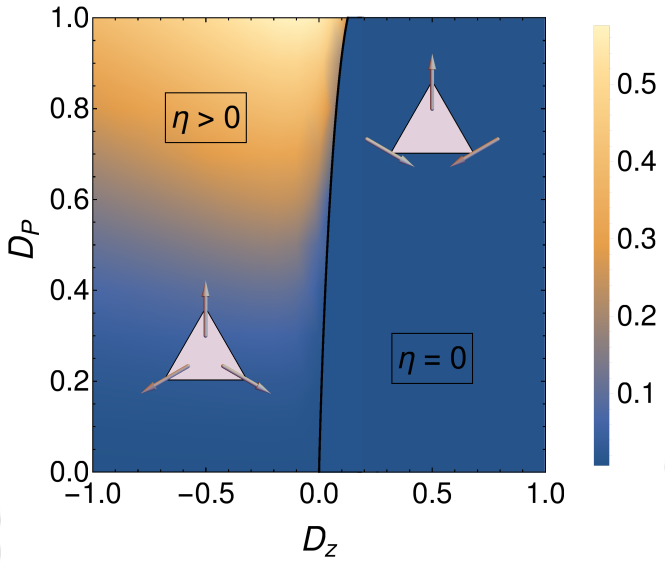

Figure 6.4: Ground state phase diagram

model only for the positive D_p. We must mention that the conclusion is made by looking at the trends of data points and extrapolation, so the accurate location of the critical point largely depends on the extrapolation function as well as cluster size and shape.

6.4 Results

We have computed the ground state phase diagram in the parameter range $0 \leq D_p \leq 1$ and $-1 \leq D_z \leq 1$ based on the chirality as well as looking at the value of ZZ-component of structure factor at Γ point. The ground state phase diagram of the present model is presented in the Fig. 6.4. The ground state is in $Q = 0$ long range order through out the parameter space. The phase boundary, shown by thick black line, is drawn on the basis of chirality. We have calculated the spin chirality that is the expectation value of

$$\chi_z = \left[\vec{S}_1 \times \vec{S}_2 + \vec{S}_2 \times \vec{S}_3 + \vec{S}_3 \times \vec{S}_1\right] \cdot \hat{\mathbf{k}} \tag{6.6}$$

where $\vec{S}_1, \vec{S}_2, \vec{S}_3$ are the spins at any arbitrary triangle. The variation of chirality as a function of D_z for fixed D_p is as shown in the Fig. 6.5(a). At $D_P = 0$ the chirality is negative for $D_z > 0$ and is postive when $D_z < 0$. When D_p is increased the transition point shifts by small amount towards the positive D_z. For $D_p = 0$ case is discussed by Cepas et al. [74] and they give evidence for spin liquid below $D_z = 0.1J$

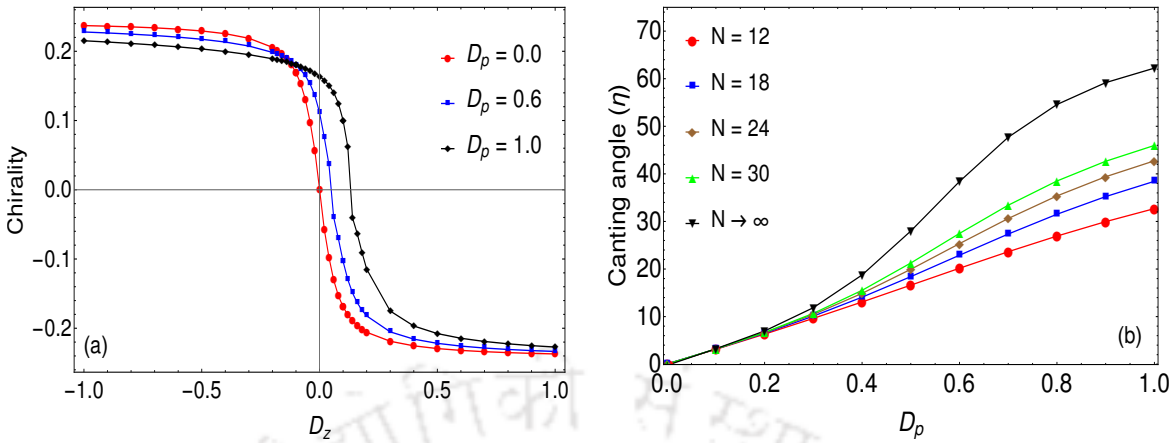

Figure 6.5: (a) Chirality as a function of D_z for different values of D_p for N=27 (b) Canting angle(in degree) as a function of D_p for $D_z = -0.1$

using the idea of tower of states. However, as soon as D_p is added, the global $U(1)$ symmetry vanishes and hence the same idea cannot be used to determine existence of spin liquid. Away from the isotropic point, the ground state is in $Q = 0$ LRO. The ground state is planar with negative chirality when $D_z > 0$. With $D_z < 0$, the state is an umbrella state with positive chirality. In this case, the canting angle varies from zero to 62.23^o as D_p changes from zero to J as shown in the Fig. 6.5(b). These results are in agreement with the SBMFT results presented earlier. In order to establish the the ground state spin configuration we have calculated the static spin structure factor. The static structure factor is defined as

$$S^{\alpha\beta}(Q) = \frac{3}{4N}\sum_{ij} e^{i[Q\cdot(R_i - R_j)]}\langle 0|S_i^{\alpha}S_j^{\beta}|0\rangle \tag{6.7}$$

where R_i and R_j is the site index and $\alpha, \beta \in \{x, y, z\}$. The Fig. 6.6 show structure factors for a representative point $D_p = D_z = 1$ along the high-symmetry line of the Brilliouin zone, for the right side of the phase diagram. The XX component of static structure shows a peak at M_e, the height of which diverges in the $N \to \infty$ limit as shown in the inset of Fig. 6.6(a) . This is a clear signature the long range magnetic order of $Q = 0$ type. In this case, the ZZ-component of static structure factor does not show any such peak(see Fig. 6.6(b)) indicating the planar arrangement of the spins i.e the spins lie in X-Y plane.

In the left part of the phase diagram ($D_z < 0$) we have taken the representative point to be $D_z = -1$ and $D_p = 1$. Here too, from Fig. 6.7(a), we see that the XX component of static structure shows a peak at M_e showing a long range magnetic

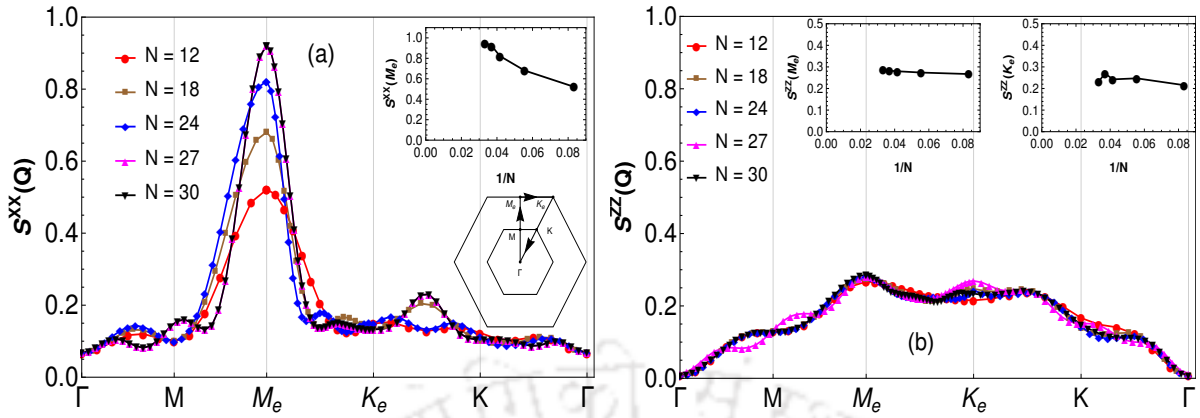

Figure 6.6: (a) XX component of static structure factor (b) ZZ component of static structure factor for $D_z = D_p = 1$

order of $Q = 0$ type. The divergent behavior of the height of the peak is shown in the inset. But the ZZ component of static structure shows a peak at Γ showing a long range ferromagnetic order which is increasing as we increase N as shown in the inset in Fig. 6.7(b). The canting angle is calculated from this data in the following way and is shown in the Fig. 6.5(b).

$$\eta = \tan^{-1}\left[\frac{\sqrt{S^{\mathrm{ZZ}}(\Gamma)}}{\sqrt{S^{\mathrm{XX}}(\mathrm{M}_e) + S^{\mathrm{YY}}(\mathrm{M}_e)}}\right] \tag{6.8}$$

Non zero canting angle implies umbrella kind of the structure of the ground state.

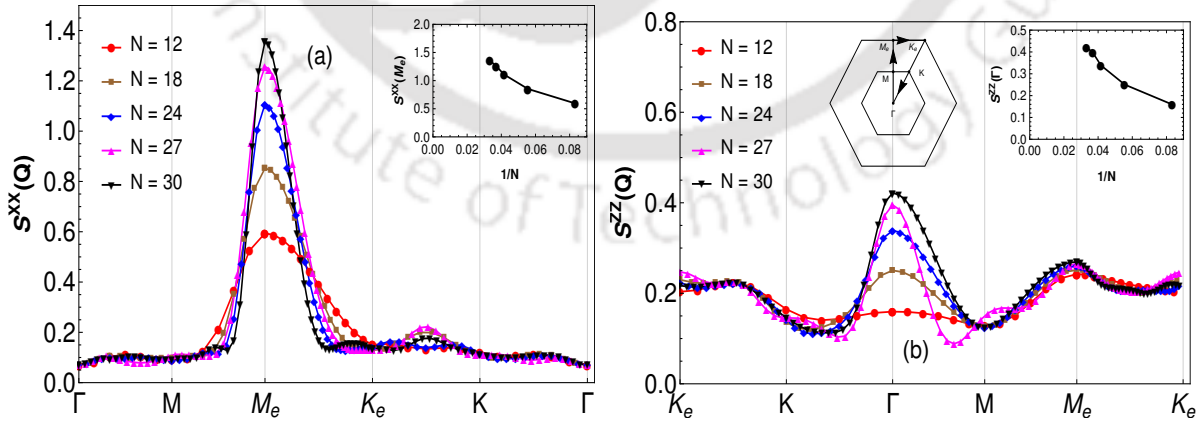

Figure 6.7: (a) XX component of static structure factor (b) ZZ component of static structure factor for $Dz = -1$ and $D_p = 1$

6.5 Discussion

For vesignieite, the measured value of in-plane component $D_p = 0.19J$ and the out-of-plane component $D_z = 0.07J$ [93] which are the two dominant term compared to other anisotropies like isotropic exchange anisotropy. The ground state is expected to be strongly influenced by the out-of-plane component of DMI. In the classical limit, any small amount of D_z will force the spin to lie in the kagome plane. In the absence of the in-plane component, the critical value $D_c = 0.1J$ predicted by ED result, there is a disordered state at one side and ordered state on the other. So, we expect that the presence of in-plane component D_p will affect this critical value. The presence of the in-plane component of DMI is responsible for the tilting of the spins towards the z-axis and giving rise to ferromagnetism. The measured value of the canting angle for vesignieite is found to be $3^o < \phi < 9^o$, as obtained from NMR data analysis.

In our phase diagram, for the spin-1/2 case, the ground state is in the magnetic LRO state. For negative values of D_z, we get the canted magnetic structure, and the canting angle increases with the increase of D_p. For $D_p = 0.2J$ and $D_z = -0.1J$, the estimated value of the canting angle is 6.98^o, which is very close to the canting angle measured in vesignieite as reported by Zorko et al. [93]. It seems the canted LRO nature of the ground state of vesignieite is dictated by the presence of DM interaction with the dominant component in the kagome plane.

In the case of SBMFT, for large boson density, the ground-state is also in the magnetic LRO region for all values of D_p and D_z. The ground-state phase diagram consists of two phases with different chiralities separated by a phase boundary. So, the ED results are in agreement with the SBMFT results.

6.6 Conclusion

We study the effect of in-plane and out of plane component of Dzyaloshinskii-Moriya interaction on the ground state of spin-1/2 kagome antiferromagnet using exact diagonalization Lanczos method up to system size $N = 30$. We found two chiralities of $Q = 0$ structure in the phase diagram for the spin-1/2 case. Positive chirality appears with a canted structure, whereas the negative chirality appears with a planar structure. For positive chirality states, the canting increases with an increase of D_p. For $D_p = 0.2$ and $D_z =$ -0.1, the estimated value of the canting angle is 6.98^o, which is in agreement with the canting angle measured in vesignieite. The obtained results are in agreement with the classical ground state and also SBMFT results.

Chapter 7

Conclusions

In this dissertation, we have extensively studied the effect of Dzyaloshinskii-Moriya interaction on the ground state of kagome Heisenberg antiferromagnet and the possible regular magnetic order in kagome and triangular lattice. Here in this chapter, we will briefly discuss the concluding remarks chapter-wise.

In Chapter-3, we study the ground-state phase diagram of kagome Heisenberg anti-ferromagnet with added Dzyaloshinskii-Moriya interaction using Schwinger boson mean-field theory. The construction of our mean-field theory is based on the assumption that the planar component of DMI is much smaller than the out-of-plane component. We have included the time-reversal symmetry breaking chiral *Ansätze* as well as the symmetric *Ansätze*. In previous mean-field calculations, only the $\mathcal{A}$ field which creates singlet at a given bond, was considered. But, here we have included the hopping field $\mathcal{B}$ in our calculation. We have computed the ground-state phase diagram for the present model. For a large value of S, even for even with small DM interaction, the spins are forced to lie in the plane, which leads to $Q = 0$ long-range order. For small S, the quantum fluctuations induce a series of spin liquid phases with increasing DM interaction. In this region, the inclusion of the hopping field seems to stabilize the $(\pi, 0)$ spin liquid phase over the $(0, \pi)$ spin liquid phase. Since the constraint of boson density is not implemented strictly, in SBMFT the spin-1/2 system can be approximated by the bosonic system at $S = 0.366$, due to the fluctuations in boson density. We find that at $S = 0.366$, the model shows a first-ordered phase transition from chiral cuboc1 spin liquid to $Q = 0$ Neel phase at $D = 0.03J$. Even though this result is qualitatively in agreement with other studies, it is not adequate in explaining the moment-free phase of herbertsmithite [112], since the estimated DM strength is $0.08J$. Probably, one may need to consider even smaller values of to obtain better numerical agreement with other studies and

experiments.

In Chapter-4, we study the possible regular magnetic order in wallpaper group $p6, p3, p3m1$, and $p31m$, which includes kagome and triangular geometry. These states can be a very good candidate to study the ground-state phase diagram of many specific spin models. We list all the possible RMOs for each of the wallpaper groups. We found new RMOs that were not reported earlier. For example, for the $p6$ wallpaper group, we have found two icosahedron states, namely icosahedron1 and icosahedron2, where the spins point towards the corner of a regular icosahedron. These two states contain 12 sub-lattices, and the unit-cell contains 12 sites. In these two cases, the relative angle between the neighboring spins is different. For $p3m1$ group, we found two new structures, namely type-I extended tetrahedral structure and type-I extended tetrahedral structure, where the spins are pointing towards the corner of a tetrahedron. In these two structures, the spins at each triangle become ferromagnetic, and it is a twelve site unit cell. For $p3$ group, we have found two similar states, namely type-I extended $Q = 0$ state. Both of them have three sub-lattices and an umbrella kind of structure. The realization of these states as a ground state of specific spin models will be interesting to study.

In Chapter-5, we study the effect of Dzyaloshinskii-Moriya interaction on the ground state of kagome Heisenberg antiferromagnet using Schwinger boson formalism. We obtained the ground-state phase diagram in the parameter space of D_P(planar component of DMI) and D_z(perpendicular component of DMI). Since in SBMFT, the spin S can be taken as a nonzero positive continuous parameter. For $S = 0.5$, we found a $Q = 0$ magnetic long-range order throughout the parameter space. The phase diagram consists of states of two different chiralities, separated by a phase boundary where there is a canted structure at one side and planar structure on the other. But at $S = 0.2$, we get a gapped topological spin liquid sandwiched between these two chiralities. By looking at the trends of data points, it seems that the gapped spin liquid region vanishes to become the phase boundary in the large S limit. Our results are in agreement with the classical ground state obtained for the present model.

In Chapter-6 Since, SBMFT is an approximate tool to identify the possible phases in the phase diagram; hence it only provides the qualitative results, not quantitative. So, to verify the results of SBMFT, we employ the exact diagonalization method to study the ground state of kagome Heisenberg antiferromagnet with added DM interaction. Here too, we found two chiralities of $Q = 0$ structure in the phase diagram for the spin-1/2 case, separated by a phase boundary that is drawn

on the basis of chirality. Positive chirality appears with a canted structure, whereas the negative chirality appears with a planar structure. The canting angle increases with the increase of the planar component of DMI for the positive chirality state. For $D_p = 0.2J$ and $D_z = 0.1J$, the estimated value of the canting angle is 6.98^o, which is in agreement with the canting angle measured in vesignieite. The obtained results are in agreement with the classical ground state and also SBMFT results.

7.1 Scopes of Future Work

The ground state of quantum kagome Heisenberg antiferromagnet is still an open problem to solve. The conclusions made from different approaches are not conclusive enough, and the ground state remains elusive, as discussed in Chapter-1. However, in this regard, we address some of the future prospects of this dissertation.

In the Schwinger boson formalism, we have described how to construct the chiral *Ansätze*. Using this formalism, the ground state of kagome Heisenberg antiferromagnet was argued to be a chiral topological spin liquid [72]. For the chiral *Ansätze*, we break the time-reversal symmetry and the minimal of lattice symmetries. In that case, the wallpaper group $p6m$ is reduced to $p3$. But there is no way one can exclude the possibilities from the other sub-groups of $p6m$. Construction of mean-field *Ansätze* from other sub-groups and the computation of the ground-state phase diagram remains an interesting topic to study.

In Chapter-4, we have listed all the possible regular magnetic orders in case of different sub-groups of $p6m$. Understanding those regular magnetic orders as a ground state of specific models remains an interesting extension of the present work.

Recent experimental results of vesignieite predict a different type of magnetic structure instead of $Q = 0$ order. Using neutron scattering results, D Boldrin et al. [94] argued that the ground state is possibly a multi-$\mathbf{k}$ co-planar variant of triple-$\mathbf{k}$ octahedral structure and the most dominant interaction is found to be the anti-ferromagnetic third neighbor exchange J_3. So, Understanding the ground state of vesignieite appears to be a fascinating problem.

In this thesis, we have only concentrated on the anisotropy Dzyaloshinskii-Moriya interaction. However, other anisotropies like single-ion anisotropy or dipole-dipole interaction may have an impact on the ground state manifold. Up to what extent these anisotropies influencees, the ground state is a potential problem to work out.

Bibliography

[1] L. Balents, Nature **464**, 199 (2010).

[2] P. Anderson, Materials Research Bulletin **8**, 153 (1973).

[3] C. Lhuillier and G. Misguich, Introduction to quantum spin liquids, in *Introduction to Frustrated Magnetism*, pages 23–41, Springer, 2011.

[4] F. Mila, European Journal of Physics **21**, 499 (2000).

[5] X.-G. Wen, Phys. Rev. B **65**, 165113 (2002).

[6] I. Dzyaloshinskii, Sov. Phys. JETP **5** (1957).

[7] T. Moriya, Physical Review **120**, 91 (1960).

[8] J. Villain, Journal de Physique **35**, 27 (1974).

[9] E. Rastelli and A. Tassi, Journal of Physics C: Solid State Physics **20**, L303 (1987).

[10] C. L. Henley, Physical review letters **62**, 2056 (1989).

[11] A. Auerbach, *Interacting electrons and quantum magnetism*, Springer Science & Business Media, 2012.

[12] N. F. MOTT, Rev. Mod. Phys. **40**, 677 (1968).

[13] N. D. Mermin and H. Wagner, Phys. Rev. Lett. **17**, 1133 (1966).

[14] A. P. Ramirez, Annual Review of Materials Science **24**, 453 (1994).

[15] Y. Shimizu, K. Miyagawa, K. Kanoda, M. Maesato, and G. Saito, Phys. Rev. Lett. **91**, 107001 (2003).

[16] T. Itou, A. Oyamada, S. Maegawa, and R. Kato, Nature Physics **6**, 673 (2010).

[17] O. Janson, J. Richter, P. Sindzingre, and H. Rosner, Phys. Rev. B **82**, 104434 (2010).

[18] M. P. Shores, E. A. Nytko, B. M. Bartlett, and D. G. Nocera, Journal of the american chemical society **127**, 13462 (2005).

[19] Y. Okamoto, H. Yoshida, and Z. Hiroi, Journal of the Physical Society of Japan **78** (2009).

[20] Y. Okamoto, M. Nohara, H. Aruga-Katori, and H. Takagi, Phys. Rev. Lett. **99**, 137207 (2007).

[21] Y. Tokiwa, T. Radu, R. Coldea, H. Wilhelm, Z. Tylczynski, and F. Steglich, Phys. Rev. B **73**, 134414 (2006).

[22] H. Bethe, Zeitschrift für Physik **71**, 205 (1931).

[23] L. Landau, Sov. Phys. JETP **8**, 70 (1959).

[24] A. Andreev and I. Grishchuk, Sov. Phys. JETP **60**, 267 (1984).

[25] A. Läuchli, J. C. Domenge, C. Lhuillier, P. Sindzingre, and M. Troyer, Phys. Rev.

Lett. **95**, 137206 (2005).
[26] A. Läuchli, F. Mila, and K. Penc, Phys. Rev. Lett. **97**, 087205 (2006).
[27] N. Shannon, T. Momoi, and P. Sindzingre, Phys. Rev. Lett. **96**, 027213 (2006).
[28] X. G. Wen and Q. Niu, Phys. Rev. B **41**, 9377 (1990).
[29] H. Iwase, M. Isobe, Y. Ueda, and H. Yasuoka, Journal of the Physical Society of Japan **65**, 2397 (1996).
[30] M. Azuma, Z. Hiroi, M. Takano, K. Ishida, and Y. Kitaoka, Phys. Rev. Lett. **73**, 3463 (1994).
[31] H. Kageyama et al., Phys. Rev. Lett. **82**, 3168 (1999).
[32] T. Nikuni, M. Oshikawa, A. Oosawa, and H. Tanaka, Phys. Rev. Lett. **84**, 5868 (2000).
[33] X.-G. Wen, Phys. Rev. Lett. **88**, 011602 (2001).
[34] X.-G. Wen, Phys. Rev. B **68**, 115413 (2003).
[35] D. A. Huse, W. Krauth, R. Moessner, and S. L. Sondhi, Phys. Rev. Lett. **91**, 167004 (2003).
[36] O. I. Motrunich and T. Senthil, Phys. Rev. B **71**, 125102 (2005).
[37] M. Hermele, M. P. A. Fisher, and L. Balents, Phys. Rev. B **69**, 064404 (2004).
[38] H.-C. Jiang, Z. Wang, and L. Balents, Nature Physics **8**, 902 (2012).
[39] A. Y. Kitaev, Annals of Physics **303**, 2 (2003).
[40] H. O. Jeschke, F. Salvat-Pujol, and R. Valentí, Phys. Rev. B **88**, 075106 (2013).
[41] T. Moriya, Physical Review Letters **4**, 228 (1960).
[42] P. W. Anderson, Physical Review **115**, 2 (1959).
[43] D. C. Mattis, *The theory of magnetism made simple: an introduction to physical concepts and to some useful mathematical methods*, World Scientific Publishing Company, 2006.
[44] A. Zorko, F. Bert, P. Mendels, P. Bordet, P. Lejay, and J. Robert, Phys. Rev. Lett. **100**, 147201 (2008).
[45] R. Moessner, Canadian journal of physics **79**, 1283 (2001).
[46] H. Diep et al., *Frustrated spin systems*, World Scientific, 2013.
[47] P. A. Lee, Science **321**, 1306 (2008).
[48] S. Yan, D. A. Huse, and S. R. White, Science **332**, 1173 (2011).
[49] P. Nikolic and T. Senthil, Phys. Rev. B **68**, 214415 (2003).
[50] R. R. P. Singh and D. A. Huse, Phys. Rev. B **77**, 144415 (2008).
[51] G. Evenbly and G. Vidal, Phys. Rev. Lett. **104**, 187203 (2010).
[52] D. Poilblanc, M. Mambrini, and D. Schwandt, Phys. Rev. B **81**, 180402 (2010).
[53] R. Budnik and A. Auerbach, Phys. Rev. Lett. **93**, 187205 (2004).
[54] M. Hermele, Y. Ran, P. A. Lee, and X.-G. Wen, Physical Review B **77**, 224413 (2008).
[55] H. C. Jiang, Z. Y. Weng, and D. N. Sheng, Phys. Rev. Lett. **101**, 117203 (2008).
[56] M. B. Hastings, Phys. Rev. B **63**, 014413 (2000).
[57] Y.-M. Lu, Y. Ran, and P. A. Lee, Physical Review B **83**, 224413 (2011).
[58] J. Marston and C. Zeng, Journal of Applied Physics **69**, 5962 (1991).

[59] S. Sachdev, Phys. Rev. B **45**, 12377 (1992).
[60] F. Mila, Phys. Rev. Lett. **81**, 2356 (1998).
[61] F. Wang and A. Vishwanath, Phys. Rev. B **74**, 174423 (2006).
[62] Y. Wan and O. Tchernyshyov, Phys. Rev. B **87**, 104408 (2013).
[63] V. Elser, Phys. Rev. Lett. **62**, 2405 (1989).
[64] P. Lecheminant, B. Bernu, C. Lhuillier, L. Pierre, and P. Sindzingre, Phys. Rev. B **56**, 2521 (1997).
[65] Y. Ran, M. Hermele, P. A. Lee, and X.-G. Wen, Phys. Rev. Lett. **98**, 117205 (2007).
[66] R. R. Singh and D. A. Huse, Phys. Rev. B **76**, 180407 (2007).
[67] S. Depenbrock, I. P. McCulloch, and U. Schollwöck, Phys. Rev. Lett. **109**, 067201 (2012).
[68] S. Nishimoto, N. Shibata, and C. Hotta, Nature communications **4**, 2287 (2013).
[69] H. Nakano and T. Sakai, Journal of the Physical Society of Japan **80**, 053704 (2011).
[70] Y. Iqbal, D. Poilblanc, and F. Becca, Phys. Rev. B **89**, 020407 (2014).
[71] Y. Iqbal, D. Poilblanc, and F. Becca, Phys. Rev. B **91**, 020402 (2015).
[72] L. Messio, B. Bernu, and C. Lhuillier, Phys. Rev. Lett. **108**, 207204 (2012).
[73] M. Elhajal, B. Canals, and C. Lacroix, Phys. Rev. B **66**, 014422 (2002).
[74] O. Cépas, C. Fong, P. W. Leung, and C. Lhuillier, Phys. Rev. B **78**, 140405 (2008).
[75] Y. Huh, L. Fritz, and S. Sachdev, Phys. Rev. B **81**, 144432 (2010).
[76] L. Messio, O. Cépas, and C. Lhuillier, Phys. Rev. B **81**, 064428 (2010).
[77] J. Nasu, M. Udagawa, and Y. Motome, Phys. Rev. Lett. **113**, 197205 (2014).
[78] Y. Li et al., Scientific reports **5**, 16419 (2015).
[79] Z. Ma et al., Phys. Rev. Lett. **120**, 087201 (2018).
[80] C. Balz et al., Nature Physics **12**, 942 (2016).
[81] M. Klanjšek et al., Nature Physics **13**, 1130 (2017).
[82] Y. Li et al., Phys. Rev. Lett. **115**, 167203 (2015).
[83] M. Hermele, T. Senthil, M. P. A. Fisher, P. A. Lee, N. Nagaosa, and X.-G. Wen, Phys. Rev. B **70**, 214437 (2004).
[84] J. Helton et al., Phys. Rev. Lett. **98**, 107204 (2007).
[85] M. A. de Vries, J. R. Stewart, P. P. Deen, J. O. Piatek, G. J. Nilsen, H. M. Rønnow, and A. Harrison, Phys. Rev. Lett. **103**, 237201 (2009).
[86] J. S. Helton et al., Phys. Rev. Lett. **104**, 147201 (2010).
[87] M. R. Norman, Rev. Mod. Phys. **88**, 041002 (2016).
[88] T.-H. Han, J. S. Helton, S. Chu, D. G. Nocera, J. A. Rodriguez-Rivera, C. Broholm, and Y. S. Lee, Nature **492**, 406 (2012).
[89] R. Colman, F. Bert, D. Boldrin, A. Hillier, P. Manuel, P. Mendels, and A. Wills, Phys. Rev. B **83**, 180416 (2011).
[90] H. Yoshida, Y. Michiue, E. Takayama-Muromachi, and M. Isobe, Journal of Materials Chemistry **22**, 18793 (2012).
[91] J. Quilliam, F. Bert, R. Colman, D. Boldrin, A. Wills, and P. Mendels, Physical Review B **84**, 180401 (2011).
[92] M. Yoshida, Y. Okamoto, M. Takigawa, and Z. Hiroi, Journal of the Physical Society

of Japan **82**, 013702 (2012).
[93] A. Zorko, F. Bert, A. Ozarowski, J. van Tol, D. Boldrin, A. S. Wills, and P. Mendels, Phys. Rev. B **88**, 144419 (2013).
[94] D. Boldrin et al., Phys. Rev. Lett. **121**, 107203 (2018).
[95] Z. Hiroi, M. Hanawa, N. Kobayashi, M. Nohara, H. Takagi, Y. Kato, and M. Takigawa, Journal of the Physical Society of Japan **70**, 3377 (2001).
[96] H. Yoshida, J.-i. Yamaura, M. Isobe, Y. Okamoto, G. J. Nilsen, and Z. Hiroi, Nature communications **3**, 860 (2012).
[97] H. Ishikawa et al., Phys. Rev. Lett. **114**, 227202 (2015).
[98] M. Yoshida, M. Takigawa, H. Yoshida, Y. Okamoto, and Z. Hiroi, Phys. Rev. Lett. **103**, 077207 (2009).
[99] Y. Okamoto, M. Tokunaga, H. Yoshida, A. Matsuo, K. Kindo, and Z. Hiroi, Phys. Rev. B **83**, 180407 (2011).
[100] R. Colman, C. Ritter, and A. Wills, Chemistry of Materials **20**, 6897 (2008).
[101] R. Colman, A. Sinclair, and A. Wills, Chemistry of Materials **22**, 5774 (2010).
[102] O. Janson, J. Richter, and H. Rosner, Phys. Rev. Lett. **101**, 106403 (2008).
[103] B. Fåk et al., Phys. Rev. Lett. **109**, 037208 (2012).
[104] L. Messio, C. Lhuillier, and G. Misguich, Phys. Rev. B **87**, 125127 (2013).
[105] N. Read and S. Sachdev, Phys. Rev. Lett. **66**, 1773 (1991).
[106] R. Flint and P. Coleman, Physical Review B **79**, 014424 (2009).
[107] G. Misguich, Phys. Rev. B **86**, 245132 (2012).
[108] J. Colpa, Physica A: Statistical Mechanics and its Applications **93**, 327 (1978).
[109] L. Savary and L. Balents, Reports on Progress in Physics **80**, 016502 (2016).
[110] P. W. Leung and V. Elser, Phys. Rev. B **47**, 5459 (1993).
[111] B. G. Levi, Physics today **60**, 16 (2007).
[112] A. Zorko et al., Phys. Rev. Lett. **101**, 026405 (2008).
[113] M. Rigol and R. R. Singh, Phys. Rev. Lett. **98**, 207204 (2007).
[114] I. Rousochatzakis, S. R. Manmana, A. M. Läuchli, B. Normand, and F. Mila, Physical Review B **79**, 214415 (2009).
[115] M. Tovar, K. S. Raman, and K. Shtengel, Physical Review B **79**, 024405 (2009).
[116] A. Mezio, C. Sposetti, L. Manuel, and A. Trumper, Europhys. Lett.) **94**, 47001 (2011).
[117] L. Manuel, C. Gazza, A. Trumper, and H. Ceccatto, Phys. Rev. B **54**, 12946 (1996).
[118] L. Messio, S. Bieri, C. Lhuillier, and B. Bernu, Phys. Rev. Lett. **118**, 267201 (2017).
[119] L. Messio, C. Lhuillier, and G. Misguich, Phys. Rev. B **83**, 184401 (2011).
[120] A. Laeuchli and C. Lhuillier, (2009).
[121] P. W. Anderson, science **235**, 1196 (1987).
[122] Y. Zhou, K. Kanoda, and T.-K. Ng, Reviews of Modern Physics **89**, 025003 (2017).
[123] P. Mendels and F. Bert, Comptes Rendus Physique **17**, 455 (2016).
[124] S. El Shawish, O. Cépas, and S. Miyashita, Phys. Rev. B **81**, 224421 (2010).
[125] W.-m. Zhang et al., Journal of the Physical Society of Japan **79**, 023708 (2010).
[126] A. Scheie, M. Sanders, J. Krizan, Y. Qiu, R. J. Cava, and C. Broholm, Phys. Rev.

B **93**, 180407 (2016).
[127] P. Laurell and G. A. Fiete, Phys. Rev. B **98**, 094419 (2018).
[128] R. Yadav et al., Phys. Rev. Materials **2**, 074408 (2018).
[129] J. C. Halimeh and M. Punk, Phys. Rev. B **94**, 104413 (2016).
[130] K. Mondal and C. Kadolkar, Phys. Rev. B **95**, 134404 (2017).
[131] Y. Saad, *Numerical methods for large eigenvalue problems*, Manchester University Press, 1992.
[132] Z. Bai, J. Demmel, J. Dongarra, A. Ruhe, and H. van der Vorst, *Templates for the solution of algebraic eigenvalue problems: a practical guide*, SIAM, 2000.

Vita

Kallol Mondal was born on 31st January, 1988 in Raniganj, West bengal, India. He did his B.Sc. with Physics Honours in 2009 from Triveni Devi Bholatia College, Raniganj, under The University of Burdwan and M.Sc. in physics from Visva-Bharati, Shantiniketan in 2012. He had enrolled into the Ph.D programme at Indian Institute of Technology Guwahati in 2012. He had qualified Graduate Aptitude Test in Engineering (GATE) in 2011 and 2012. He has earned the Senior Research Fellowship in 2014 by Indian Institute of Technology Guwahati.